ISTANBUL TECHNICAL UNIVERSITY ★ GRADUATE SCHOOL

HIGH-RATE ACTIVATED SLUDGE PROCESS FOR ENERGY EFFICIENT WASTEWATER TREATMENT

Ph.D. THESIS

Hazal GÜLHAN

Department of Environmental Engineering

Environmental Sciences Engineering and Management Programme

OCTOBER 2023

ISTANBUL TECHNICAL UNIVERSITY ★ GRADUATE SCHOOL

HIGH-RATE ACTIVATED SLUDGE PROCESS FOR ENERGY EFFICIENT WASTEWATER TREATMENT

Ph.D. THESIS

Hazal GÜLHAN
(501172704)

Department of Environmental Engineering

Environmental Sciences Engineering and Management Programme

Thesis Advisor: Prof. Dr. İzzet ÖZTÜRK

OCTOBER 2023

ISTANBUL TEKNİK ÜNİVERSİTESİ ★ LİSANSÜSTÜ EĞİTİM ENSTİTÜSÜ

ENERJİ VERİMLİ ATIKSU ARITIMI İÇİN YÜKSEK YÜKLEMELİ AKTİF ÇAMUR PROSESİ

DOKTORA TEZİ

Hazal GÜLHAN
(501172704)

Çevre Mühendisliği Anabilim Dalı

Çevre Bilimleri Mühendisliği ve Yönetimi Programı

Tez Danışmanı: Prof. Dr. İzzet ÖZTÜRK

EKİM 2023

Hazal GÜLHAN, a Ph.D. student of İTU Graduate School student ID 501172704, successfully defended the dissertation entitled "HIGH-RATE ACTIVATED SLUDGE PROCESS FOR ENERGY EFFICIENT WASTEWATER TREATMENT", which she prepared after fulfilling the requirements specified in the associated legislations, before the jury whose signatures are below.

Thesis Advisor : **Prof. Dr. İzzet ÖZTÜRK** ....
İstanbul Technical University

Jury Members : **Prof. Dr. Bülent İNANÇ** ....
Istanbul Technical University

Prof. Dr. Barış ÇALLI ....
Marmara University

Prof. Dr. Özlem KARAHAN ÖZGÜN ....
Istanbul Technical University

Assist. Prof. Recep Kaan DERELİ ....
University College Dublin

Date of Submission : 1 July 2023
Date of Defense : 25 October 2023

To my family,

FOREWORD

After completing my master's thesis, I told my dad over the phone that I had no intention of pursuing a Ph.D. Back then, I was discouraged by seeing how drained and exhausted Ph.D. candidates seemed. Yet, it has been six years since the conversation with him, and now, at eleven o'clock on a Sunday night, I find myself writing the foreword of my Ph.D. thesis.

Throughout this period, I've realized that my personal growth outweighs the knowledge I've gained in my field. I've found that I have a genuine passion for learning. Despite eagerly planning tasks, I found myself completing them at the last minute with a heightened focus, leading to increased stress. Still, this process taught me to stay composed in tough situations and focus on the next steps. And most significantly, I've found fulfillment in contributing to scientific progress rather than chasing financial gains. The saying "one cannot grow unless they step out of their comfort zone" deeply resonates with me. Looking back, the Ph.D. journey pushed me out of my comfort zone, fostering personal growth and leaving me content with my current state.

I extend my heartfelt gratitude to Prof. İzzet ÖZTÜRK, my advisor. His insatiable curiosity for science and respect for all has been a great source of inspiration to me. Next, I would like to express my thanks to Assoc. Professors Hale ÖZGÜN and Evren ERŞAHİN. From Assoc. Prof. Hale, I have learned the importance of focusing on the purpose behind every task I undertake. And if I could follow the discipline of consistent study from Assoc. Prof. Evren, it would undoubtedly make everything easier for me. Additionally, I am sincerely appreciative of Assis. Professors Kaan DERELİ, Hüseyin GÜVEN, and Türker TÜRKEN for sharing their knowledge and experiences generously. I would like to acknowledge the Istanbul Water and Sewerage Administration, ITU Scientific Research Projects Coordination Unit, and National Research Center on Membrane Technologies for their financial and technical support in my Ph.D. study.

During my doctoral journey, I had the support and friendship of many individuals. I sincerely thank Onur, Amr, Şadiye, Malhun, Büşra, Muhammed, Reza, Beyda, Kadir, Bahriye, Yasemin, Ali, and Erol ERTÜRK for their unwavering support.

I am deeply grateful to Orhun for being an inspiration and providing unwavering support, living life to the fullest with profound purpose and meaning.

My heartfelt thanks go to my mom, Gülten, my dad, Erol, and my dearest sister, İzel. Your constant presence by my side fills me with an indescribable sense of lightness and reassurance.

July 2023

Hazal GÜLHAN
(Environmental Engineer)

TABLE OF CONTENTS

Page

ABBREVIATIONS

A/B	:	Adsorption/Bio-oxidation
Alum	:	Aluminum Sulfate
ANOVA	:	Analysis of Variance
ASM1	:	Activated Sludge Model No. 1
ASM2	:	Activated Sludge Model No. 2
ASM3	:	Activated Sludge Model No. 3
BMP	:	Biomethane Potential
BOD	:	Biological Oxygen Demand
BOD_5	:	5 Days BOD
BSA	:	Bovine Serum Albumin
CAS	:	Conventional Activated Sludge
cCOD	:	Colloidal COD
cEPS	:	Carbohydrate EPS
cfu	:	Colony Forming Units
CHP	:	Combined Heat and Power
COD	:	Chemical Oxygen Demand
CST	:	Capillary Suction Time
DMF	:	Direct Membrane Filtration
DO	:	Dissolved Oxygen
E. coli	:	*Escherichia coli*
EEA	:	The European Environment Agency
EQI	:	Effluent Quality Index
ESEM	:	Environmental Scanning Electron Microscopy
EU	:	The European Union
EUCO	:	The European Council
HRT	:	Hydraulic Retention Time
IC	:	Ion Chromatography
ICP-OES	:	Inductively Coupled Plasma-Optical Spectrometer
LB-EPS	:	Loosely Bound EPS
MAE	:	Mean Absolute Error

MF : Microfiltration
MLSS : Mixed Liquor Suspended Solids
MLVSS : Mixed Liquor Volatile Suspended Solids
ND : Not Detected
NF : Nano Filtration
O&M : Operations and Maintenance
OLR : Organic Loading Rate
PACl : Polyaluminium Chloride
PE : Population Equivalent
pEPS : Protein EPS
PSD : Particle Size Distribution
PVDF : Polyvinylidene Difluoride
PWWTP : Preliminary Wastewater Treatment Plant
RAS : Return Activated Sludge
RMSE : Root Mean Squared Error
RO : Reverse Osmosis
rpm : Revolutions per Minute
RWQI : Reclaimed Water Quality Index
SCADA : Supervisory Control and Data Acquisition
sCOD : Soluble COD
SD : Standard Deviation
SLR : Surface Loading Rate
SRT : Sludge Retention Time
SS : Suspended Solids
SVI : Sludge Volume Index
TB-EPS : Tightly Bound EPS
tCOD : Total COD
TDS : Total Dissolved Solids
TMP : Transmembrane Pressure
TN : Total N
TS : Total Solids
TSS : Total Suspended Solids
UF : Ultrafiltration
US EPA : The United States Environmental Protection Agency
USA : The United States of America

UV	**:** Ultraviolet
VS	**:** Volatile Solids
VSS	**:** Volatile Suspended Solids
WAS	**:** Waste Activated Sludge
WTP	**:** Water Treatment Sludge
WWTP	**:** Wastewater Treatment Plant
xCOD	**:** Particulate COD

SYMBOLS

μ	: Maximum specific growth rate
μS	: Microsiemens
AC	: Annual capital costs
Al	: Aluminum
$Al_2(SO_4)_3$	: Aluminum sulfate
Au	: Gold
b	: Decay rate
Ca	: Calcium
$CaCO_3$	: Calcium carbonate
Cd	: Cadmium
CH_4	: Methane
Cl^-	: Chloride
CO_2	: Carbon dioxide
$COD_{biomass}$	: COD used for biomass growth
$COD_{biosorption}$	: Biosorbed COD
COD_{eff}	: COD concentration in the effluent
COD_{EPS}	: COD used for EPS production
COD_{inf}	: COD concentration in the influent
$COD_{redirected}$	: Redirected COD
COD_{WAS}	: COD concentration in WAS
Con	: Concentration
d_{50}	: Median particle size
Da	: Dalton
f_{col}	: Colloidal fraction generated via hydrolysis of X_S
Fe	: Iron
$FeCl_3$	: Iron(III) chloride
f_p	: Inert fraction generated via decay of X_B
i	: Interest rate
$i_{chargeNH}$	: Conversion factor for NH_4^+ in charge
$i_{chargePO}$	: Conversion factor for PO_4^- in charge

i_{NXB} : N fraction of X_B

i_{NXI} : N fraction of X_I

i_{NXS} : N fraction of X_S

i_{PXB} : P fraction of X_B

i_{PXI} : P fraction of X_I

i_{PXS} : P fraction of X_S

k_{ADS} : Adsorption rate

kDa : Kilodalton

k_H : Maximum specific hydrolysis rate

$K_{max,j}$: Maximum value of the j^{th} model output

$K_{min,j}$: Minimum value of the j^{th} model output

K_j : Average value of the j^{th} model output

K_{NH} : Ammonia (as nutrient) half-saturation coefficient

K_O : Oxygen half-saturation coefficient

K_{S1} : S_S half-saturation coefficient for growth

K_{S2} : S_S half-saturation coefficient for storage

K_{SP} : Phosphorus (as nutrient) half-saturation coefficient

k_{STO} : Storage rate

K_{XS} : X_S half-saturation coefficient

K_{XSTO} : X_{STO} half-saturation coefficient

$L(\theta_i/Y_j)$: Likelihood for the j^{th} model output

$L(\theta_i/Y_j)_j$: Average likelihood for the j^{th} model output of the i^{th} model parameter

$L(\theta_i/Y_j)_{max,j}$: Maximum likelihood for the j^{th} model output of the i^{th} model parameter

$L(\theta_i/Y_j)_{min,j}$: Minimum likelihood for the j^{th} model output of the i^{th} model parameter

$MgSO_4$: Magnesium sulfate

M_i : Model outputs

Mn : Manganese

n : Sample size

N : Nitrogen

NaCl : Sodium chloride

NH_4^+ : Ammonium ion

NH_4-N : Ammonium nitrogen

Ni : Nickel

O_i	: Observed values
P	: Phosphorus
Pb	: Lead
PC	: Present capital cost
Pd	: Palladium
p-value	: Significance level
Q_{inf}	: Influent flow rate
Q_{WAS}	: WAS flow rate
r	: Correlation coefficient
S_{COL}	: Colloidal COD
S_I	: Soluble inert organics
S_i	: Sensitivity index
SiO_2	: Silica
S_{NH}	: Ammonia
S_O	: Oxygen
SO_4^{2-}	: Sulfate
S_P	: Ortho-Phosphate
S_S	: Readily biodegradable organics
TN_{eff}	: TN concentration in the effluent
TP_{eff}	: TP concentration in the effluent
TSS_{eff}	: TSS concentration in the effluent
$V_{reactor}$	: Volume of the reactor
w	: Weighting factor
X_B	: Biomass
X_{eff}	: TSS concentration in the effluent
X_I	: Particulate inert organics
X_{MLSS}	: MLSS concentration
X_S	: Slowly biodegradable organics
X_{STO}	: Stored substrate
X_{WAS}	: TSS concentration of the WAS
y	: Years of operation
Y_H	: Growth yield
Y_{STO}	: Storage yield
β_{COD}	: Weighting factor for COD
β_{TN}	: Weighting factor for TN

β_{TSS} : Weighting factor for TSS

β_{TP} : Weighting factor for TP

$\sigma^2_{M_j - O_j}$: Sum of squared errors

LIST OF TABLES

Page

LIST OF FIGURES

Page

HIGH-RATE ACTIVATED SLUDGE PROCESS FOR ENERGY EFFICIENT WASTEWATER TREATMENT

SUMMARY

The conventional activated sludge (CAS) process used in wastewater treatment is inefficient in terms of energy and requires a large space. CAS plants can only recover around 33% of the energy in wastewater, which is a significant drawback. The growing urban population and wastewater volume pose a challenge in land-constrained areas like Istanbul. Therefore, it is important to adopt innovative treatment processes that minimize land requirements, maximize organic matter capture, and reduce carbon dioxide (CO_2) losses. This approach, known as carbon capture, redirection, or harvesting, focuses on diverting carbon from wastewater to the sludge line for biogas production in anaerobic digesters.

High-rate activated sludge (HRAS) systems, developed in the 1980s, aim to redirect carbon from wastewater to anaerobic digesters for energy production, offering an alternative to primary sedimentation in wastewater treatment plants (WWTPs). They are operated at high organic loading rates and have short sludge retention times (SRTs) and hydraulic retention times (HRTs). In the B-stage, pollutant removal primarily occurs through biological oxidation at lower organic loading rates.

The HRAS process has proven to be superior to CAS and primary sedimentation units with regard to carbon redirection and methane generation during anaerobic digestion. However, several areas for improvement have been identified based on existing literature. Firstly, there is a lack of information regarding the performance of HRAS systems when equipped with lamella clarifiers, which can enhance the performance of solid-liquid separation in WWTPs. Secondly, existing mathematical modeling studies of the HRAS process are either overly complex or overly simplistic, often overlooking important processes like adsorption and focusing primarily on carbon removal. Furthermore, sensitivity and uncertainty analyses, commonly employed to assess the robustness of models, have not been extensively applied to HRAS system models. Thirdly, despite its potential, there is a scarcity of literature on integrating the HRAS process into water reclamation practices, which could benefit from its smaller spatial footprint, lower energy consumption, and nutrient-rich effluent. Lastly, it is essential to address the fact that the use of coagulants in the HRAS process improves phosphorus removal efficiency while increasing operational costs. Limited research has been conducted on the impact of using water treatment plant (WTP) sludge on the anaerobic digestion of waste sludge in WWTPs and its influence on HRAS process performance and energy recovery. This thesis explores the potential of the HRAS process in sustainable wastewater treatment and investigates the following research topics: **Study 1**, optimum operational conditions for the HRAS process with a lamella clarifier, **Study 2**, mathematical modelling of the HRAS process to provide a practical tool for future implementations of HRAS plants, **Study 3**, integration of membrane filtration for reclaimed water production for industries, **Study 4**, post-treatment alternatives for HRAS process effluent for irrigation purposes, and **Study 5**, the reuse

of WTP sludge to enhance treatment performance and resource circularity. These topics were investigated through pilot and laboratory scale studies using real municipal wastewater. A pilot-scale HRAS plant with a lamella clarifier was constructed in a full-scale preliminary WWTP (PWWTP) in Istanbul. The plant was operated under various conditions for two years to address the research topics. Laboratory-scale experiments involving membrane filtration and chemical precipitation were conducted using real municipal wastewater collected from the same PWWTP.

Study 1 focused on determining the optimal operational conditions for the pilot-scale HRAS system coupled with a lamella clarifier. The study found that using a lamella clarifier resulted in lower total suspended solids (TSS) concentrations in the effluent and required a smaller footprint compared to a conventional clarifier. The optimum operational condition was identified as Stage 1, with an HRT of 75 minutes and a dissolved oxygen (DO) concentration of 0.5 mg/L. This condition demonstrated the best effluent quality, highest carbon capture, and highest production of extracellular polymeric substance (EPS). The study also found that reducing the HRT increased biosorption but led to increased chemical oxygen demand (COD) loss through the effluent. Lower DO concentrations promoted carbon redirection but resulted in weak floc formation and increased particulate COD (xCOD) loss. Meanwhile, higher DO concentrations enhanced COD oxidation but allowed more particles to escape through the effluent. Overall, the HRAS process with a lamella clarifier showed promising particulate matter removal efficiency and the potential for reclaimed water production. Studies 3 and 4 further investigated the inclusion of the HRAS process in reclaimed water production systems.

Study 2 developed and calibrated a mathematical model for HRAS systems by integrating Activated Sludge Models No. 1 and 3 (ASM1 and ASM3), accounting for substrate adsorption and storage. The calibration utilized dynamic data from the pilot-scale HRAS plant and identified influential parameters like maximum specific growth rate (μ), growth yield (Y_H), storage yield (Y_{STO}), storage rate (k_{STO}), decay rate (b), and readily biodegradable substrate half-saturation coefficient (K_{S1}). The calibrated model demonstrated satisfactory efficiencies for mixed liquor suspended solids (MLSS), total COD (tCOD), soluble COD (sCOD), xCOD, total nitrogen (TN), ammonia nitrogen (SNH), total phosphorus (TP), soluble TP (sTP), and particulate TP (xTP), all above 70%. However, an uncertainty analysis exposed discrepancies in sCOD. The study also highlighted the potential to enhance sTP dynamic behavior estimation. The low model efficiency is likely due to variations in wastewater characteristics, especially the phosphorus (P) fractions, which were not dynamically considered in the model. Another reason could be the precipitation of phosphate salts, which was not included in the model. Overall, the study offers valuable insights into influential parameters and opportunities for refining the HRAS process modeling.

Study 3 encompassed both experimental and cost analyses to evaluate different treatment configurations for water reclamation. Six configurations were examined, incorporating pre-treatment options like direct membrane filtration (DMF) via microfiltration (MF) and ultrafiltration (UF) membranes, and HRAS, and final treatment alternatives such as nanofiltration (NF) and reverse osmosis (RO). The performance of NF and RO membranes ensured that the reclaimed water from each scenario met the required quality standards for cooling tower makeup water. Despite HRAS producing effluent with higher turbidity compared to MF and UF membranes, the cost analysis revealed that the HRAS+NF configuration (C3) offered the most cost-effective treatment, with a cost of 0.38 €/m^3 of wastewater. This cost advantage was due to the lower expenses associated with the HRAS process compared to MF and UF membranes. The study concluded that the C3 configuration has the potential to produce reclaimed water suitable for cooling towers, thereby reducing the water footprint of industries and promoting water circularity.

Study 4 compared various post-treatment alternatives for generating irrigation water from the effluent of the HRAS process. UF membrane filtration showed the best treatment performance compared to MF membrane filtration, iron(III) chloride ($FeCl_3$) coagulation, and aluminum sulfate (alum) coagulation. Ultraviolet (UV) disinfection was implemented in all options to ensure pathogen removal. The membrane filtration techniques effectively removed particulate matter, while coagulant doses were adjusted to achieve TSS concentrations below 10 mg/L in the supernatant. Among the alternatives, only UF membrane filtration followed by UV disinfection (referred to as A2) produced Class A quality reclaimed water, meeting the highest standards. However, A2 also had the highest operating cost. Alternatives A1, A3, and A4 produced Class B quality reclaimed water, with operating costs decreasing as the reclaimed water quality decreased. A3 (coagulation with $FeCl_3$+UV disinfection) had the lowest operating cost. The energy consumption per unit volume was consistent with previous studies. The findings demonstrated that the HRAS process's effluent can be effectively utilized for irrigation water production with comparable costs to traditional CAS systems.

Study 5 investigated the impact of using WTP sludge in a HRAS system. Jar tests compared the performance of iron sludge and alum sludge in terms of removal efficiency, with iron sludge proving more effective in removing particulates. Incorporating iron sludge into the HRAS system resulted in slight improvements in TSS and xCOD removal efficiencies. The environmental impact, measured by the effluent quality index (EQI), improved by 2% through WTP sludge use. Additionally, adding WTP sludge increased the particle size of sludge in the aeration tank, enhancing settleability and dewaterability, which reduces sludge treatment costs. However, biomethane potential (BMP) tests showed that the addition of iron sludge decreased the BMP of HRAS process sludge. Cost estimations were conducted for different sludge management scenarios, considering transfer, disposal, and wastewater treatment costs, along with energy savings from biogas production. Using WTP sludge in the HRAS plant led to an estimated 11% reduction in the total cost, indicating the potential for mutual benefits for WTPs and WWTPs in terms of finances and the environment. Integrating water and wastewater treatment plants can promote resource circularity and maximize resource utilization efficiency.

This thesis highlights the potential of the HRAS process in contributing to water and material recovery in the circular economy. To enhance the model's accuracy in estimating sTP, simulating phosphate salt precipitation may be necessary. However, this improvement would necessitate additional data on wastewater characteristics and increase the model's complexity. To further explore water reuse and nutrient recovery, a more comprehensive economic analysis could be conducted, investigating various treatment combinations at the pilot scale. In this study, the direct integration of WTP sludge into the HRAS process resulted in limited improvement in treatment performance. Future research could be conducting pilot-scale tests to enhance this approach for increased treatment efficiency and biogas production, possibly through coagulant recovery processes like acidification. Such research would offer valuable insights into the circularity between water and wastewater treatment plants.

ENERJİ VERİMLİ ATIKSU ARITIMI İÇİN YÜKSEK YÜKLEMELİ AKTİF ÇAMUR PROSESİ

ÖZET

Atıksu arıtımında kullanılan konvansiyonel aktif çamur (KAS) prosesinin en önemli kısıtları yüksek enerji tüketimi ve alan ihtiyacıdır. KAS prosesi ile atıksuyun enerji içeriğinin %30'u karbon dioksit (CO_2) olarak atmosfere kaybedilirken yaklaşık %33'ünü geri kazanabilir. Artan kentsel nüfus ve atıksu hacmi, İstanbul gibi nüfus yoğunluğunun yüksek olduğu yerleşim yerlerinde KAS sistemlerinin uygulanabilirliğini kısıtlamaktadır. Bu nedenle, alan gereksinimlerini en aza indiren ve enerji geri kazanımını en üst düzeye çıkaran yenilikçi arıtma prosesleri önem kazanmaktadır. Karbon yakalama olarak bilinen bu yaklaşım, anaerobik çürütücülerde proses çamurundan biyogaz üretimini artırmak için atıksudaki karbonu çamur hattına yönlendirmeye odaklanır.

İki kademeli adsorpsiyon/biyo-oksidasyon (A/B) prosesinin A kademesi, atıksudaki karbonu mineralize edip CO_2 olarak kaybetmektense, çamur hattına yönlendirerek anaerobik çamur çürütücülerde daha fazla biyogaz üretmeyi amaçlar. 1980'lerde geliştirilen yüksek yüklemeli aktif çamur (YYAÇ) sistemleri, A/B prosesinde A kademesi olarak tercih edilir ve atıksu arıtma tesislerindeki (AAT) birincil çökeltime bir alternatiftir. Yüksek organik yük ile işletilen YYAÇ prosesi oldukça kısa çamur yaşı ve hidrolik bekletme süresine (HBS) sahiptir. A/B prosesinin B kademesinde ise daha düşük organik yükleme hızlarında biyolojik oksidasyon yoluyla nütrient giderimi hedeflenir.

YYAÇ prosesinin, karbon yakalama ve enerji geri kazanımı açısından KAS ve birincil çökeltim proseslerine göre üstün olduğu bilinmekle beraber, döngüsel ekonomi kapsamındaki su ve maddesel geri kazanım konularında literatür çalışması sınırlıdır. Döngüsel ekonomi, sürdürülebilir üretimi teşvik eden ve ulaşım maliyetlerini ve kaynak ticaretini de azaltarak iklim değişikliğinin etkilerini azaltmayı amaçlayan bir iş modelidir. Bu tez, YYAÇ prosesinin döngüsel ekonomi ilkeleriyle uyumlu bir şekilde sürdürülebilir atıksu arıtımındaki potansiyelini araştırmayı amaçlamaktadır.

Literatürdeki çoğu çalışmada ve tam ölçekli uygulamalarda YYAÇ sistemlerindeki katı-sıvı ayrımı konvansiyonel çökeltim tankları ile sağlanmaktadır. Lamelli çökeltim tankları, konvansiyonel çökeltim tanklarına göre daha küçük alanda daha yüksek verimde katı-sıvı ayrımı sağlayabilmektedir. Bu nedenle YYAÇ prosesinde konvansiyonel yerine lamelli çökeltim tankı tercih edilerek prosesin ayak izi daha da azaltılabilir. Ancak literatürde lamelli çökeltim tankı ile katı-sıvı ayrımı yapan YYAÇ prosesi kapsamlı bir şekilde çalışılmamıştır.

Bu tezde, sürdürülebilir atıksu arıtımında YYAÇ prosesinin potansiyelini beş ayrı alt çalışma ile araştırılmıştır: **Çalışma 1**, lamelli çökeltim tankı bulunan bir YYAÇ prosesi için optimum çalışma koşullarının belirlenmesi; **Çalışma 2**, gelecekteki YYAÇ prosesi uygulamaları için uygulamaya yönelik bir araç sağlamak üzere YYAÇ prosesinin matematiksel modellemesi; **Çalışma 3**, YYAÇ prosesi ve membran

filtrasyonu entegrasyonu ile endüstriler için geri kazanılmış su üretiminin test edilmesi; **Çalışma 4,** YYAÇ prosesinin çıkış suyunun farklı prosesler ile arıtılıp sulama suyu elde edilmesi; ve **Çalışma 5**, YYAÇ prosesinin arıtma performansını ve döngüsel ekonomi kapsamında kaynak döngüselliğini artırmak için SAT çamurunun YYAÇ prosesinde yeniden kullanımının araştırılması. Bahsi geçen araştırma konuları, gerçek kentsel atıksu kullanılarak pilot ve laboratuvar ölçekte incelenmiştir. İstanbul'da tam ölçekli bir ön arıtma tesisinde lamelli çökeltim tankı bulunan pilot ölçekli bir YYAÇ tesisi inşa edilmiştir. Tesis, iki yıl boyunca çeşitli koşullar altında çalıştırılmıştır. Membran filtrasyonu ve kimyasal çökeltimi içeren laboratuvar ölçekli deneyler ise aynı atıksu ön arıtma tesisinden alınan gerçek kentsel atıksu ile gerçekleştirilmiştir.

Çalışma 1 ile lamelli çökeltim tankı içeren pilot ölçekli YYAÇ sistemi için en uygun çalışma koşulları belirlenmiştir. Lamelli çökeltim tankı ile konvansiyonel çökeltim tankına göre daha az yer kaplayarak çıkış suyunda daha düşük konsantrasyonda askıda katı madde (AKM) elde edilmiştir. YYAÇ sisteminin optimum çalışma koşulu, 75 dk'lık HBS ve 0,5 mg/L'lik çözünmüş oksijen (ÇO) konsantrasyonu olarak belirlenmiştir. Bu koşulda, en iyi çıkış kalitesi elde edilmiş ve en yüksek oranda karbon çamur hattına yönlendirilmiştir. Ayrıca en fazla hücre dışı polimerik madde (extracellular polymeric substance (EPS)) üretimi de bu koşulda gözlenmiştir. Çalışma ile HBS'yi azaltmanın biyosorpsiyonu artırdığı ancak çıkış suyundaki kimyasal oksijen ihtiyacı (KOİ)'nı da artırdığı ortaya konmuştur. Düşük ÇO konsantrasyonlarının ise organik madde mineralizasyonunu azalttığı, ancak zayıf flok oluşumuna ve dolayısıyla çıkış suyunda yüksek partiküler KOİ (xKOİ) konsantrasyonuna sebep olduğu bulunmuştur. Daha yüksek ÇO konsantrasyonları KOİ oksidasyonunu artırmış ve çamur hattına yönlendirilen karbon miktarını azaltmıştır. YYAÇ prosesinin çıkış suyundaki azot ve fosfor içeriği bu akımın yeniden kullanımının özellikle tarımsal uygulamalar için faydalı olabileceğini işaret etmektedir.

Atıksu arıtma sistemlerinin matematiksel modellemesi, AAT'lerin tasarımı ve optimizasyonunda çok önemli bir rol oynamaktadır. Modelleme çalışmalarında atıksudaki karbon ve nütrientlerin biyokimyasal dönüşümünü analiz edilerek, sistemin değişen koşullar altındaki performansı tahmin edilir. Mevcut YYAÇ proses modelleri aşırı derecede karmaşık veya adsorpsiyon gibi önemli prosesleri dikkate almayacak kadar basittir. Mevcut modellerde esas olarak karbon giderimine odaklanılmış ve modellerin doğruluğunun değerlendirilmesinde yaygın olarak kullanılan duyarlılık ile belirsizlik analizleri uygulanmamıştır.

Çalışma 2'de, Aktif Çamur Modeli No. 1 ve 3 (AÇM1 ve AÇM3) modifiye edilerek, adsorpsiyon ve depolama proseslerini de içeren uygulamaya yönelik yeni bir YYAÇ modeli oluşturulmuştur. Model, pilot ölçekli YYAÇ tesisinden alınan dinamik veriler ile kalibre edilmiştir. Modelleme çalışması ile maksimum spesifik büyüme hızı (μ), büyüme verimi (Y_H), depolama verimi (Y_{STO}), depolama hızı (k_{STO}), ölüm hızı (b), ve kolay ayrışabilir substrat yarı doygunluk sabiti (K_{S1}) model parametrelerinin YYAÇ sistemi için etkili olduğu ortaya konmuştur. Böylelikle kalibrasyon adımında sadece önemli parametreler kalibre edilmiş ve işlem sadeleştirilmiştir. Kalibre edilen YYAÇ modeli, havalandırma tankındaki AKM konsantrasyonu ile çıkış suyundaki toplam toplam KOİ (tKOİ), çözünmüş KOİ (sKOİ), xKOİ, azot (TN), amonyum azotu (SNH), toplam fosfor (TP), çözünmüş TP (sTP) ve partiküler TP (xTP) konsantrasyonlarını %70'in üzerinde bir verimle oldukça iyi bir şekilde tahmin etmiştir. Ancak belirsizlik analizleri, modelin çıkış suyundaki sKOİ konsantrasyonunu daha yüksek tahmin ettiğini ortaya koymuştur. Ayrıca, belirsizlik analizi ile modelin çıkış suyundaki sTP konsantrasyonu tahminin, pilot ölçekli sistemden elde edilen verilere göre yeterince dinamik olmadığı gösterilmiştir. YYAÇ modeline dahil edilmeyen ama çıkıştaki sTP konsantrasyonunu etkileyebilen bazı atıksu karakterizasyon parametrelerinin buna neden olduğu düşünülmektedir. Bu parametreler, konvansiyonel atıksu karakterizasyon parametreleri olmadığı için modele dahil edilmemiştir. Bir başka neden ise çözünmüş fosforun atıksudaki başka maddelerle birleşerek çökelmesi prosesinin modele dahil edilmemesi olabilir.

YYAÇ prosesi düşük enerji tüketimi ve çıkış suyundaki yüksek azot ve fosfor içeriği ile suyun yeniden kullanımına oldukça uygun olmasına rağmen, az yer kaplayan alternatiflerle suyun geri kazanılması hakkında yapılan çalışma sayısı azdır. **Çalışma 3**'te**,** endüstriyel kullanıma uygun su geri kazanımı için farklı arıtma konfigürasyonları deneysel ve maliyet analizleri ile karşılaştırılmıştır. Endüstriler genelde soğutma kulelerinde, işletme sırasında kaybedilen suyun telafisi için geri kazanılan su tercih etmektedir. Telafi suyunun kalitesi, soğutma kulesinin tasarımına bağlı olarak değişmektedir. Bu çalışmada, evsel atıksu, altı farklı arıtma konfigürasyonu ile arıtılarak soğutma kuleleri için telafi suyu üretimi hedeflenmiştir. Bu kapsamda, gerçek kentsel atıksu, üç farklı ön arıtma (mikrofiltrasyon (MF) ve ultrafiltrasyon (UF) ile direkt membran filtrasyonu (DMF) ve YYAÇ prosesi) ve iki farklı son arıtma alternatifinin (nanofiltrasyon (NF) ve ters ozmos (TO)) kombinasyonları ile arıtılmıştır. NF ve RO membranlarının arıtma performansı, her arıtma konfigürasyonunda geri kazanılan suyun soğutma kulesi telafi suyu için gerekli kalite standartlarını karşılamasını sağlamıştır. Ön arıtma alternatifleri karşılaştırıldığında, YYAÇ prosesinin çıkış suyundaki bulanıklığın, MF ve UF membranları ile DMF prosesine göre daha yüksek olduğu gözlenmiştir. Buna rağmen, maliyet analizi ile YYAÇ+NF konfigürasyonunun 0,38 €/m^3'lük arıtma maliyetiyle en uygun maliyetli arıtmayı sunduğunu ortaya konmuştur. Bunun sebebi DMF prosesinin enerji maliyetinin YYAÇ prosesinin enerji maliyetinden daha yüksek olmasıdır.

Çalışma 4'te, YYAÇ prosesinin çıkış suyundan sulama suyu elde etmek için dört farklı son arıtma alternatifi karşılaştırılmıştır. UF membran filtrasyonu, MF membran filtrasyonu, demir(III) klorür ($FeCl_3$) ve alüminyum sülfat (alum) ile kimyasal çökeltim alternatifleri laboratuvar ölçekli sistemlerde karşılaştırılmıştır, her bir arıtma alternatifi sonunda ultraviyole (UV) dezenfeksiyonu ile patojen giderimi sağlanmıştır. Geri kazanılan su kalitelerini karşılaştırmak için Avrupa Birliği minimum su kalite kriterine uygun bir geri kazanılan su kalite indeksi (GSKİ) kullanılmıştır. GSKİ hesaplarına, tarım için faydalı olan arıtılmış suyun azot ve fosfor içeriği de dahil edilmiştir. Alternatifler arasında yalnızca UF membran filtrasyonu ve ardından UV dezenfeksiyonu ile en iyi kalitede sulama suyu (A Sınıfı) üretilmiştir. Diğer alternatifler ile ise B Sınıfı kalitede sulama suyu elde edilmiştir. Maliyet analizi ile UF+UV alternatifinin en yüksek, $FeCl_3$ ile çökeltim+UV alternatifinin ise en düşük işletme maliyetine sahip olduğu bulunmuştur. Çalışmada hesaplanan birim enerji maliyetleri literatür ile uyumludur. Elde edilen bulgular, YYAÇ çıkış suyunun, KAS prosesi çıkış suyu ile karşılaştırılabilir maliyetlerde sulama suyu üretimi için kullanılabileceğini göstermiştir.

Tam ölçekli YYAÇ proseslerinde koagülant yardımı ile partiküler madde ve fosfor giderimi iyileştirilmekte, ancak bu uygulama işletme maliyetlerini artırmaktadır. Su arıtma tesislerinde (SAT) ham sudaki partikülleri ve kolloidal maddeleri gidermek için çeşitli koagülantlar kullanılmakta ve bunun sonucu olarak inorganik içeriği yüksek çamur oluşmaktadır. Geleneksel olarak, bu çamur düzenli depolama alanlarında bertaraf edilmektedir. Ancak, döngüsel ekonomi modelinin ilkeleriyle uyumlu atıksu arıtma sektöründeki mevcut eğilim, kaynakların yeniden kullanımına odaklanmaktadır. Bu bağlamda, SAT çamurunun, AAT'lerde çeşitli uygulamalar için doğrudan veya dolaylı olarak kullanımı öne çıkmaktadır. Ancak bu çalışmaların çoğu uygulamanın AAT'nin arıtma verimini iyileştirdiğini laboratuvar ölçekli deneylerle göstermiştir ve AAT proses çamurunun anaerobik çürütülebilirliği üzerindeki etkisi genellikle göz ardı edilmiştir.

Çalışma 5 ile SAT çamurunun YYAÇ sisteminde yeniden kullanılmasının arıtma verimi ve enerji geri kazanımı üzerindeki etkisi araştırmıştır. Jar test ile demir ve alum çamurunun YYAÇ prosesine etkisi karşılaştırılmış ve demir çamurunun partiküllerin giderilmesinde daha etkili olduğunu bulunmuştur. Ardından pilot ölçekli YYAÇ sistemine demir çamuru sürekli olarak ilave edilmiştir. SAT çamurunun eklenmesinin, YYAÇ prosesinin havalandırma tankındaki çamurun partikül boyutunu arttırdığı, çökelebilirliğini ve susuzlaştırılabilirliğini iyileştiği gözlenmiştir. Ancak çıkış suyu kalite indeksi (ÇSKİ) hesaplarına göre, SAT çamurunun yeniden kullanımı ile YYAÇ prosesi çıkış suyunda yalnızca %2'lik bir iyileşme olduğu bulunmuştur. Bunun sebebi, YYAÇ proses çamuruna dahil olacak SAT çamuru miktarını sınırlamak için SAT çamuru dozunun minimum tutulmasıdır. Çünkü SAT çamurunun organik içeriği çok düşüktür ve YYAÇ proses çamurundan geri kazanılacak enerji miktarını azaltması beklenir. Biyometan potansiyeli (BMP) testleri ile sınırlı miktarda SAT çamuru ilavesinin bile YYAÇ proses çamurunun BMP'sini azalttığını görülmüştür. Bununla birlikte, maliyet analizi ile SAT çamurunun YYAÇ tesisinde yeniden kullanılmasının, çamur transfer/bertaraf ve atıksu arıtma maliyetleri ile biyogaz üretiminden elde edilen enerji tasarrufunu kapsayan toplam maliyette %11'lik bir azalmaya yol açacağı tahmin edilmiştir. Bu çalışma ile su ve atıksu arıtma tesislerinin entegre edilmesi ve kaynak döngüselliğinin önünde maliyetin bir engel olmadığı ortaya konmuştur.

Bu tez, YYAÇ prosesinin döngüsel ekonomi çerçevesinde enerjiye ek olarak su ve maddesel geri kazanıma katkıda bulunma potansiyelini vurgulamaktadır. Modelin sTP'yi tahmin etmedeki doğruluğunu arttırmak için fosfor çökelmesini simüle edilebilir. Ancak çökelme prosesinin modele tanımlanması, atık su özellikleri hakkında ek veri gerektirecek ve modelin karmaşıklığını artıracaktır. Su ve nütrient geri kazanımı için çeşitli arıtma kombinasyonlarının pilot ölçekte araştırılması daha kapsamlı bir ekonomik analiz yapılmasını sağlayabilir. Bu çalışmada, SAT çamuru YYAÇ prosesine doğrudan ilave edilmiş, bu da arıtma performansında sınırlı bir iyileşme ile sonuçlanmıştır. İleride, SAT çamurundan asidifikasyon gibi yöntemlerle geri kazanılan koagülantların YYAÇ prosesine ilave edilmesi pilot ölçekli olarak çalışılabilir. Böylelikle YYAÇ sistemine dahil olan inert çamur miktarı sınırlanır. Ancak SAT çamurundan koagülant geri kazanımı maliyeti de dikkate alınmalıdır. Böyle bir çalışma, su ve atıksu arıtma tesislerinin entegrasyonu ile maddeler döngüsellik konusuna ışık tutacaktır.

1. INTRODUCTION

1.1 Background and Problem Statement

The conventional activated sludge (CAS) process, widely used for over a century in wastewater treatment, is the most prevalent method globally (Jenkins and Wanner, 2014). However, its low energy efficiency stands as a significant drawback. In CAS treatment plants, only approximately 33% of the energy potential present in wastewater can be recovered (Garrido et al., 2013). Additionally, about 30% of the organic carbon content in wastewater is lost in the form of carbon dioxide (CO_2) (Wan et al., 2016). Another disadvantage of CAS is its substantial footprint requirement. As urban populations grow, so does the volume of wastewater generated, necessitating larger treatment areas. This issue poses a significant challenge in cities like Istanbul, which has a substantial population but limited available space. Consequently, it is crucial to adopt innovative treatment processes that can minimize the footprint while maximizing the capture of organic matter and reducing CO_2 losses. This contemporary approach, known as carbon capture, redirection, or harvesting, aims to divert a significant amount of carbon from wastewater to the sludge line to be used for biogas production in anaerobic digesters (Liu et al., 2019).

The A-stage of the adsorption/bio-oxidation (A/B) process has emerged as a fundamental component in energy-efficient methods for treating wastewater. Its primary objective is redirecting carbon from wastewater to anaerobic sludge digesters for energy generation (Modin et al., 2015). High-rate activated sludge (HRAS) was introduced in the 1980s as the A-stage of the A/B process (Boehnke et al., 1998; Versprille et al., 1985). However, its popularity grew with the start of the energy-neutral treatment concept due to its energy efficiency and minimal spatial requirements. HRAS systems which are modifications of CAS systems serve as an alternative for primary sedimentation in wastewater treatment plants (WWTPs) and are now commonly used to enhance energy recovery from wastewater. The HRAS process comprises a biological reactor and a sedimentation unit. It typically is operated at a high sludge-specific loading rate exceeding 2 g biological oxygen demand (BOD)/g volatile suspended solids (VSS)/d, with a low sludge retention time (SRT) ranging from 0.5 to 4 days, and a relatively short hydraulic retention time (HRT) of 0.5 to 4 hours (Jimenez et al., 2015; Meerburg et al., 2016). In the B-stage, the organic loading rate is lower, and biological oxidation serves as the primary mechanism for pollutant removal (Guven et al., 2019).

In addition to energy recovery, water and chemical reuse plays an important role in ensuring resource circularity. The circular economy is a business model that promotes sustainable production and aims to mitigate the effects of climate change by focusing on economic benefits, including reductions in transportation costs and resource trade (Mannina et al., 2022). However, scientific studies focused on the integration of the HRAS process into water and material circularity are scarce.

After undergoing preliminary treatment, approximately 70% of Istanbul's wastewater is directed to the anoxic part of the Bosporus through deep-sea discharge. While there are plans to enhance the discharge quality by upgrading the existing preliminary wastewater treatment plants (PWWTPs), the main challenge lies in the limited space resulting from dense urbanization in Istanbul. The HRAS process exhibits superior treatment efficiency compared to preliminary treatment methods and offers a smaller footprint than conventional biological treatment, all while ensuring energy efficiency. Moreover, the water and nutrient circularity opportunities of the HRAS process hold the potential to move forward towards the circular economy. So, exploring the HRAS process improvement possibilities in this matter is extremely important for sustainable economic growth.

1.2 Purpose and Scope of the Thesis

This thesis aims to investigate the potential of the HRAS process in sustainable wastewater treatment, aligning it with the principles of the circular economy. To achieve this objective, the thesis is structured to explore the following research topics:

- The optimum operational conditions for the HRAS process with lamella clarifier from the effluent quality and carbon capture point of view
- Mathematical modeling of the HRAS process to provide a practical tool for future HRAS process applications

- Membrane filtration integration with the HRAS process to produce reclaimed water for industrial use
- Post-treatment alternatives for the effluent of the HRAS process for irrigational purposes
- The reuse of water treatment plant (WTP) sludge in the HRAS process to increase the treatment performance and resource circularity

The research topics listed above were explored by pilot and laboratory scale studies with real municipal wastewater. A pilot-scale HRAS plant with lamella clarifier was built in a full-scale PWWTP in Istanbul. The plant was operated for two years under different operational conditions according to the research topic. Membrane filtration and chemical precipitation experiments were conducted with the real municipal wastewater collected from the same PWWTP in laboratory scale.

1.3 Outline of the Thesis

The thesis consists of five chapters listed below:

Chapter 1 serves as the introduction to the HRAS process and problem statement, outlining the aim of the thesis.

Chapter 2 provides a comprehensive review of the literature, focusing on the performance and mechanisms of the HRAS process, modelling studies, and the importance of integrating it with other processes for achieving material circularity and water reuse.

Chapter 3 details the materials and methods employed in this thesis, including information on wastewater characteristics, sludge properties, experimental setups, analytical methods, and modelling approach.

Chapter 4 presents the findings of five individual studies conducted to address the gaps identified in the literature review outlined in Chapter 3. These studies encompass:

- **Study 1:** Optimization of operational conditions for the HRAS process with the implementation of a lamella clarifier.
- **Study 2:** Mathematical modeling of the HRAS process to provide a practical tool for future HRAS process applications.

- **Study 4:** Investigation of the integration of membrane filtration and the HRAS process to produce reclaimed water suitable for industrial use.
- **Study 5:** Exploration of alternative post-treatment options to the HRAS process for producing water suitable for irrigation purposes.
- **Study 3:** Examination of the impact of adding WTP sludge to the HRAS process.

Chapter 5 summarizes the overall conclusions drawn from the studies given in Chapter 4 and highlights the main concluding remarks. Furthermore, it provides insights into potential future research directions and perspectives.

2. LITERATURE REVIEW

2.1 HRAS Process

Theoretically, medium-strength wastewater contains sufficient chemical energy content (1.93 kWh/m^3) (McCarty et al., 2011) to meet the energy requirements of WWTPs (0.3-0.8 kWh/m^3) (Garrido et al., 2013). In the CAS process, the biomass present in the system has two primary functions: oxidizing organics in wastewater to carbon dioxide through aerobic respiration or utilizing them as a carbon source for biomass growth. After the treatment process, when the biomass and treated wastewater are separated in final clarifiers, the organic content within the biomass can be harnessed and utilized in anaerobic digesters. Anaerobic digestion is a process that converts the organic matter in the biomass into biogas, with a methane (CH_4) content typically ranging from 60% to 70% (Appels et al., 2008). This biogas can be further utilized as an energy source for various purposes. The primary clarifiers in WWTPs have an important role in diverting a portion of the organic matter found in the wastewater to the sludge stream, referred to as primary sludge. However, it is important to note that primary clarifiers can only capture around 40% of the organic content present in the wastewater, while the remaining portion escapes to subsequent treatment processes (Wan et al., 2016). Thus, CAS systems can only recover approximately 33% of the energy potential in wastewater and around 30% of the organic carbon content in wastewater is lost as metabolic heat through aerobic respiration (Wan et al., 2016). Therefore, the implementation of up-concentration processes has garnered attention in next-generation WWTPs, allowing for maximized organic carbon capture from wastewater and minimized CO_2 losses (Jenkins and Wanner, 2004).

The HRAS process, which is operated at around 20 times higher organic loading rates (OLR) compared to CAS systems (Versprille et al., 1985), is a carbon capture technology. The HRAS process is an alternative to primary sedimentation and offers higher efficiency in redirecting organics to the sludge stream for anaerobic digestion and subsequent energy production. Approximately 60% of the organics in the wastewater can be successfully directed to the sludge stream in the HRAS process (Guven et al., 2017; Rahman et al., 2019). Notably, studies have shown that the anaerobic digestion of sludge derived from the HRAS process generates around 15% more CH_4 compared to primary sludge (Abdelrahman et al., 2022). This highlights the potential of the HRAS process for enhanced energy recovery from wastewater treatment.

The HRAS process, also known as the A-process, serves as the initial stage of the A/B process (Figure 2.1). Its primary objective is to collect the majority of organics from wastewater without undergoing biological assimilation and reduce the pollution load directed to the B-stage, where residual organic matter and nutrients are removed with sludge withdrawal (Wan et al., 2016; de Graff et al., 2016). Key operational differences between HRAS and CAS systems include parameters such as HRT, SRT, and dissolved oxygen (DO) concentration. HRAS processes are typically operated at high sludge loading rates exceeding 2 g BOD/g VSS/d, low SRTs (1-4 d), and short HRTs (20-90 min) (Jimenez et al., 2015; Meerburg et al., 2016). Keeping the DO concentration below 1 mg/L in the HRAS process limits the mineralization of organic matter present in wastewater, resulting in lower aeration energy consumption compared to CAS systems (Guven et al., 2019).

In a study by Jimenez et al. (2015) investigating the effect of HRT (5 to 60 min) and DO concentration (0.1 to 2 mg/L) on chemical oxygen demand (COD) removal in an HRAS system, it was found that COD removal efficiency decreased when HRT was reduced by less than 30 min. Guven et al. (2017) operated a pilot-scale HRAS system with different HRTs (130, 95, and 60 min) and low DO concentrations (0.3-0.4 mg/L) for municipal wastewater treatment. The optimum HRT of 60 min resulted in the highest COD removal efficiency of 59% and the lowest concentration of total suspended solids (TSS) in the effluent (90 mg/L). Trzcinski et al. (2017) examined the impact of DO concentration on the removal efficiency of soluble COD (sCOD) by increasing DO from 0.2 mg/L to 1 mg/L. They found that sCOD removal efficiency gradually declined when DO concentrations exceeded 0.4 mg/L. The decrease in sCOD removal efficiency was attributed to increased particulate COD (xCOD) hydrolysis rate and floc destruction due to increased shear force.

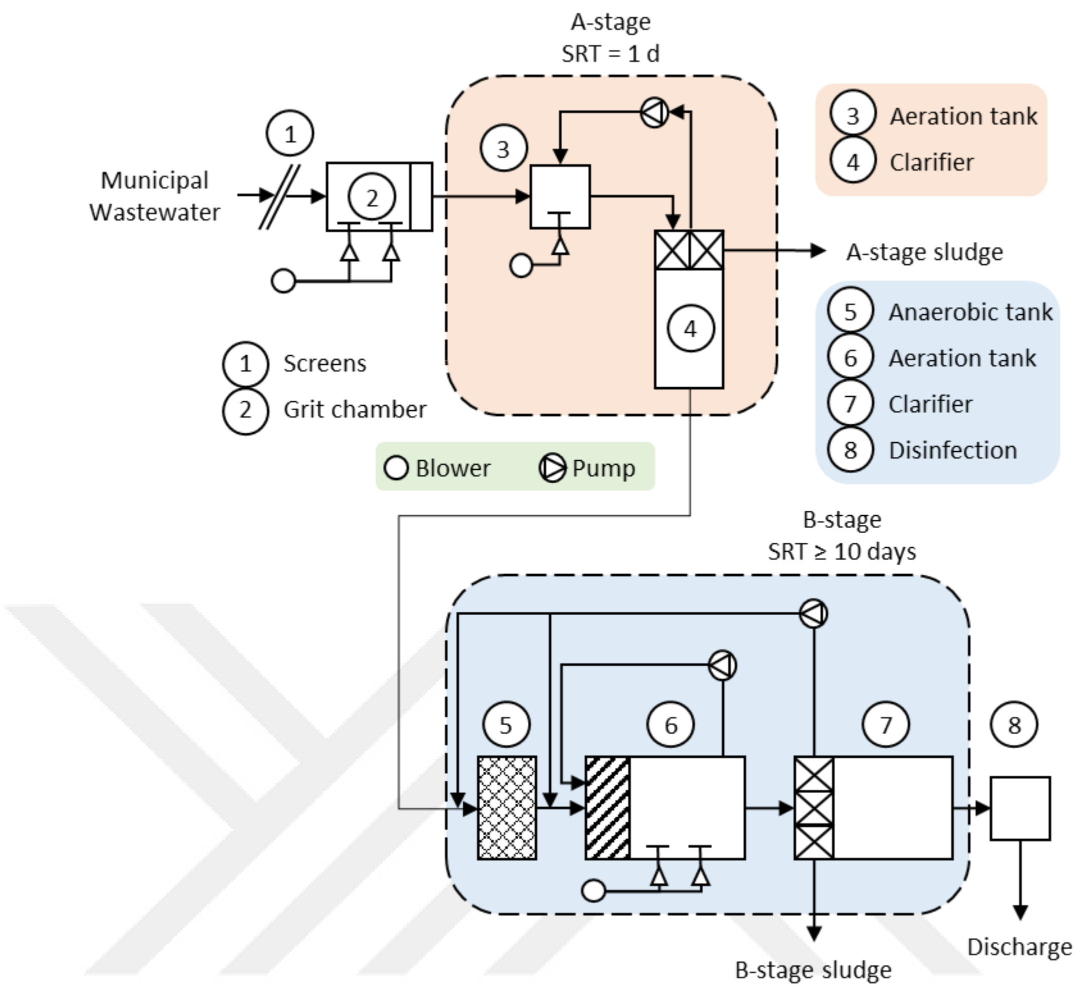

Figure 2.1 : The flow diagram of A/B process.

To reduce the footprint of sedimentation tanks and increase their capacity in WWTPs, lamella clarifiers or tube settlers are recommended. Lamella clarifiers allow higher surface loading rates (SLR) compared to conventional clarifiers, resulting in improved solid separation from wastewater (Kolish and Schirmer, 2004; Fujisaki, 2010). Most studies in the literature have focused on the conventional sedimentation unit within the HRAS process. Cao et al. (2020) compared the treatment performance of a HRAS system with and without aeration in the reactor. Their study found that the condition without aeration yielded higher organic recovery but slightly lower COD removal efficiency.

2.2 Modelling of HRAS Process

Mathematical modelling of activated sludge systems plays a crucial role in the design and optimization of WWTPs. By analyzing the biochemical transformation of substrate and nutrients, these models estimate the system's performance under varying conditions (Gernaey et al., 2004). Complex models like Activated Sludge Model No. 1, 2, and 3 (ASM1, ASM2, and ASM3) are developed based on microbiology and biochemistry knowledge. These three models vary in complexity (Henze et al., 2000). ASM1 simulates the removal of COD and nitrogen (N), in which COD is removed via oxidation and assimilation, and N is removed via nitrification, denitrification, and assimilation. ASM2 is an extension of ASM1 by integrating biological phosphorous (P) removal. ASM3 simulates COD and N removal, taking into consideration the stored polymers in the heterotrophic conversion of organics, unlike ASM1 (Krishna and van Loosdrecht, 1999). However, the ASM family of models does not apply to HRAS systems due to their short SRT and the importance of adsorption and bioflocculation mechanisms (Guven et al., 2019).

Previous studies have attempted to modify existing models to simulate HRAS systems, but they have limitations. Winkler et al. (2001) modified ASM1 and ASM3 to incorporate simultaneous growth on the readily biodegradable substrate and stored substrate in a two-stage WWTP. However, their model lacked the adsorption process, which is crucial for particulate and colloidal matter removal. Karahan et al. (2006) also modified ASM1 and ASM3 similarly to Winkler et al. (2001) but included the adsorption of the slowly biodegradable substrate. Nevertheless, their SRT of 5 days was higher than typical HRAS systems. Makinia et al. (2006) modified ASM3 to account for adsorption and storage capacity in an activated sludge system with a selector reactor. They calibrated their model using steady-state simulations, which may not capture dynamic behavior. Smitshuijzen et al. (2016) added a parameter for particulate substrate adsorption to ASM1, while Nogaj et al. (2015) introduced new state variables to account for various organic compounds. Hauduc et al. (2019) further modified the model of Nogaj et al. (2015) by including fast-growing adsorptive biomass, colloidal biodegradable substrate production, and flocculation/deflocculation processes. However, these model parameters are not commonly measured in WWTPs and increase the model's complexity (Sancho et al., 2019). Additionally, the focus of these modelling studies has been primarily on carbon removal/capture in HRAS systems. Furthermore, sensitivity and uncertainty analyses, which have proven effective for assessing the robustness of activated sludge or membrane bioreactor models in the literature, have not been extensively applied to HRAS system models

(Mannina et al., 2018; Koch et al., 2001; Chen et al., 2012; Sweetapple et al., 2017). These analyses are valuable for identifying influential model parameters and reducing the complexity of model calibration.

2.3 Membrane Filtration Integration with the HRAS Process for Industrial Reuse

The industrial sector accounts for a significant portion of global water withdrawal, with an estimated 3,971 km^3/year in 2020, representing 18% of total global water withdrawal (AQUASTAT, 2020). To address water scarcity issues, one approach is to reduce the industrial water footprint through water reuse. In regions where freshwater resources are limited, industries are treating their wastewater and reusing it within their own facilities (US EPA, 2012). Some countries have also implemented economic incentives to encourage water reuse in industries, and the feasibility of water reuse is influenced by water tariffs set by water authorities (Kehrein et al., 2021). Minimizing the cost of water reclamation is another important aspect of making water reuse economically viable.

The primary method of water reuse in industries is through the use of reclaimed water in cooling towers (US EPA, 2012). Cooling water is lost during the operation, and make-up water is required to replenish these losses (Judd and Jefferson, 2003). The design of cooling towers can vary, and the required quality of cooling water depends on the specific design. Depending on the availability of water resources and the type of cooling tower, facilities may choose to use tap water, surface water, or even seawater as cooling water (Tchobanoglous et al., 2003). Replacing the use of treated seawater or transferring freshwater to industrial facilities with reclaimed water from wastewater for cooling tower operations can be a financially feasible option.

The United States Environmental Protection Agency (US EPA) has provided water quality guidelines for reusing water in cooling towers. These guidelines limit the concentration of TSS to 30 mg/L, BOD to 30 mg/L, fecal coliform to 200 colony forming units (cfu)/100 mL, and pH to a range of 6-9 (US EPA, 2012). However, in the context of cooling towers, concerns related to scaling (caused by calcium (Ca) and silica (SiO_2)) and metallic corrosion (caused by manganese (Mn), iron (Fe), and aluminum (Al)) are important considerations in terms of cooling water quality (Cherchi et al., 2019). Industries should ensure that the quality of the cooling water aligns with their specific cooling tower designs and, if necessary, apply additional treatment to the reclaimed water obtained from domestic/municipal WWTPs.

Membrane filtration, particularly nanofiltration (NF) and reverse osmosis (RO) is commonly used for water reclamation due to their high removal efficiency of particles and pathogens (Kehrein et al., 2021). NF membranes can capture multivalent ions and charged/polar molecules, while RO membranes can capture inorganic ions (Judd and Jefferson, 2003). Depending on the design of the cooling tower, NF or RO membranes can be preferred for producing cooling water from municipal/domestic wastewater. However, the high operational and maintenance costs associated with membrane fouling are reported as significant drawbacks of NF and RO membrane applications, necessitating pre-treatment of the wastewater (Kehrein et al., 2021). Membrane filtration is typically applied as an advanced treatment step following conventional wastewater treatment processes, such as the CAS process. However, the CAS process has a large footprint, high energy consumption, and inadequate energy recovery from wastewater due to the loss of organic matter through oxidation (Hube et al., 2020). To enhance the sustainability of WWTPs, efforts are being made to capture organic matter from wastewater in the process sludge (sewage sludge) and convert it into biogas through anaerobic digestion.

Direct membrane filtration (DMF) aims to achieve carbon capture from wastewater while having smaller footprints, similar to the HRAS process (He et al., 2021). DMF, which involves filtering raw wastewater directly through low-pressure membranes (microfiltration (MF) or ultrafiltration (UF)), has gained popularity due to its small footprint (Nascimento et al., 2018). The main advantage of low-pressure DMF is its high particle capture efficiency, with reported permeate turbidity values as low as 0.15 Nephelometric Turbidity Units (NTU) (Ravazzini et al., 2005), 1.7 NTU (Kim et al., 2007), and even below 1 NTU (Zhao et al., 2019). However, it should be noted that DMF systems have high operational and maintenance costs (He et al., 2021). However, higher particulate matter removal of DMF is an advantage over HRAS since the TSS concentrations in the effluent range from 90 to 120 mg/L and turbidity from 42 to 88 NTU (Guven et al., 2017; Rey-Martinez et al., 2021).

2.4 Post-treatment of HRAS Process Effluent for Irrigational Reuse

The agricultural sector, due to its water-intensive nature, is particularly vulnerable to the impacts of climate change. As a result, the sector is seeking alternative water sources, especially in regions facing or anticipating water scarcity (Chen et al., 2021). Treated wastewater plays a significant role in supplying water and nutrients (N and P) to crops (Ricart and Rico, 2019). Therefore, water reuse in agriculture can help reduce the water footprint and decrease indirect greenhouse gas emissions associated with fertilizer production and transport. Recognizing these benefits, the European Council (EC) issued regulation No. 2020/741, which establishes minimum reclaimed water quality criteria to promote water reuse in Europe (EC, 2020). The regulation defines four classes of reclaimed water quality with varying applicability in agriculture. Class A represents the highest quality and permits the use of reclaimed water on all food crops, including those consumed raw. Class D represents the lowest quality and is limited to industrial, energy, and non-food crops.

To produce reclaimed water of appropriate quality, secondary treatment of wastewater is typically followed by tertiary and/or advanced treatment processes, such as membrane filtration, coagulation, and advanced oxidation (Perez et al., 2022). Membrane filtration, particularly UF, is commonly preferred for water reuse due to its high removal efficiency for particles (>99% TSS removal) and pathogens (5-6 log removal) (Kehrein et al., 2021). Coagulation is another process used to remove particles from secondary effluents. Üstün et al. (2011) observed a TSS removal efficiency of 64% when coagulating secondary effluent with alum. Ultraviolet (UV) irradiation is a physical disinfection process that does not require chemicals and does not produce disinfection by-products. Recent advancements in energy-efficient and cost-effective UV disinfection technologies have further increased their advantages over chemical disinfection methods (US EPA, 2012).

The CAS process is the most commonly used secondary treatment technology preceding tertiary or advanced treatment processes to produce irrigation water (Lazarova et al., 2013). However, the HRAS process, which operates under low DO concentrations of around 1 mg/L, consumes less energy compared to CAS processes (Guven et al., 2019). HRAS also enhances biogas production through anaerobic digestion of the process sludge (He et al., 2021). While nutrient removal in HRAS systems is limited to biomass growth or biosorption, the N and P in treated wastewater can serve as potential resources for agriculture (Cosenza et al., 2022). Therefore, the effluent from the HRAS process may offer advantages over CAS systems in terms of energy-efficient operation and potential nutrient reuse in agriculture.

2.5 Addition of WTP Sludge to HRAS Process

In full-scale HRAS plants, the addition of coagulants can be employed to enhance P removal efficiency, which can reach levels of up to 68%. This approach helps reduce the P load received by the B-stage of the A/B process (de Graaff et al., 2016). However, it is important to note that the use of coagulants increases operational costs (Taboada-Santos et al., 2020).

WTPs typically utilize various coagulants to remove particles and colloids from raw water, resulting in the generation of a significant amount of inorganic sludge. Traditionally, this sludge has been disposed of in landfills (Gitis and Hankins, 2018). However, the current trend in the wastewater treatment sector, aligned with the principles of the circular economy model, focuses on resource reuse (Smol et al., 2020). WTP sludge, containing coagulants, can be regarded as a valuable resource in this context. Incentives such as increasing landfill fees and taxes aim to promote the reuse of treatment sludge (Bolan et al., 2013). Due to its low combustibility and nutritional value, incineration or digestion is not a viable disposal option for WTP sludge (Turner et al., 2019). Consequently, there is a growing interest in researching alternative reuse options for WTP sludge.

One potential option for reusing WTP sludge is its utilization in the production of cement, ceramic materials, or lightweight aggregates (Ahmad et al., 2016). Additionally, WTP sludge can be employed as a substrate in constructed wetlands or utilized as a coagulant in wastewater treatment plants (WWTPs) to facilitate solids removal and improve sludge settleability and dewatering (Guan et al., 2005). These reuse options not only provide a sustainable approach to sludge management but also offer potential benefits in terms of waste reduction, resource recovery, and cost savings.

WTP sludge has been utilized directly or indirectly, with the recovery of chemicals, for various applications in wastewater treatment. Guan et al. (2005) observed that the addition of alum sludge, derived from a WTP using aluminum sulfate ($Al_2(SO_4)_3$ or alum) as a coagulant, improved the removal efficiency of suspended solids (SS) and COD in domestic wastewater. Alum sludge addition increased the SS removal from 52-66% to 72-90% and the COD removal from 28-38% to 43-53%. Furthermore, the settleability and dewaterability of the sludge were enhanced by alum sludge addition. WTP sludge has also proven to be effective in adsorbing heavy metals, particularly lead (Pb), cadmium (Cd), and nickel (Ni) (Abo-El-Enein et al., 2017). Rebosura Jr et al. (2020) investigated the impact of dosing iron-based WTP sludge into a sewer line on the performance of a WWTP. They found that the addition of WTP sludge improved the removal of dissolved sulfur and P without adversely affecting the effluent quality of the WWTP. Nair and Ahammed (2014) indirectly utilized WTP sludge by recovering polyaluminium chloride (PACl) from PACl-based WTP sludge. The recovered PACl was then used for polishing the effluent of an upflow anaerobic sludge blanket reactor. The recovered PACl exhibited high removal efficiencies for COD, turbidity, P, SS, and total coliforms, achieving removal rates of 71%, 80%, 89%, 77%, and 99.5%, respectively. It is important to note that most studies focusing on the reuse of WTP sludge in wastewater treatment have been conducted at the laboratory scale. Furthermore, while the addition of WTP sludge to WWTPs aims to enhance the treatment performance, its effect on the anaerobic digestion of waste sludge in WWTPs has often been overlooked. More importantly, there is no study on how WTP sludge affects the HRAS process performance and energy recovery.

2.6 Overall Evaluation

The HRAS process outperforms CAS and primary sedimentation units in redirecting carbon to the sludge line and generating more CH_4 during anaerobic digestion. However, several areas of improvement have been identified based on existing literature. Firstly, there is a lack of information regarding the performance of HRAS systems with lamella clarifiers, which can enhance sedimentation tank capacity in WWTPs. Secondly, existing mathematical modelling studies of the HRAS process are either overly complex or too simplistic, often neglecting important processes like adsorption and focusing primarily on carbon removal. Additionally, sensitivity and uncertainty analyses, commonly used in assessing the robustness of other models, have not been extensively applied to HRAS system models. Thirdly, despite its potential, there is a lack of literature on integrating the HRAS process into water reclamation practices, which could benefit from its smaller spatial footprint, lower energy consumption, and high nutrient content in the effluent. Lastly, the use of coagulants in the HRAS process increases operational costs but improves phosphorus removal efficiency. However, there is limited research on the impact of reused water treatment plant (WTP) sludge on the anaerobic digestion of waste sludge in WWTPs and its effect on HRAS process performance and energy recovery.

3. MATERIALS AND METHODS

The thesis encompasses five individual studies aimed at addressing the gaps identified in the literature review presented in Chapter 3. The structures of these studies are as follows (Figure 3.1):

- Study 1: The study comprises four distinct stages to compare various operational conditions for the HRAS process.
- Study 2: The HRAS system was operated in two periods for calibration and validation of the HRAS model.
- Study 3: This study evaluated six different treatment configurations to produce industrial water.
- Study 4: Four different post-treatment alternatives were examined in this study for irrigation water production.
- Study 5: The system was operated in two stages to examine the effects of introducing WTP sludge into the HRAS process.

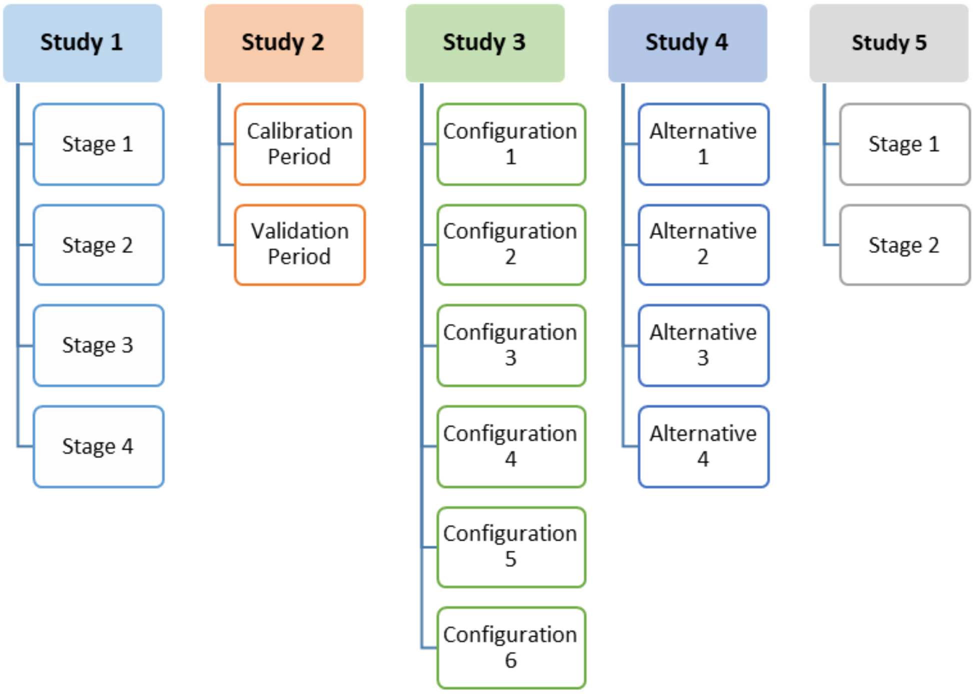

Figure 3.1 : Thesis structure.

3.1 Characteristics of Seed Sludge and Wastewater

3.1.1 Study 1 (Optimization of a Pilot-Scale HRAS Process with Lamella Clarifier)

The HRAS system was initially inoculated with sludge obtained from the RAS line of a full-scale municipal WWTP that implemented biological nutrient removal. The seed sludge used had an average total solids (TS) concentration of 18,388±13 mg/L and a total COD (tCOD) concentration of 13,824±177 mg/L (Table 3.1).

Characteristics of wastewater are given in Table 3.2. The tCOD and sCOD concentrations were in the range of 362-553 mg/L and 98-250 mg/L, respectively. The maximum and minimum concentrations observed during operation period for ammonium nitrogen (NH_4-N) was 55.6 mg/L and 26.1 mg/L, respectively.

Table 3.1 : Characterization of the seed sludge.

Parameter	Unit	Value (Average±SD*)
TS	mg/L	18,388±13
Volatile solids (VS)	mg/L	12,843±3
TSS	mg/L	11,420±20
VSS	mg/L	8568±7
tCOD	mg/L	13,824±177
sCOD	mg/L	209±7
pH	-	6.6±0.01
Capillary suction time (CST)	sec	72.8
Sludge volume index (SVI)	mL/g	103±6
Median particle size (d_{50})	µm	42.29±0.32

* Standard deviation

Table 3.2 : Characterization of the wastewater in Study 1.

Parameter	Unit	Value (Average±SD)	Number of data
TSS	mg/L	284±44	44
tCOD	mg/L	463±53	44
sCOD	mg/L	188±33	44
TN	mg/L	56.3±9.0	20
NH_4-N	mg/L	40.1±8.8	20
TP	mg/L	5.5±0.8	20
pH	-	7.55±0.16	44
Turbidity	NTU	258±43	44

3.1.2 Study 2 (Modelling of High-Rate Activated Sludge Process)

The wastewater characterization is given in Table 3.3 for Study 2. The concentration ranges for TSS and tCOD were 206-219 mg/L and 286-356 mg/L, respectively.

Table 3.3 : Characterization of the wastewater in Study 2.

Parameter	Unit	Value (Average±SD)	Number of data
TSS	mg/L	245±24	56
tCOD	mg/L	317±19	56
sCOD	mg/L	127±18	56
TN	mg/L	59.3±5.9	28
NH_4-N	mg/L	39.0±6.8	28
TP	mg/L	5.2±0.3	28
pH	-	7.63±0.23	56
Turbidity	NTU	238±45	56

3.1.3 Study 3 (Integration of Membrane Filtration and The HRAS Process to Produce Industrial Water)

In Study 3, parameters that are specified in water reuse guidelines for cooling tower make-up water were monitored and wastewater characterization is given in Table 3.4. The average 5 days BOD (BOD_5) to tCOD ratio was 0.52±0.09. The concentrations of tCOD, BOD_5, and TSS, as well as the total and fecal coliform counts in the raw wastewater, indicated that it possessed a medium strength according to the classification by Tchobanoglous et al. (2003). However, certain parameters such as total dissolved solids (TDS), ammonium ion (NH_4^+), chloride (Cl^-), and sulfate (SO_4^{2-}) exceeded the values typically found in medium-strength domestic wastewater (as shown in Table 1, Tchobanoglous et al., 2003). This discrepancy could likely be attributed to the presence of industrial discharges and infiltration of seawater into the sewer system, which ultimately reaches the WWTP. Furthermore, the high conductivity observed in the raw wastewater can also be attributed to the interference of seawater in the sewer lines.

3.1.4 Study 4 (Alternative Post-Treatment Options to The HRAS Process for Producing Irrigation Water)

In Study 4, parameters specified in the minimum water quality criteria for water reuse regulation (EC, regulation no. 2020/741) were monitored in the effluent of the pilot-scale HRAS process and the performances of post-treatment alternatives were explored. Additionally, NH_4-N and ortho-phosphate concentrations were monitored since these nutrients can substitute fertilizers in agriculture. Table 3.5 summarizes the characterization of the pilot-scale HRAS effluent accordingly.

Table 3.4 : Characterization of the wastewater in Study 3.

Parameter	Unit	Value (Average±SD)	Medium-Strength Domestic Wastewater*
TSS	mg/L	268±21	210
TDS	mg/L	4,039±55	500
tCOD	mg/L	412±8	430
BOD_5	mg/L	213±15	190
Turbidity	NTU	245±24	-
Total coliform	cfu/100 mL	$2.81\times10^8\pm1.79\times10^8$	10^7-10^9
Fecal coliform	cfu/100 mL	$22.8\times10^6\pm6.30\times10^6$	10^4-10^6
Total hardness	mg calcium carbonate ($CaCO_3$)/L	828±28	-
Ca hardness	mg $CaCO_3$/L	208±8	-
Alkalinity	mg $CaCO_3$/L	769±210	60-120
Conductivity	µS/cm	6,280±405	-
pH	-	7.5±0.1	-
Cl^-	mg/L	3,109±24	20-50
SO_4^{2-}	mg/L	607±200	15-30
NH_4^+	mg/L	89±3	25**
Fe	mg/L	0.278±0.120	-
Mn	mg/L	0.069±0.053	0.2-0.4
Al	mg/L	0.080±0.003	0.1-0.2
Si	mg/L	3.910±0.259	-

* Tchobanoglous et al. (2003)
** 25 mg/L as NH_4-N. Its NH_4^+ equivalent is 25×1.2878=32 mg/L.

Table 3.5 : Characterization of the effluent of pilot-scale HRAS process in Study 4.

Parameter	Unit	Value (Average±SD)
TSS	mg/L	46±4
BOD_5	mg/L	120±3
Turbidity	NTU	40±2
Escherichia coli (*e. coli*)	cfu/100 mL	$3.0\times10^6\pm1.2\times10^6$
pH	-	7.35±0.4
NH_4-N	mg/L	31.2±5.4
PO_4-P	mg/L	1.2±0.4

3.1.5 Study 5 (Examination of The Impact of Adding WTP Sludge to The HRAS Process)

Wastewater characteristics are given in Table 3.6 for Study 5. TN and TP were in the range of 50.0-61.0 mg/L and 4.3-5.2 mg/L, respectively.

Table 3.6 : Characterization of the wastewater in Study 5.

Parameter	Unit	Value (Average±SD)	Number of data
TSS	mg/L	243±23	22
tCOD	mg/L	343±25	22
sCOD	mg/L	143±16	22
TN	mg/L	57.2±3.9	12
NH_4-N	mg/L	37.4±3.3	12
TP	mg/L	4.9±0.3	12
pH	-	7.28±0.07	22
Turbidity	NTU	221±48	22

3.2 Experimental Set-ups

3.2.1 Study 1 (Optimization of a Pilot-Scale HRAS Process with Lamella Clarifier)

The pilot-scale HRAS system was equipped with several components, including a feeding tank, an aeration tank, a lamella clarifier, and various electromechanical instruments (Figure 3.2). The wastewater from the effluent of an aerated grit chamber unit of a full-scale WWTP was fed to the feeding tank via a wastewater pump ((Masdaf, Türkiye)). The feeding tank had a volume of 2 m^3, contained a mixer and a feeding pump (Masdaf, Türkiye). The aeration tank had a volume of 4 m^3 and was equipped with TSS (S40-SWW Quadbeam, New Zealand), pH (Zirkon 203072100, Kuntze Instrument, Germany), and DO and temperature (OPTOD Aqualabo, France) probes for real-time monitoring. The DO concentration in the aeration tank was controlled using an on-off control strategy, with minimum and maximum DO values set and an offset value of 0.2 mg/L to maintain the desired average DO concentration. The lamella clarifier had a volume of 4 m^3 and a surface area of 2.3 m^2. The clarifier included lamella plates arranged at a 60-degree angle with a 10 cm gap between each plate. Part of the sludge collected from the bottom of the clarifier was recirculated to the head of the aeration tank via return activated sludge (RAS) pump (Seepex, Germany), while the remaining sludge was removed from the system via waste activated sludge (WAS) pump (Seepex, Germany). Electromagnetic flow meters were used to measure the flow rates of the influent and sludge streams. The pilot-scale plant was connected to a computer running Supervisory Control and Data Acquisition (SCADA) software, which allowed for remote access. Sludge pumps, SCADA, and office space were located inside a container near the HRAS system (Figure 3.3).

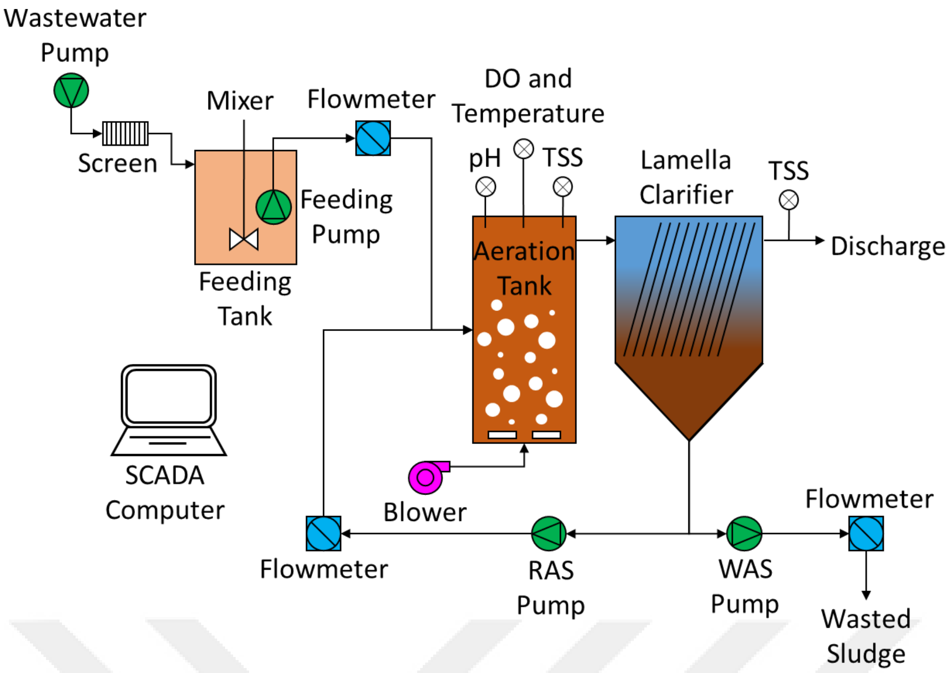

Figure 3.2 : The flow scheme of the pilot-scale HRAS process.

Figure 3.3 : Pictures of the pilot-scale HRAS plant.

3.2.2 Study 2 (Modelling of High-Rate Activated Sludge Process)

The data to calibrate and validate the HRAS model was collected from the pilot-scale HRAS plant described in section 3.2.1.

3.2.3 Study 3 (Integration of Membrane Filtration and The HRAS Process to Produce Industrial Water)

In Study 3, the effluent of HRAS process was collected from the configuration given in Figure 3.2 while a laboratory-scale cross-flow membrane filtration system was utilized for membrane filtration experiments (Figure 3.4). This system consisted of various components, including a feeding tank, cartridge filter, feeding pump, membrane filtration cell, permeate tank, pressure sensor, and computer for data collection. Before entering the filtration system, the wastewater is pre-filtrated using a cartridge filter with a pore size of 100 µm (Aquafer, Turkey) to remove large particles and protect the instruments. The filtration experiments were conducted in batches, and each experiment concluded when the permeate volume reached the desired recovery rate. The effective membrane area used in the experiments was 140 cm^2. The permeate, which passed through the membrane, was collected in the permeate tank, and its quantity was measured, while the concentrate flow was recirculated back to the feeding tank.

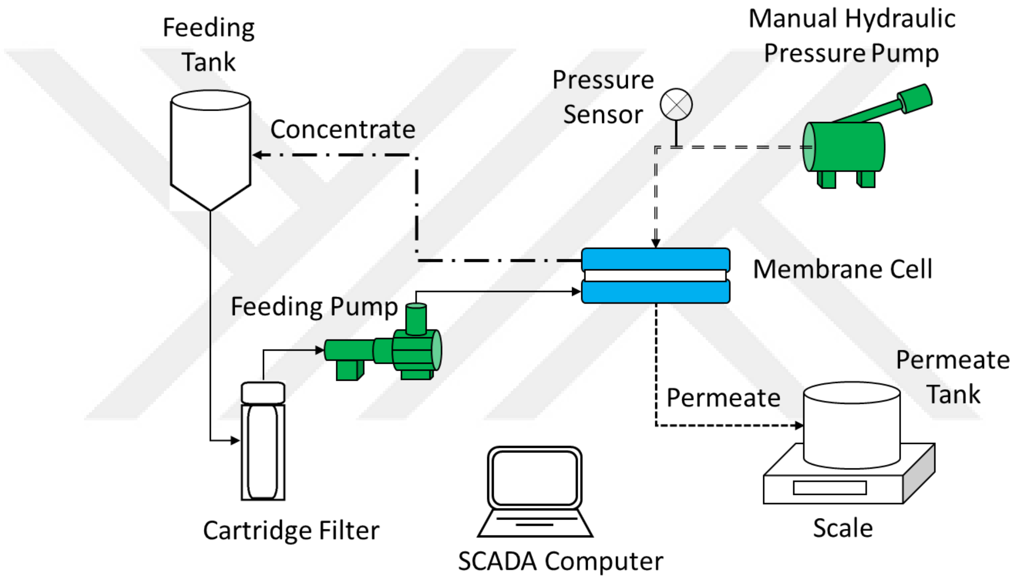

Figure 3.4 : The flow diagram of the laboratory-scale membrane filtration system.

3.2.4 Study 4 (Alternative Post-Treatment Options to The HRAS Process for Producing Irrigation Water)

The effluent of HRAS process was collected from the configuration given in section 3.2.1 and the membrane filtration experiments were conducted with the laboratory-scale membrane filtration system described in Figure 3.4.

3.2.5 Study 5 (Examination of The Impact of Adding WTP Sludge to The HRAS Process)

In Study 5, the pilot-scale HRAS process was modified to have a continuous feeding of WTP sludge to the aeration tank (Figure 3.5). The WTP sludge was mixed with tap water in the WTP sludge feeding tank to have desired solid content and a peristaltic pump (Longer Pump, USA) was used to dose the WTP sludge.

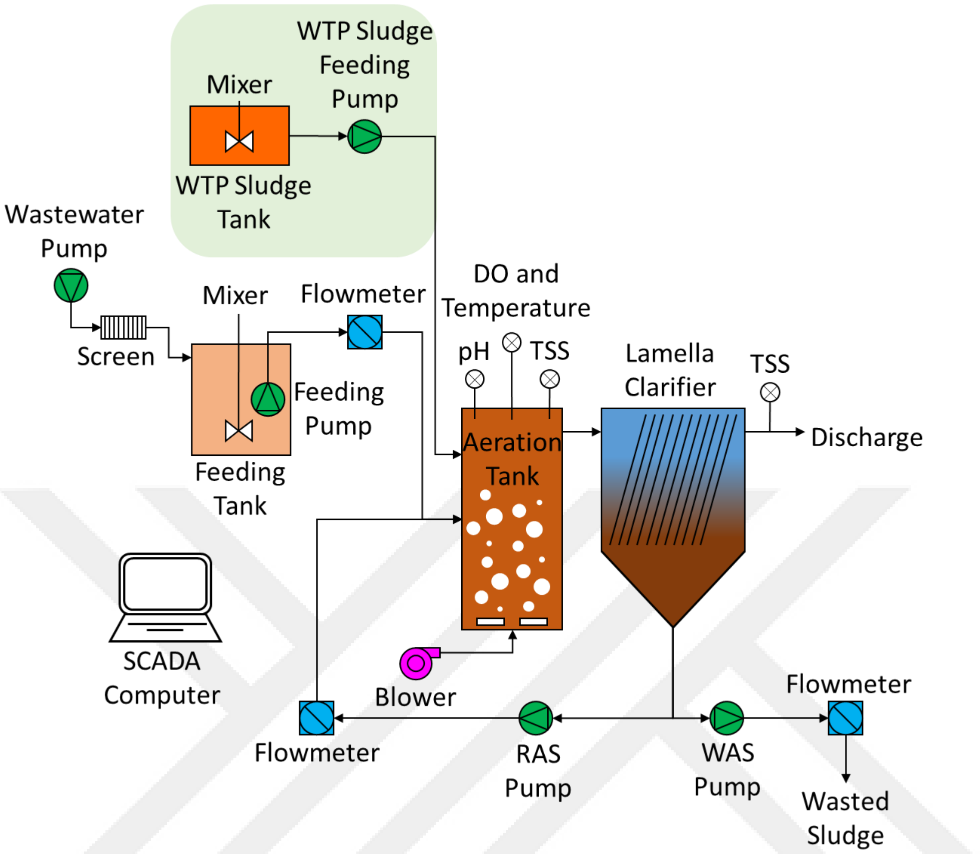

Figure 3.5 : The flow diagram of the modified pilot-scale HRAS process.

3.3 Experimental Procedures

3.3.1 Study 1 (Optimization of a Pilot-Scale HRAS Process with Lamella Clarifier)

The influence of HRT and DO on the performance of the HRAS process was examined across four stages, as outlined in Figure 3.6. The evaluation of performance at each stage encompassed assessing effluent quality and the fraction of captured organics in the WAS. Initially, two HRT values of 75 minutes and 50 minutes were tested at Stage 1 and Stage 2, respectively, while maintaining a constant DO concentration of 0.5 mg/L. The influent flow rates for Stage 1 and Stage 2 were 75 m^3/day and 115 m^3/day, respectively. Based on the results obtained, the HRT that yielded superior effluent quality and higher carbon capture was selected. At this selected HRT, DO concentrations of 0.2 mg/L and 0.8 mg/L were then tested at Stage 3 and Stage 4, respectively, with an influent flow rate of 75 m^3/day for both stages. The SRT calculations took into consideration the solids present in both the effluent and waste sludge. The SRT of the system was maintained at 0.5±0.1 days, and the ratio of the RAS flow rate to the influent flow rate was fixed at 25% throughout the study. The SLR of the lamella clarifier, based on the tank surface area, was approximately 35 $m^3/d/m^2$ in stages 1, 3, and 4, while it was 51 $m^3/d/m^2$ in Stage 2.

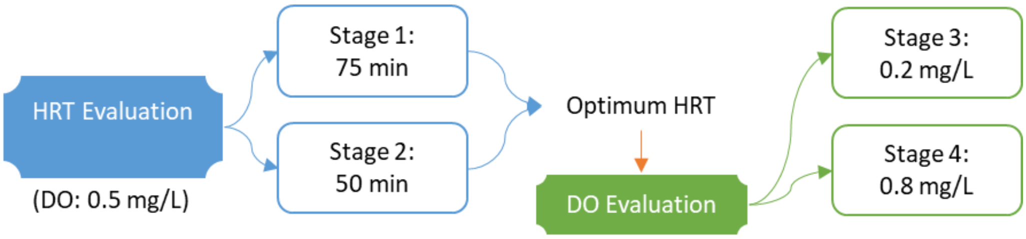

Figure 3.6 : The operational plan of Study 1.

3.3.2 Study 2 (Modelling of High-Rate Activated Sludge Process)

The pilot-scale HRAS plant was operated with a HRT of 75 minutes and a SRT of 0.5 days. The concentration of DO was kept at 0.5 mg/L and mixed liquor suspended solids (MLSS) concentrations between 2000-3000 mg/L. The ratio of the RAS flowrate to the influent flowrate was maintained at 0.25. The system was operated 46 days in for calibration period and 45 days for validation period.

3.3.3 Study 3 (Integration of Membrane Filtration and The HRAS Process to Produce Industrial Water)

This study comprised six different treatment configurations, each consisting of a combination of various pre-treatment and final-treatment options (Figure 3.7). The pre-treatment options included DMF via MF, DMF via UF, and HRAS process. The final treatment options were filtration via NF and filtration via RO.

DMF via MF and UF were operated at a constant transmembrane pressure (TMP) of 2 and 2.5 bar, respectively. The recovery rates, which represent the permeate flowrate to feed flowrate ratio, for MF and UF membranes were set to 0.9.

The pilot-scale HRAS plant was operated with the operational conditions given in section 3.2.2.

NF and RO membrane filtrations were also operated at a constant TMP of 10 and 15 bar, respectively, while the recovery rate for each of them was maintained at 0.5.

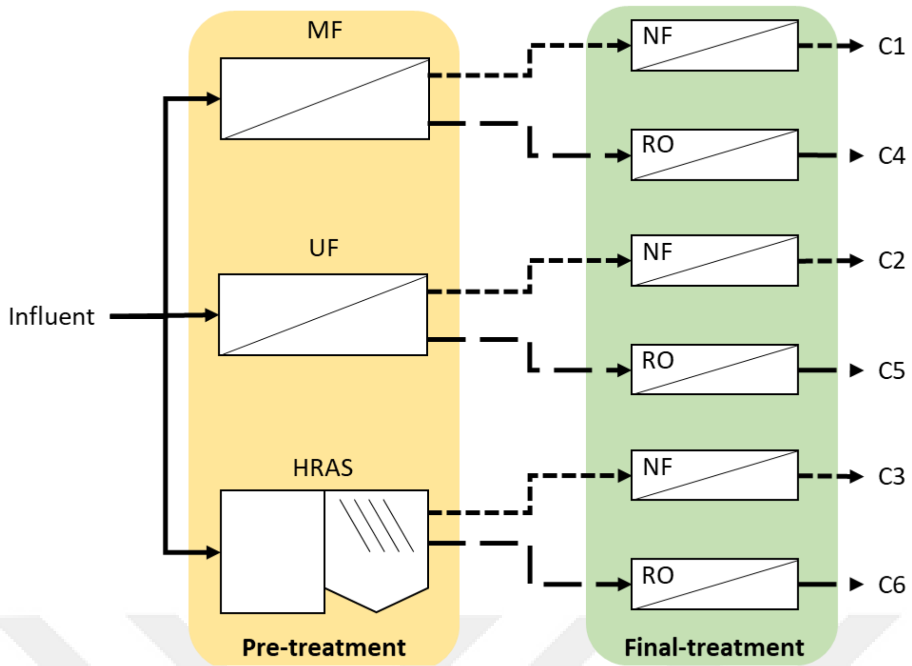

Figure 3.7 : Treatment configurations in Study 3.

3.3.4 Study 4 (Alternative Post-Treatment Options to The HRAS Process for Producing Irrigation Water)

Figure 3.8 summarizes post-treatment alternative in Study 4. The pilot-scale HRAS plant was operated using the operational conditions specified in section 3.2.2. MF and UF membrane filtrations were conducted as stated in section 3.2.3. The coagulation tests were conducted using jar tests. Different doses of coagulants were tested, including 10 mg/L, 30 mg/L, and 50 mg/L for iron(III) chloride ($FeCl_3$), and 30 mg/L, 90 mg/L, and 150 mg/L for alum.

After the membrane filtration process, the permeates from the MF and UF membranes, as well as the supernatants from the $FeCl_3$ and alum coagulation, underwent UV disinfection. The UV disinfection unit used had an active reactor volume of 2.5 L and a power capacity of 20 W (Ao Smith-Purfect 06, United States of America (USA)). The unit was operated with a feeding time of 9 minutes and a discharge time of 1.5 minutes. The selected UV dose for disinfection was 10 mW s/cm^2.

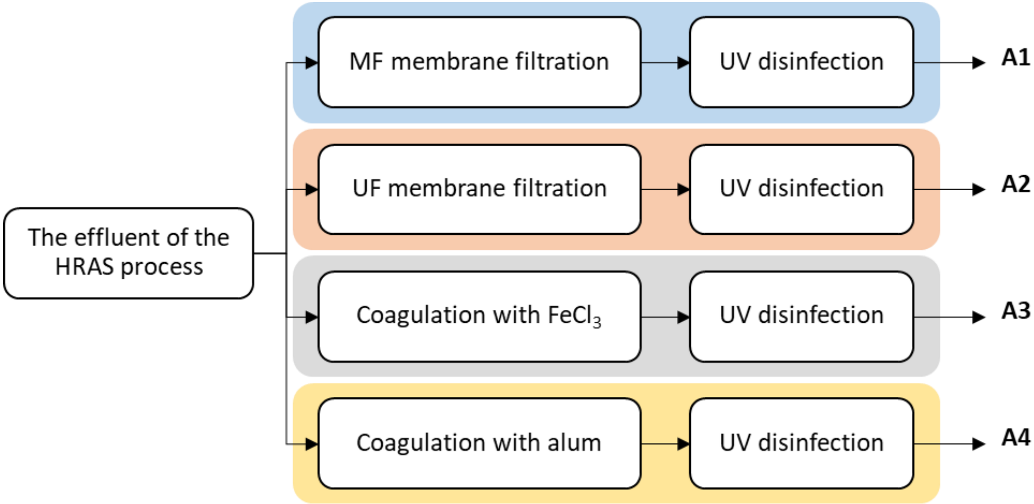

Figure 3.8 : Post-treatment alternatives in Study 4.

3.3.5 Study 5 (Examination of The Impact of Adding WTP Sludge to The HRAS Process)

At Stage 1 of Study 5, the pilot-scale HRAS process was operated without the addition of WTP sludge to the aeration tank. However, in Stage 2, the system was operated with the addition of WTP sludge. The operation of the HRAS process followed the procedures described in section 3.2.3.

Before Stage 2 of Study 5, in laboratory-scale experiments, two different WTP sludges obtained from different sources were compared. Jar tests were performed to assess the impact of iron sludge and alum sludge on the removal efficiency of TSS, COD, and TP parameters.

During Stage 2, the flow rate of the selected WTP sludge was maintained at 40 mL/min, and the dosage was 20.1±1.6 mg of dry matter/L of wastewater. The primary objective of the HRAS process was to recover energy through the digestion of waste sludge. Consequently, the addition of WTP sludge was kept relatively low during Stage 2 to minimize the introduction of inorganic content from the WTP sludge into the HRAS process sludge.

3.4 Model Development

3.4.1 Definition and assumptions

Figure 3.9 provides an overview of the HRAS model developed in Study 2, which is a modified version of the combination of ASM1 and ASM3. The model focuses on the processes conducted by heterotrophic microorganisms, assuming them to be the dominant microorganisms in the biomass. To simplify the model, the anoxic growth of heterotrophs was excluded since the HRAS system operates as an aerated system. Model continuity was verified following the method proposed by Hauduc et al. (2010).

Table 3.7 compares the features of the HRAS model with previous models that served as inspiration, such as those developed by Smitshuijzen et al. (2016) and Hauduc et al. (2019). The HRAS model includes six processes: growth on readily biodegradable organics, growth on stored organics, storage of readily biodegradable organics, adsorption of colloidal organics on slowly biodegradable organics, decay, and hydrolysis of slowly biodegradable organics. The stoichiometric matrix and process rates for the HRAS model are presented in Table 3.8 and Table 3.9, respectively.

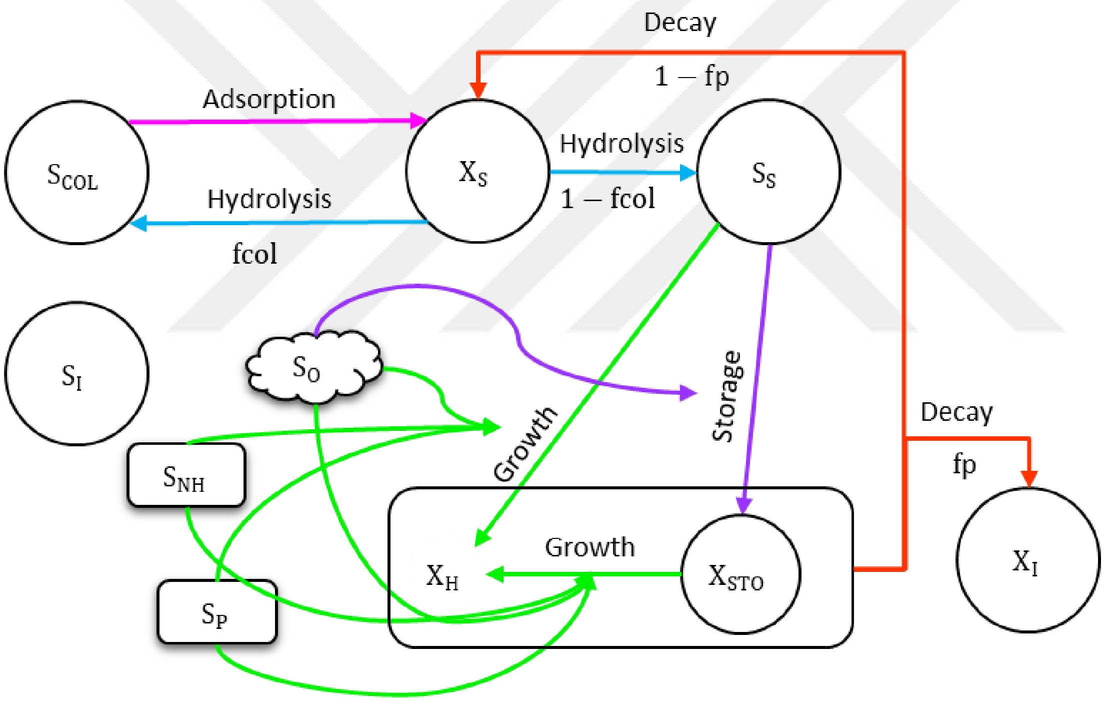

Figure 3.9 : The schematic overview of the HRAS model.

In the model, colloidal organic (S_{COL}) is present in the wastewater and is produced during the hydrolysis of slowly biodegradable organics (X_S), along with readily biodegradable organics (S_S). The parameter fcol determines the fraction of produced colloidal organic after the hydrolysis of X_S. It is assumed that S_{COL} is adsorbed onto X_S without requiring energy (Makinia et al., 2006).

While ASM3 defines the storage process as an energy-requiring process where growth occurs only over the stored substrate (X_{STO}) (Henze et al., 2000), the HRAS model assumes that growth can happen simultaneously on both X_{STO} and S_S. Two half-saturation coefficients, K_{S1} and K_{S2}, are defined in the HRAS model to represent the half-saturation constants for growth and storage on S_S, respectively. The growth rates for direct growth on S_S and growth on X_{STO} are kept the same. However, a switching function ($K_{S1}/(S_S+K_{S1})$) is implemented for growth on X_{STO} to dominate over direct growth, favoring the storage of S_S (Karahan et al., 2006).

In the HRAS model, biomass decay (X_B) is assumed to generate particulates, including X_S and inert particulate organics (X_I). The fraction f_p determines the proportion of generated X_I. X_I can be present in the influent wastewater or produced during decay, and it leaves the system through the excess sludge. The soluble inert fraction (S_I) in the influent wastewater, however, exits the system through the effluent without undergoing any change.

Table 3.7 : The HRAS model with comparison to inspired previous models.

Model features	ASM1	ASM3	Karahan et al. (2006)	Makinia et al. (2006)	Smitshuijzen et al. (2016)	Hauduc et al. (2019)	This study
Mono soluble readily substrate	X	X	X	X	X		X
Dual soluble readily substrate						X	
Sequential storage and growth		X					
Parallel storage and growth			X	X	X	X	X
Mono heterotrophic biomass	X	X	X	X	X		X
Dual heterotrophic biomass						X	
Decay	X				X	X	X
Endogenous respiration		X	X	X			
Adsorption			X	X			X

Due to the low SRT in the HRAS system, S_S in the influent wastewater are not completely consumed. As a result, the sCOD concentration in the effluent of the HRAS system is the sum of the S_I and the remaining S_S. In some modelling studies of HRAS systems, the S_S in the influent is divided into two fractions: monomers (representing the portion used in the HRAS process) and polymers (representing the remaining S_S at the end of the HRAS process) (Nogaj et al., 2015; Hauduc et al., 2019). However, in this study, the dual fraction approach for SS was not employed to maintain model simplicity.

Table 3.8 : The matrix for the HRAS model.

	Component → Process ↓	S_I	S_S	S_{COL}	X_S	X_I	X_{STO}	X_B	S_{NH}	S_P	S_O	S_{ALK}
1	Growth on readily biodegradable organics		$-\frac{1}{Y_H}$					1	$-i_{NXB}$	$-i_{PXB}$	$-\frac{1-Y_H}{Y_H}$	$(-i_{NXB}) \times i_{charge_{NH}} + (-i_{XBP}) \times i_{charge_{PO}}$
2	Growth on stored organics						$-\frac{1}{Y_H}$	1	$-i_{NXB}$	$-i_{PXB}$	$-\frac{1-Y_H}{Y_H}$	$(-i_{NXB}) \times i_{charge_{NH}} + (-i_{XBP}) \times i_{charge_{PO}}$
3	Storage of readily biodegradable organics		-1				Y_{STO}				$-(1 - Y_{STO})$	
4	Adsorption of colloids on particulates			-1	1							
5	Decay				$1 - f_p$	f_p		-1	$-f_p \times i_{NXI} - (1-f_p) \times i_{NXS} + i_{NXB}$	$-f_p \times i_{PXI} - (1-f_p) \times i_{PXS} + i_{PXB}$		
6	Hydrolysis		$1 - f_{col}$	f_{col}	-1				i_{NXS}	i_{PXS}		$i_{NXS} \times i_{charge_{NH}} + i_{PXS} \times i_{charge_{PO}}$

Table 3.9 : Process rates of the HRAS model.

	Process	Process Rate ($M / L^3 T^1$)
1	Growth on readily biodegradable organics	$\mu \times \left(\frac{S_O}{K_O+S_O}\right) \times \left(\frac{S_S}{K_{S1}+S_S}\right) \times \left(\frac{S_{NH}}{K_{NH}+S_{NH}}\right) \times \left(\frac{S_P}{K_{SP}+S_P}\right) * X_B$
2	Growth on stored organics	$\mu \times \left(\frac{S_O}{K_O+S_O}\right) \times \left(\frac{X_{STO}}{K_{X_{STO}}+X_{STO}}\right) \times \left(\frac{S_{NH}}{K_{NH}+S_{NH}}\right) \times \left(\frac{S_P}{K_{SP}+S_P}\right) \times \left(\frac{K_{S1}}{K_{S1}+S_S}\right) \times X_B$
3	Storage of readily biodegradable organics	$k_{STO} \times \left(\frac{S_O}{S_O+K_O}\right) \times \left(\frac{S_S}{K_{S2}+S_S}\right) \times X_B$
4	Adsorption of colloids on particulates	$k_{ADS} \times S_{COL}$
5	Decay	$b \times X_B$
6	Hydrolysis	$k_H \times \left(\frac{X_S/X_B}{K_{XS}+X_S/X_B}\right) \times X_B$

In the HRAS model, the ratio of S_I to tCOD was assumed to be 0.08, which falls within the typical range of 0.06-0.10 for municipal wastewater after primary treatment (Orhon and Artan, 1994). The concentration of S_S was calculated by subtracting S_I from the sCOD. The concentration of xCOD was considered to be the sum of the X_S and the X_I. The fraction of X_I in TCOD was assumed to be 0.13, which is typically between 0.08-0.13 for primarily treated municipal wastewater (Orhon and Artan, 1994).

The SRT of the HRAS system was defined to include the TSS removed by excess sludge (WAS), along with the TSS exiting the system through the effluent. The calculation of SRT is represented by equation 3.1 as proposed by Smitshuijzen et al., (2016). Where X_{MLSS} is the MLSS concentration in the A reactor, X_{EFF} is the TSS concentrations in the effluent X_{WAS} is the TSS concentrations in the excess sludge, $V_{reactor}$ is the volume of the A reactor, Q_{inf} and Q_{WAS} are the influent and WAS flowrates, respectively.

$$\mathrm{SRT} = \frac{X_{MLSS} \times V_{reactor}}{(Q_{WAS} \times X_{WAS}) + ((Q_{inf} - Q_{WAS}) \times X_{eff})} \tag{3.1}$$

3.4.2 Model calibration

Simulations of the HRAS system were performed using the GPS-X 6.5.1 software developed by Hydromantis in Canada. The "Model Developer" tool provided in the software was utilized to construct the HRAS model based on the model matrix specified in Table 3.8. For the clarifier model, the one-direction nonreactive "simple1d" model available in GPS-X was chosen, and the use of lamella was enabled in the model configuration.

Operational data from 91 days of the pilot-scale HRAS plant was employed for the simulations. The first 46 days of data were used for model calibration, while the remaining 45 days were used for model validation. Various input parameters were considered for the dynamic simulations, including flow rates, measured characterization parameters, the temperature of the liquid and environment, DO concentration in the reactor, and SVI of the sludge.

The calibration of the HRAS model followed a systematic procedure outlined in Figure 3.10. First, representative model outputs were identified based on the data collected from the pilot-scale HRAS system (Step 1). These outputs served as reference points for the calibration process. Next, a manual calibration approach was employed to adjust the model parameters (Step 2). This process involved iteratively modifying the parameters to achieve a better fit between the model outputs and the observed data. Process engineering knowledge and expertise were used to guide the parameter adjustment process. To perform sensitivity analysis, the range of each model parameter was defined based on the work of Fortela et al. (2019), and delta values were calculated to generate 100 different values within each parameter range (Step 3.1). Subsequently, simulations were conducted for each parameter by selecting the "Analyze Mode" with "Time Dynamic" in the software (Step 3.2). This allowed for the evaluation of the model's sensitivity to variations in each parameter. Sensitivity indexes (Si) were calculated for all model parameters for each model output using the methods described by Mannina et al. (2011) (Step 3.3). Likelihood measurements were first computed for each parameter using equations 3.2, 3.3, and 3.4, and then sensitivity indexes were determined using equation 3.5. Where $L(\theta_i/Y_j)$ is the likelihood for the jth model output of the ith model parameter, θ_i is the ith set of model parameters, $\sigma^2_{M_j-O_j}$ is the sum of squared errors between model outputs and observation, $\sigma^2_{O_j}$ is the sum of squared errors between observation and the average value of the observations, $M_{j,i}$ is the model output of the jth model parameter, $O_{j,i}$ is the observation of the jth model parameter, and $\overline{O_j}$ is the average value of the observation of the jth model output. $S_{i,j}$ is the S_i for the jth model output of the ith model parameter, $L(\theta_i/Y_j)_{max,j}$ is the maximum likelihood for the jth model output of the ith model parameter, $L(\theta_i/Y_j)_{min,j}$ is the minimum likelihood for the jth model output of the ith model parameter, and $L(\theta_i/Y_j)_j$ is the average likelihood for the jth model output of the ith model parameter. $K_{max,j}$, $K_{min,j}$, and K_j is the maximum, minimum and average value of the jth model output, respectively. The model efficiency, E_i, was calculated using equation 3.6. Where α_j is the normalizing constant that represents the weight of the jth model output and calculated according to equation 3.7.

These sensitivity indexes were then scaled to the maximum sensitivity index value and sorted in descending order. To identify influential model parameters, a threshold value of 0.25 was used. If the sensitivity index value for a parameter exceeded this threshold, it was considered to have a significant influence on the model outputs. By following this calibration procedure, the HRAS model was refined and adjusted to better represent the behavior of the pilot-scale HRAS system and capture the observed data.

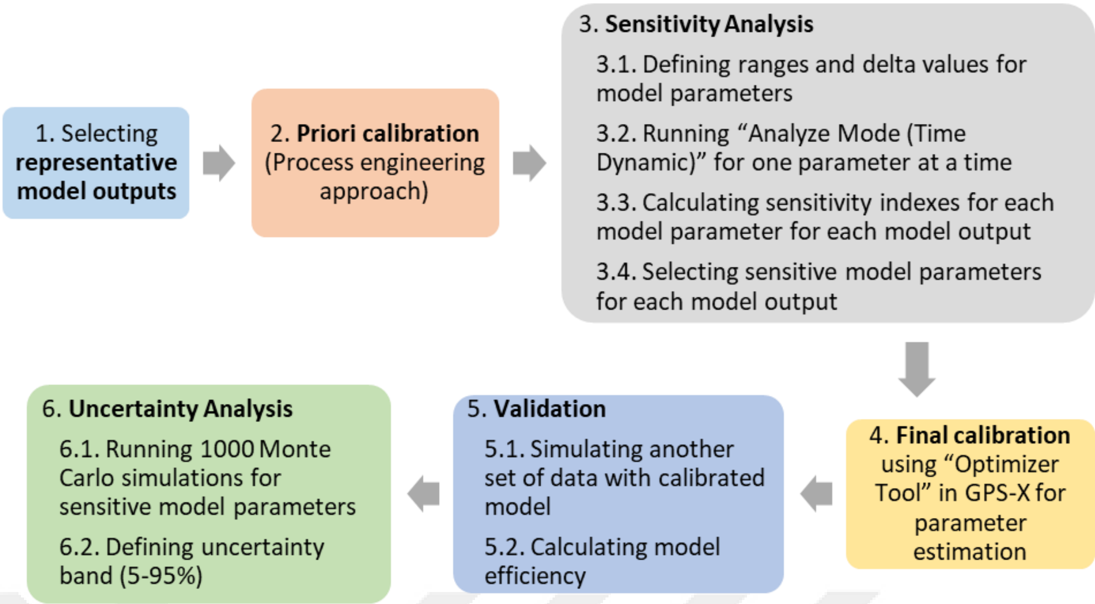

Figure 3.10 : Model calibration protocol.

$$L(\theta_i/Y_j) = \exp\left(\frac{-\sigma^2_{M_j-O_j}}{\sigma^2_{O_j}}\right) \tag{3.2}$$

$$\sigma^2_{M_j-O_j} = \Sigma_i^K\left(M_{j,i} - O_{j,i}\right)^2 \tag{3.3}$$

$$\sigma^2_{O_j} = \Sigma_i^K\left(O_{j,i} - \bar{O}_j\right)^2 \tag{3.4}$$

$$S_{i,j} = \left|\frac{\left(L(\theta_i/Y_j)_{max,j} - L(\theta_i/Y_j)_{min,j}\right)/L(\theta_i/Y_j)_j}{(K_{max,j} - K_{min,j})/K_j}\right| \tag{3.5}$$

$$E_i = \Sigma_j^n \propto_j L(\theta_i/Y_j)_{max,j} \tag{3.6}$$

$$\propto_j = \frac{L(\theta_i/Y_j)_{max,j}}{\Sigma_j^n L(\theta_i/Y_j)_{max,j}} \tag{3.7}$$

In the final calibration step (Step 4), influential model parameter values were estimated using the "Optimizer Tool" in the GPS-X software, utilizing the maximum likelihood function. The model outputs were grouped and prioritized based on their relevance to TSS, COD, N, and P parameters, following the approach described by Mannina et al. (2011).

After the final calibration, the model was validated using a different dataset in Step 5.1. The efficiency of the model was assessed using mean absolute error (MAE) and root mean squared error (RMSE) metrics. These metrics provided quantitative measures of how well the calibrated model could simulate the observed data.

To assess the uncertainty of the model, a Monte Carlo simulation approach was employed in Step 6, following the methodology outlined by Mannina et al. (2012). The range of sensitive parameters, as determined in Step 3.1, was utilized to generate 1000 sets of randomly sampled parameter values from a uniform distribution. Each set of parameter values was used to run a simulation, and the cumulative likelihood of the selected model outputs was calculated for each Monte Carlo simulation. The 5th and 95th percentiles of the cumulative likelihood distribution were then used to define the uncertainty band, providing an estimation of the model's uncertainty.

By completing these steps, the HRAS model underwent a comprehensive calibration, validation, and uncertainty analysis process, allowing for a more accurate representation of the pilot-scale HRAS system and an assessment of the model's predictive capabilities.

3.5 Membrane Characteristics

3.5.1 Study 3 (Integration of Membrane Filtration and The HRAS Process to Produce Industrial Water)

The properties of the commercial membranes employed in Study 3 are provided in Table 3.10. Specifically, the PV024 MF membrane (Philos, South Korea) and PV250 UF membrane (Philos, South Korea) were utilized for the pre-treatment experiments. For the final treatment experiments, the NF90 NF membrane (Dow-Filmtec, USA) and the RO-XLE RO membrane (specifically designed for brackish water treatment, Dow-Filmtec, USA) were employed.

3.5.2 Study 4 (Alternative Post-Treatment Options to The HRAS Process for Producing Irrigation Water)

In Study 4, MF and UF membranes specified in section 3.5.1 were used.

3.6 Jar Tests

The jar tests involved 1 min of rapid mixing (120 revolutions per minute (rpm)), followed by 20 min of slow mixing (consisting of approximately 10 min at 40 rpm and 10 min at 20 rpm), and finally, 30 min of settling (Guan et al., 2005).

Table 3.10 : Properties of commercial membranes used in Study 4.

Parameter	PV024	PV250	NF90	RO-XLE
Membrane material	Polyvinylidene difluoride (PVDF)	PVDF	Polyamide Thin-Film Composite	Polyamide Thin-Film Composite
Pore size	0.24 µm	250 kDa*	200-400 Da*	100-200 Da*
Maximum operating temperature (°C)	-	-	45	45
Maximum operating pressure (bar)	-	-	41	41
Operating pH range	-	-	3-10	2-11
Sodium chloride (NaCl) rejection (%)	-	-	-	99.5
Magnesium sulfate ($MgSO_4$) rejection (%)	-	-	>97	-

** Cut-off molecular weight*

3.7 Mass Balance Calculations

A COD mass balance was performed to determine the pathways of COD within the pilot-scale HRAS system. The mass balance assumed that the tCOD load in the influent is equal to the combined load in the effluent, wasted sludge, and oxidized COD, as suggested by Barker and Dold (1995). tCOD loads in the influent, effluent, and waste sludge were calculated based on experimental data. The fraction of oxidized COD ($COD_{oxidized}$) was determined using equation 3.8, where COD_{inf} represents the daily tCOD load in the influent (g/d), COD_{eff} represents the daily tCOD load leaving the system with the effluent (g/d), and COD_{WAS} represents the daily tCOD load in the waste sludge (g/d).

$$COD_{oxidized}\ (\%)=\frac{COD_{Inf}\text{-}COD_{Eff}\text{-}COD_{WAS}}{COD_{Inf}}\times 100 \tag{3.8}$$

COD redirection was determined using the approach outlined by Rahman et al. (2017). According to this method, it was assumed that the portion of COD_{inf} that is not redirected undergoes oxidation or exits the system through the effluent as non-biomass components such as sCOD and cCOD. Conversely, the redirected COD leaves from the system via the effluent as xCOD and captured in the waste sludge as COD_{WAS}. This relationship is described by equation 3.9, where COD_{WAS} represents the captured or harvested COD. In order to keep the mass balance simple, it is assumed that the XCOD in the wastewater leaves the system with excess sludge (WAS), not with effluent, and that all of the xCOD in the effluent is the biomass produced in the system. The redirected COD ($COD_{redirected}$) was presumed to be utilized for the production of extracellular polymeric substances (EPS) (COD_{EPS}) and the growth of biomass ($COD_{biomass}$). Any remaining $COD_{redirected}$ was assumed to be biosorbed by the cells as $COD_{biosorption}$ (equation 3.10). The amount of COD utilized for EPS production and biomass growth was determined based on experimental data of EPS, assuming a heterotrophic yield coefficient of 0.67 g cell COD/g $COD_{oxidized}$. Biosorption, which includes adsorption and storage mechanisms, accounted for a portion of the $COD_{redirected}$. The percentage of $COD_{redirected}$ allocated to biosorption was determined by balancing the COD mass equation (equation 3.10). The percentage of $COD_{oxidized}$ used for EPS production was calculated using equation 3.12, where the total EPS quantity was measured in g COD/g VSS. The fraction of $COD_{oxidized}$ contributed to biomass growth was calculated using equation 3.13. The portion of $COD_{redirected}$ allocated to biosorption was determined by closing the COD mass balance as defined in equation 3.14. Actual percentages of EPS production, biomass growth, and biosorption were calculated using equations 3.15, 3.16, and 3.17, respectively (Rahman et al., 2017).

$$COD_{redirected}\ (\%)=\frac{xCOD_{eff}+COD_{WAS}}{COD_{inf}}\times 100 \tag{3.9}$$

$$COD_{Redirected}(\text{g COD/d})=COD_{Biomass}+COD_{EPS}+COD_{Biosorption} \tag{3.10}$$

$$(COD_{Biomass} + COD_{EPS})\ (g\ COD/d) = COD_{Oxidized} \times \frac{Y}{1-Y} \tag{3.11}$$

$$COD_{EPS}(\%) = \frac{\text{Total EPS amount (g COD/g VSS)}}{(xCOD/VSS)_{reactor}} \times 100 \tag{3.12}$$

$$COD_{Biomass}\ (\%) = \frac{COD_{Biomass+EPS}}{COD_{inf}} \times 100 - COD_{EPS}(\%) \tag{3.13}$$

$$COD_{Biosorption}(\%) = 100 - COD_{Biomass}\ (\%) - COD_{EPS}(\%) \tag{3.14}$$

$$\text{Actual } COD_{EPS}(\%) = \frac{\text{equation 3.10}}{100} \times COD_{Redirected}\ (\%) \tag{3.15}$$

$$\text{Actual } COD_{Biomass}\ (\%) = \frac{\text{equation 3.11}}{100} \times COD_{Redirected}\ (\%) \tag{3.16}$$

$$\text{Actual } COD_{Biosorption}(\%) = \frac{\text{equation 3.12}}{100} \times COD_{Redirected}\ (\%) \tag{3.17}$$

For the N and P mass balance, it was assumed that these nutrients only exited the system through the effluent and waste sludge. In fully-aerated HRAS systems with low SRT and DO levels, processes such as nitrification and enhanced biological phosphorus removal do not occur (Barker and Dold, 1997). As a result, the main mechanisms for N and P removal are biomass uptake and adsorption (Ge et al., 2017).

3.8 Scenario Analysis

In Study 3, apart from the experimental investigations, scenario analysis was performed to assess different sludge management options. The costs associated with sludge transfer and disposal, net energy consumption of a full-scale HRAS system, and chemical consumption for sludge dewatering were estimated for various scenarios. The study focused on a HRAS plant serving a city with a population equivalent (PE) of 1,000,000, where the distances between the WTP, HRAS plant, and landfill were set at 50 km.

Scenario 1 involved the separate disposal of sludges from the WTP and HRAS plants. Figure 3.11 provides an overview of this scenario. On the other hand, in Scenario 2, the HRAS plant received the sludge from the WTP. The dosage of WTP sludge was the same as in experiments in Stage 2 of Study 3. The cost estimation for different sludge management scenarios considered expenses related to sludge transfer from the WTP and HRAS plant to the landfill, as well as from the WTP to the HRAS plant. Furthermore, landfilling costs were taken into account.

In addition to the above-mentioned costs, the analysis also encompassed the chemical expenses for sludge dewatering and the energy costs associated with the HRAS plant. The energy costs included the consumption of energy for various processes such as preliminary treatment, blowers, pumps, sludge thickening, anaerobic digestion, and sludge dewatering. Moreover, the energy production from biogas was factored into the overall energy balance of the HRAS system.

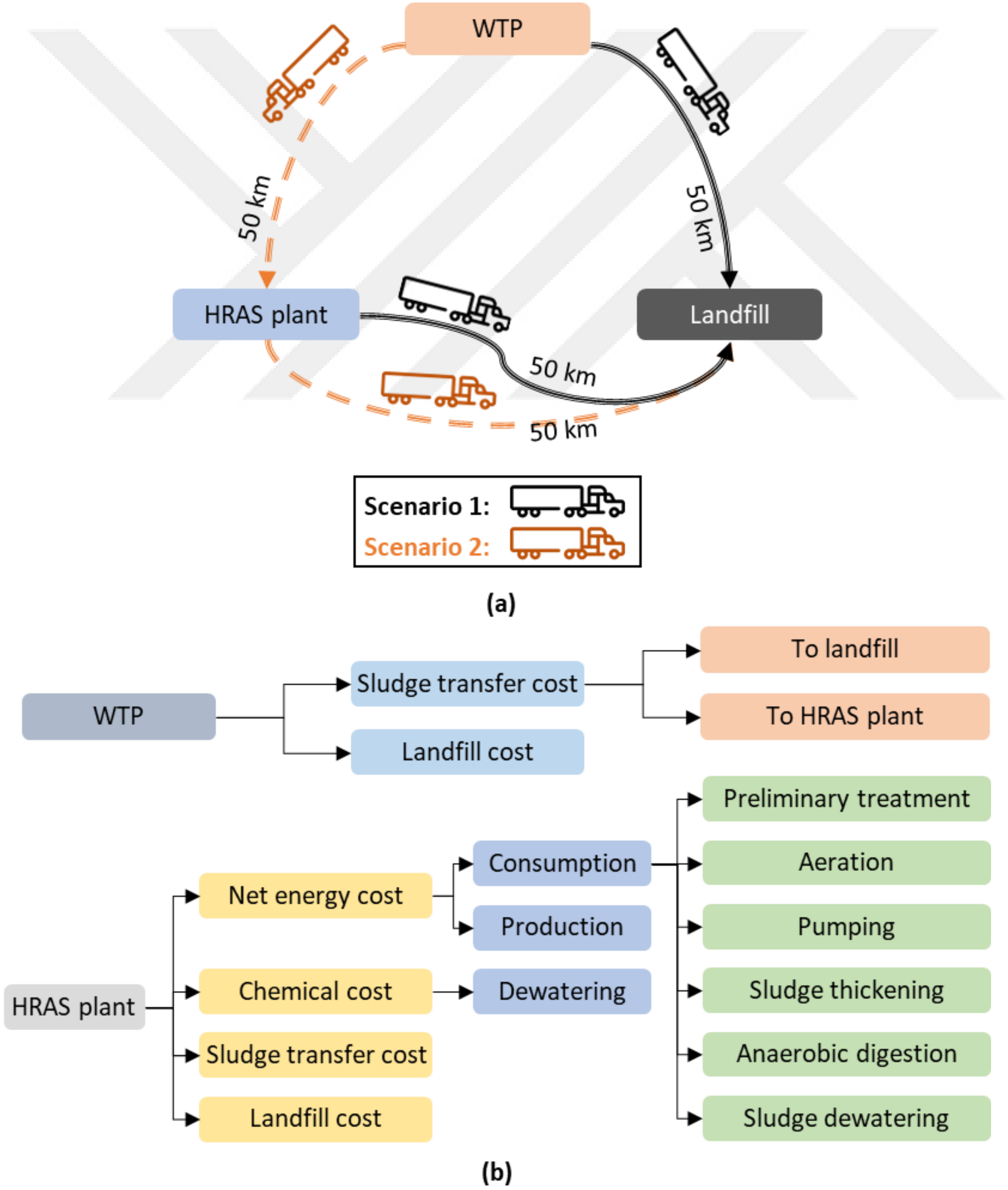

Figure 3.11 : Scenario analysis of different treatment sludge management scenarios in Study 3.

By considering these factors, the study aimed to evaluate the economic and energy implications of different sludge management scenarios within the context of the HRAS plant serving a city with a PE of 1,000,000.

3.9 Effluent Quality Indexes

3.9.1 Reclaimed Water Quality Index (RWQI)

RWQI is a metric used to evaluate the quality of treated water in different post-treatment alternatives in Study 4. The calculation method for RWQI is described in the study conducted by Cosenza et al. (2022). In this method, certain parameters specified in the European Union's minimum reclaimed water quality criteria (EUCO 2020/741), such as TSS, turbidity, *E. coli*, and BOD_5, were considered undesired parameters. On the other hand, NH_4-N and PO_4-P were selected as desired parameters. Each desired and undesired parameter was assigned a weighting factor (w). The weighting factor for desired parameters was set at 0.5.

For undesired parameters, the weighting factor for *E. coli* was -0.4, indicating its higher importance in determining the reclaimed water quality class. The weighting factors for BOD_5, TSS, and turbidity were -0.2 each. These weighting factors reflect the relative significance of each parameter in the overall water quality assessment.

The RWQI calculation involves the weighted summation of the desired and undesired parameters using equation 3.18 where i is the parameter and Con is the concentration. The resulting sums are then normalized by dividing them by the maximum sums of the desired and undesired parameters. The normalized RWQI values range between 0 and 1 for desired parameters and between -1 and 0 for undesired parameters. The RWQIs of different post-treatment alternatives are calculated by summing the normalized RWQI values of the desired and undesired parameters.

$$\mathrm{RWQI} = \sum_{\mathrm{i}=1}^{\mathrm{n}} \mathrm{w_i\ Con_i} \tag{3.18}$$

3.9.2 Effluent Quality Index (EQI)

The EQI calculations (equation 3.19) in this study considered the concentrations of TSS, COD, TN, and TP) parameters in the effluent of the HRAS plant at both Stage 1 and Stage 2 of Study 5. To determine the overall EQI, weighting factors were assigned to each parameter based on established guidelines. For TSS (β_{TSS}) and COD (β_{COD}), the weighting factors of 2 and 1, respectively, were selected following the recommendation by Copp (2002). The weighing factor for TP (β_{TP}) was chosen to be the same as the weighing factor for TN (β_{TN}), which was 20, as suggested by Gernaey and Jorgensen (2004). The effluent concentrations of TSS, COD, TN, and TP were is represented with TSS_{eff}, COD_{eff}, TN_{eff}, and TP_{eff}, respectively in equation 3.16.

$$\mathrm{EQI} = \sum \beta_{TSS} \times TSS_{eff} + \beta_{COD} \times COD_{eff} + \beta_{TN} \times TN_{eff} + \beta_{TP} \times TP_{eff} \qquad (3.19)$$

3.10 Cost Estimations

3.10.1 Study 3 (Integration of Membrane Filtration and The HRAS Process to Produce Industrial Water)

Cooling towers can have varying flow rates depending on their size, with large systems reaching up to 31,500 L/s, while small systems typically have flow rates ranging from 190-315 L/s (US EPA, 2012). The makeup water requirement for cooling towers is typically around 2% of the nominal flow rate (Perry et al., 2018). In Study 3, a conceptual medium-sized industry was considered, and the makeup water requirement was set at 5 L/s. Six different wastewater treatment plant configurations, each capable of treating approximately 7 L/s of domestic wastewater to produce the required cooling makeup water (5 L/s), were compared based on treatment cost. The treatment cost was divided into capital and operations and maintenance (O&M) costs. The capital cost included expenses related to construction, equipment, and installation, while the O&M cost encompassed energy consumption (such as pumping energy for membrane filtration and sludge lines, and aeration energy for HRAS), chemical usage (for membrane cleaning), membrane replacement, labor, and maintenance costs. The unit capital and O&M costs were derived from information gathered from commercial membrane manufacturers and wastewater treatment plant contractors. The different scenarios were compared in terms of the total unit treatment cost, which combined the annual capital and O&M costs. It was assumed that the WWTP would be operational for 30 years (n), with an interest rate (i) of 3%. The uniform annual capital cost (AC) was calculated using equation 3.20, where the present capital cost (PC) was considered. The unit capital cost for DMF via MF and UF was estimated at 4.7 and 5.2

€ cents/m^3 permeate, respectively. For the HRAS plant, the unit capital cost was set at 2.4 € cents/m^3 of treated water. The unit O&M costs were 24 and 27 € cents/m^3 permeate/year for DMF via MF and UF, respectively. The assumed O&M cost for the HRAS plant was 2.7 € cents/m^3 treated water/year. Regarding the final-treatment, the unit capital costs for N) and RO membrane filtration were taken as 3.3 and 3.4 € cents/m^3 permeate, respectively. The unit O&M costs for NF and RO membrane filtrations after pre-treatment with UF membrane was estimated at 21 € cents/m^3 permeate/year and 22 € cents/m^3 permeate/year, respectively. Experimental observations revealed flux variations in NF and RO membranes when fed with different pre-treated effluents. The unit O&M costs of NF and RO membrane filtrations after DMF via MF and HRAS processes were normalized based on the flux change resulting from different pre-treatment efficiencies.

$$\mathrm{AC} = \mathrm{PC} \times \frac{\mathrm{i}(1+\mathrm{i})^{\mathrm{y}}}{(1+\mathrm{i})^{\mathrm{y}} - 1} \tag{3.20}$$

3.10.2 Study 4 (Alternative Post-Treatment Options to The HRAS Process for Producing Irrigation Water)

In Study 4, the operation cost of the post-treatment alternatives includes energy, chemical, and labor costs. Information regarding unit operation costs was gathered from membrane manufacturers, UV manufacturers, and chemical suppliers. The electricity consumption for MF and UF membranes was assumed to be 0.12 kWh/m^3 and 0.15 kWh/m^3, respectively. The energy consumption for UV units was estimated at 0.09 kWh/m^3. For the coagulation system, the pumping energy consumption was set at 0.03 kWh/m^3. The price of $FeCl_3$ and alum, which are commonly used coagulants, was taken as 230 €/ton and 180 €/ton, respectively. A part-time technician labor cost for a well automated system was assumed to be 5,000 €/year. The operation cost of the post-treatment alternatives was estimated based on a treatment capacity of 2,000 m^3/d.

3.10.3 Study 5 (Examination of The Impact of Adding WTP Sludge to The HRAS Process)

In Study 5, the cost of sludge transfer was estimated based on the assumption that trucks with a capacity of 40 m^3 were used for transportation. The sludge transportation cost consisted of two components: a fixed cost of 4 \$/m^3 that remained constant regardless of the transfer distance, and a variable cost of 0.059 \$/m^3/km that depended on the distance of transfer (Marufuzzaman et al., 2015).

Regarding sludge landfill disposal costs, it is observed that these costs have been increasing globally (Campo et al., 2021). Different countries set their prices for landfilling fees and taxes. In Europe, the average cost of landfill disposal for sludge was around 75 €/ton in 2013, according to the European Environment Agency (EEA, 2013). In 2015, the range of sludge disposal costs in European countries varied between 125 and 255 €/ton (Kacprzak et al., 2017). Although water treatment sludge has lower organic content compared to wastewater treatment sludge, it is typically not considered inert waste (Hidalgo et al., 2017). The European Union (EU) classifies wastewater and water treatment sludges together as "common sludges" based on EUCO Regulation No: 2150/2002 (European Parliament, 2002). Therefore, the landfill disposal cost for both water and wastewater treatment sludges was assumed to be 250 €/ton of dewatered sludge in this study, considering the increasing trend in landfill disposal costs worldwide.

The specific energy consumption of the HRAS plant was determined by summing the energy demands of various processes such as wastewater and sludge pumping, preliminary treatment (screening and grit removal), aeration, settling, sludge thickening, anaerobic digestion, and sludge dewatering (Table 3.11). The energy production from anaerobic digestion was calculated using the Biomethane Potential (BMP) values of the HRAS process sludge at Stage 1 and Stage 2. The energy production from biogas combustion through a combined heat and power (CHP) unit was estimated assuming that 2.9 kWh of electricity (30%) and 4.9 kWh of heat (50%) could be generated from 1 m^3 of CH_4 (with an energy content of 9.9 kWh/m^3) (Tchobanoglous et al., 2003). The energy price considered in the analysis was 0.1208 €/kWh, which represented the average energy price for non-household consumers in EU countries (Eurostat, 2022).

Table 3.11 : The unit energy consumption of the treatment units in HRAS plant.

Treatment units	Specific energy consumption (kWh/m^3 wastewater)	Reference
On-site pumping of wastewater	0.03	Taboada-Santos et al. (2020)
Aeration	0.07	
Sludge recirculation	0.03	
Waste sludge pumping	0.02	
Sludge thickening	0.02	
Sludge dewatering	0.03	
Screening and grit removal	0.0027	Longo et al., (2016)
Settling	0.0084	
Anaerobic digestion	0.0375	

3.11 Statistical Analysis

3.11.1 Study 1 (Optimization of a Pilot-Scale HRAS Process with Lamella Clarifier)

For the statistical analysis, the analysis of variance (ANOVA) test, specifically the Single Factor ANOVA, was conducted using the Microsoft Excel 2016 Data Analysis Tool. The significance level (p-value) was set at 0.05, indicating that results with p-values less than 0.05 were considered statistically significant. Strong correlations were identified when the correlation coefficient (r) was lower than -0.7 or higher than 0.7.

3.11.2 Study 2 (Modelling of High-Rate Activated Sludge Process)

MAE serves as a metric to assess the performance of a regression model. It quantifies the average absolute difference between predicted values and actual values within a dataset. A lower MAE suggests a better fit of the model to the dataset. MAE is calculated according to equation 3.21 where O_i is the observed values, M_i is the model output, an is the sample size (Dai et al., 2017).

$$\mathrm{MAE} = \frac{1}{\mathrm{n}} \times \sum_{\mathrm{i}=1}^{\mathrm{n}} |\mathrm{O_i} - \mathrm{M_i}| \tag{3.21}$$

Similarly, RMSE is a metric employed to evaluate regression models (equation 3.22). It measures the average difference between predicted values and actual values, incorporating the squared errors (Dai et al., 2017). A smaller RMSE value signifies a superior fit of the model to the dataset. RMSE is considered more sensitive than MAE since it takes into account the squared errors, thereby penalizing larger errors to a greater extent.

$$RMSE = \sqrt{\frac{1}{n} \times \sum_{i=1}^{n} (O_i - M_i)^2} \tag{3.22}$$

3.12 Analytical Methods

3.12.1 Conventional parameters

The measurements of COD, BOD_5, TSS, VSS, TS, VS, TN, NH_4-N, total P (TP), soluble TP (STP), total hardness, Ca hardness, alkalinity and SVI were conducted following the Standard Methods outlined in APHA (2017).

For tCOD measurements, unfiltered samples were used, and sludge samples were diluted with distilled water prior to tCOD analysis. sCOD samples were filtered through syringe filters with a pore size of 0.45 µm before analysis. The cCOD value was calculated by subtracting the sCOD from the COD value, which was measured after filtration through a 1.5 µm glass fiber filter. To calculate xCOD, the sum of cCOD and sCOD was subtracted from tCOD, as described by Rahman et al. (2016).

Analysis for pathogens were conducted following APHA (2017). Total coliform and fecal coliform analyses were performed using the membrane filtration technique with the 14049 Chromogenic Coliform and 140068 m FC Sartorius Stedim Biotech kits (Germany), respectively. *E. coli* were counted using the membrane filtration method (140068 mFC Sartorius Stedim Biotech, Germany).

The turbidity of influent and effluent samples was measured using a turbidimeter (Hach 2100 P, USA) with a detection range of 0-1000 NTU. The CST of the sludge was measured using a CST analyzer (Triton Electronics, Type 304 M, UK). The conductivity was measured with a portable conductivity meter (Hach HQ40d, USA).

3.12.2 Particle size distribution (PSD)

The PSDs of influent and effluent samples were measured using a Zetasizer Nano-S instrument from Malvern Instruments (UK). This instrument has a detection range between 0.3 nm and 10 µm, allowing for the analysis of particles within this size range.

For the determination of the PSDs of sludge samples, a Mastersizer 2000 instrument from Malvern Instruments with a Hydro 2000 MU attachment was utilized. This instrument has a detection range between 0.6 μm and 6000 μm.

3.12.3 EPS

The analysis of reactor sludge samples aimed to determine the fractions of EPS, including carbohydrate and protein fractions, as well as the loosely bound EPS (LB-EPS) and tightly bound EPS (TB-EPS). The following procedure was conducted:

1. The sludge samples (21 mL each) were subjected to centrifugation at 4 ℃ and 4000g for 5 minutes using a Sigma 3-30 K centrifuge (Germany).
2. The resulting sludge pellet obtained after centrifugation was utilized for EPS measurement. A modified version of the heat extraction method developed by Li and Yang (2007) was employed for the extraction of LB-EPS and TB-EPS.
3. The sludge pellets were re-suspended in 21 mL of phosphate buffer solution (PBS), consisting of 14 mL of PBS at room temperature and 7 mL of PBS preheated to 60 ℃. The samples were vigorously shaken using a vortex mixer for 1 minute.
4. After cooling the samples to room temperature, they were centrifuged at 20 ℃ and 4000g for 10 minutes. The supernatant obtained from this step was used for LB-EPS measurement.
5. The pellet was then re-suspended in 21 mL of pre-heated PBS at 60 ℃ and heated to 60 ℃ for 30 minutes. After cooling the samples to room temperature, they were centrifuged at 4000g for 15 minutes. The supernatant obtained from this step was used for TB-EPS measurement.
6. Carbohydrate measurement followed the method described by Dubois et al. (1956), while protein measurement was conducted using the modified Lowry method (Frølund et al., 1995). Bovine serum albumin (BSA) and glucose standard (D-glucose monohydrate) were used as standards for protein and carbohydrate measurements, respectively.

3.12.4 Ions and heavy metal analysis

Ions (Cl^-, NH_4^+, PO_4^{3+}, and SO_4^{2-}) were quantified using an ion chromatography (IC) system, specifically the Dionex ICS-300 model manufactured by Thermo Fisher Scientific (USA). Heavy metals (Al, Si, Mn, Fe) were analyzed using an inductively coupled plasma-optical spectrometer (ICP-OES), specifically the Optima 7000 model from Perkin Elmer (USA).

3.12.5 BMP tests

In Study 5, to evaluate the impact of adding WTP sludge on CH_4 production from the HRAS process sludge, BMP tests were conducted. The Automatic Methane Potential Test Systems II from Bioprocess Control (Sweden) was employed for these tests. The BMP tests were performed under mesophilic conditions at a temperature of 35 ℃.

HRAS process sludge samples were collected at the end of each stage for the BMP tests. The inoculum used in the tests was obtained from a full-scale anaerobic digester that treated waste sludge from a municipal WWTP. Before the BMP test, the inoculum was kept at a temperature of 35 ℃ for 4 days to deplete any residual organic matter.

The sludge samples and a blank (used to measure the BMP of the inoculation sludge) were analyzed in triplicates. To remove oxygen, nitrogen gas was flushed into 500 mL test bottles (with a working volume of 400 mL) before the BMP tests. Sodium acetate was used as the substrate in the tests. The mixing ratio of the inoculum and sludge sample was adjusted so that the VS concentration of the mixture was twice the COD concentration of the substrate.

3.12.6 Morphological analyses

To visualize the structure of the HRAS process sludge, Environmental Scanning Electron Microscopy (ESEM) was employed. The ESEM equipment used for this purpose was the FEI Quanta FEG 250 ESEM from Thermo Fisher Scientific Inc. (USA). To prepare the samples for imaging, a vacuum evaporator (Quorum SC7620, UK) was utilized to coat the surfaces of the samples with a thin layer of Palladium and Gold (Pd-Au) measuring approximately 3-4 nm in thickness.

4. RESULTS AND DISCUSSION

4.1 Study 1 (Optimization of a Pilot-Scale HRAS Process with Lamella Clarifier)

4.1.1 Sludge characteristics

The concentration of MLSS is an important parameter in carbon adsorption as it is related to the active biomass in activated sludge processes. Typically, HRAS systems are operated within a range of 900 to 5400 mg/L for MLSS concentration (Sancho et al., 2019). However, MLSS concentrations exceeding 3000 mg/L can harm the oxygen transfer rate without improving COD removal efficiency (Miller, 2015). Therefore, in this study, the MLSS concentration was maintained between 2000 and 3000 mg/L. The variations in MLSS and mixed liquor volatile suspended solids (MLVSS) concentrations in the bioreactor, as well as the MLVSS/MLSS ratio, are depicted in Figure 4.1. Throughout the long-term operation, the average MLSS concentration was 2613±363 mg/L, and the MLVSS/MLSS ratio was 64±4%.

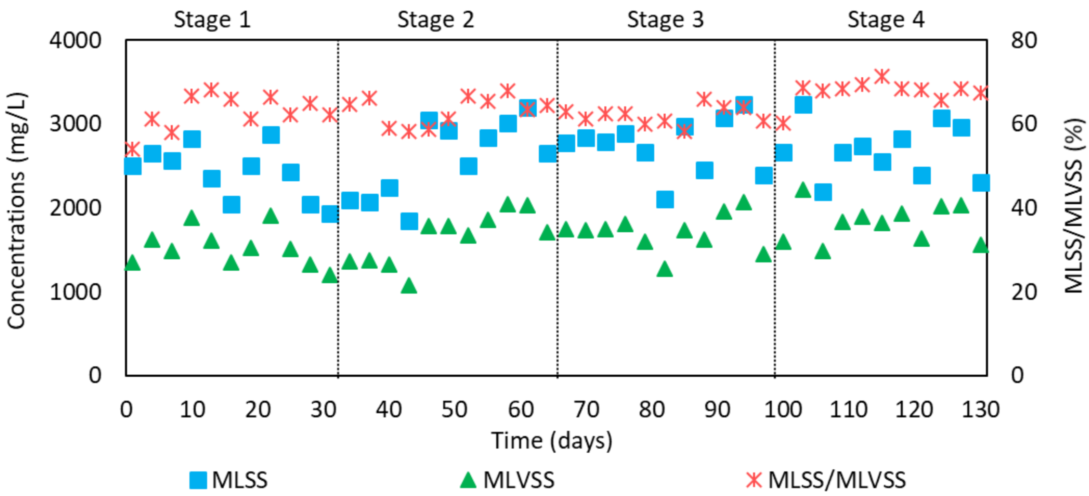

Figure 4.1 : MLSS and MLVSS concentrations, and MLVSS/MLSS ratios obtained at each stage.

Quantifying EPS is crucial in HRAS systems as it provides valuable information about floc formation. Table 4.1 presents the EPS production, LB-EPS/TB-EPS ratio, and protein EPS to carbohydrate EPS (pEPS/cEPS) ratio obtained at each operational stage. At Stage 1 (HRT: 77±1 min, DO: 0.5±0.03 mg/L), the highest EPS production was observed, reaching 237±36 mg COD/g VSS. Lowering the HRT to 54±6 min at Stage 2 (DO: 0.5±0.04 mg/L) and reducing the DO concentration to 0.2±0.02 mg/L at Stage 3 (HRT: 76±3 min) resulted in decreased EPS production to 140±34 and 119±27 mg COD/g VSS, respectively, consistent with the findings of Jimenez et al. (2015). At Stage 4, with a DO concentration of 0.8±0.05 mg/L, the EPS production was higher than at Stage 3 (DO: 0.2±0.02 mg/L) but lower than at Stage 1 (DO: 0.5±0.03 mg/L). Rahman et al. (2019) highlighted that EPS production was observed when DO exceeded a certain threshold (>0.4 mg/L) in their study. They reported an increase in EPS production with increasing DO concentration. However, Kinyua et al. (2017) observed a decrease in EPS concentration from 293.3 to 199.8 mg COD/g VSS as the DO concentration increased from 0.5 to 1 mg/L. In this study, the findings showed that a DO concentration of 0.2±0.02 mg/L was not sufficient to achieve EPS levels as high as Stages 2 and 3, as reported by Rahman et al. (2019). On the other hand, increasing the DO concentration from 0.5±0.03 mg/L to 0.8±0.05 mg/L hindered EPS production, similar to the study conducted by Kinyua et al. (2017). According to Shin et al. (2000), cEPS concentration increases with increasing DO concentration, while pEPS remains unchanged, leading to deflocculation. Based on the statistical analysis, total EPS production exhibited a high correlation with HRT ($r=0.81$, $p<0.05$), but a low correlation with DO ($r=0.37$, $p<0.05$). The average LB-EPS/TB-EPS ratio remained around 0.46 at all stages except Stage 2. The LB-EPS/TB-EPS ratio showed a strong correlation with HRT ($r=0.90$, $p<0.05$), but a weak correlation with DO concentration ($r=-0.03$, $p=0.63$). A low pEPS/cEPS ratio indicates poor floc formation (van Winckel et al., 2019). Generally, pEPS was the dominant fraction, accounting for over 70% of the total EPS in the sludge, which could be attributed to the presence of a large amount of concentration of exoenzymes trapped in the EPS (Dignac et al., 1998; Miller, 2015). The pEPS/cEPS ratio was moderately affected by changes in HRT ($r=0.76$, $p<0.05$) and DO ($r=0.73$, $p<0.05$) values. Increased HRT and DO values resulted in an increased pEPS/cEPS ratio.

PSD measurements were carried out on five different samples collected at each stage. The highest and lowest d_{50} values of the reactor sludge were observed at Stage 3 and Stage 1, measuring 157±15 μm and 84±15 μm, respectively. The reactor sludges at Stage 2 and Stage 4 exhibited d_{50} values of 135±17 μm and 126±13 μm, respectively.

At Stage 1, particles smaller than 100 μm accounted for more than 50% of the total sludge volume, while they constituted approximately 40% of the total sludge volume at the other stages.

Table 4.1 : Total EPS production, LB-EPS/TB-EPS ratio, and pEPS/cEPS ratio obtained at each stage.

Stage	EPS (mg COD/g VSS)	LB-EPS/TB-EPS	pEPS/cEPS
1	237±36	0.46±0.04	4.96±1.29
2	140±34	0.23±0.07	2.57±0.68
3	119±27	0.46±0.08	4.15±0.29
4	170±20	0.45±0.04	6.33±0.58

The HRT of 54±6 min at Stage 2 resulted in the lowest observed SVI of 20±3 mL/g. The average SVI values ranged from 26 to 30 mL/g at the other stages. This finding aligns with the SVI values reported in the study conducted by Guven et al. (2017), where SVI decreased from 29 to 18 mL/g with a reduction in HRT from 130 to 60 min. The difference in d_{50} values between Stage 1 and Stage 3 did not appear to have an impact on SVI.

CST is a parameter that indicates the dewaterability of sludge, where lower CST values indicate better dewaterability. The average normalized CST values for the waste sludge at Stages 1, 2, 3, and 4 were 1.31±0.25 sec/g TSS/L, 1.78±0.49 sec/g TSS/L, 1.33±0.16 sec/g TSS/L, and 1.23±0.38 sec/g TSS/L, respectively. The statistical analysis revealed that HRT had a stronger impact on CST ($r=-0.69$, $p<0.05$) and SVI ($r=0.69$, $p<0.05$) compared to DO concentration (CST: $r=0.18$, $p<0.05$; SVI: $r=0.31$, $p<0.05$). However, the effect of HRT on CST and SVI was moderate.

4.1.2 Treatment performance

According to the findings, the average TSS concentration in the influent ranged from 265 to 309 mg/L at each stage, as shown in Figure 4.2. The TSS removal efficiency was 79.6±5% at Stage 1 and 74.4±4.3% at Stage 2. Decreasing the HRT from 77±1 min to 54±6 min led to a decrease in TSS removal efficiency ($r=0.50$, $p<0.05$). Consequently, DO concentration trials were conducted at an HRT of 75 min. The average TSS concentration in the effluent ranged from 60 to 93 mg/L across all stages.

In a study by Guven et al. (2017), the minimum TSS concentration in the effluent of a HRAS system with a 4 m^3 aeration tank and a 10 m^3 conventional sedimentation tank, treating municipal wastewater at an HRT of 60 min, was reported as 161 mg/L.

Although the aeration tank volumes, studied HRT values, and influent characteristics were similar, lower TSS concentrations were achieved in the effluent compared to the study by Guven et al. (2017). This can be attributed to the increased separation performance provided by the lamella clarifier with 60% less settler volume compared to the 10 m^3 conventional settler used by Guven et al. (2017). Rahman et al. (2020) emphasized that the settleability of sludge is influenced by both the performance of the sedimentation tank and the operational conditions.

The SVI values obtained at Stage 2 were lower than those at Stage 1; however, the effluent TSS concentration (68±17 mg/L) was not lower than that obtained at Stage 1 (60±17 mg/L). This indicates that although SVI is an important indicator of sludge settling performance, it cannot be directly linked to effluent quality (Mancell-Egala et al., 2017). The influent and effluent turbidity ranged between 245-268 NTU and 42-88 NTU, respectively, at all stages. Turbidity removal exhibited a similar trend to TSS removal, with the lowest turbidity in the effluent recorded as 42 NTU at Stage 1.

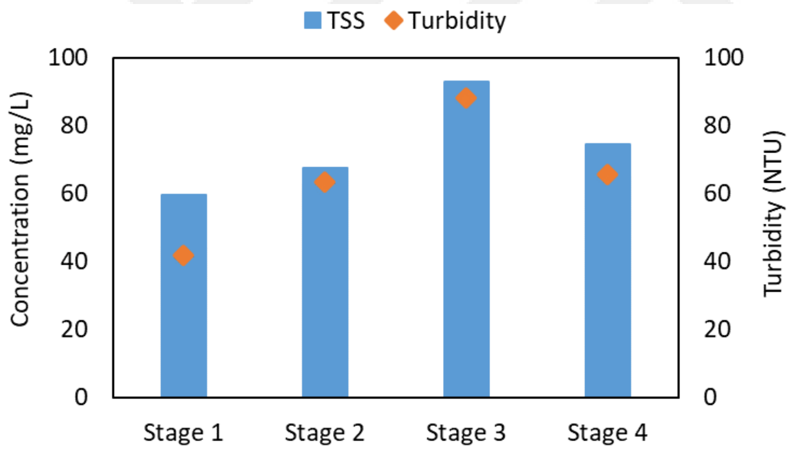

Figure 4.2 : TSS concentrations and turbidity values obtained in the effluent at each stage.

Figure 4.3 illustrates the influent and effluent concentrations as well as the removal efficiencies of COD, TN, NH_4-N, and TP at each stage. The highest total COD removal efficiency was observed at the first stage (58.3±2.9%), which coincided with the highest EPS production and the lowest d_{50} value of the reactor sludge among all stages. This suggests that the presence of small flocs may be advantageous for adsorption due to their larger specific surface area (Morgenroth et al., 2002). Previous studies on HRAS processes have reported total COD removal efficiencies ranging from 28% to 72% (Guven et al., 2019). Cao et al. (2020) investigated an HRAS process with a lamella clarifier and achieved a COD removal efficiency of 54.3%, which is consistent with the results obtained in this study. The average total COD removal efficiency slightly decreased from 58.3±2.9% to 49.5±3.2% when the HRT decreased from 77±1 min to 54±6 min in Stage 2. Total COD removal efficiency showed a moderate correlation with EPS production ($r=0.64$, $p<0.05$) and a strong negative correlation with the d_{50} value ($r=-0.87$, $p<0.05$).

The xCOD removal efficiencies were 78±2%, 65±9%, 64±5%, and 77±6% at Stage 1, Stage 2, Stage 3, and Stage 4, respectively. In HRAS systems, the removal mechanism for xCOD begins with the rapid attachment of particles to flocs (bioflocculation) before being hydrolyzed or removed from the system as excess sludge (Morgenroth et al., 2002). Increased EPS production enhances bioflocculation and, consequently, xCOD removal (Wilen et al., 2003; Jimenez et al., 2007), which aligns with the findings of this study. At Stage 1, the low effluent COD concentration and smaller d_{50} value in the sludge are consistent with the results reported by van Winckel et al. (2019). The authors mentioned that when the available spots on the EPS were occupied by the substrate, floc formation was hindered, which could explain the smaller d_{50} value observed in the sludge at Stage 1.

The effect of DO concentration on COD removal is significant, as it is correlated with the biodegradation of organics and floc breakage due to shear effects (Trzcinski et al., 2017). Jimenez et al. (2015) demonstrated that increasing DO concentration from 0 mg/L to 2 mg/L increased EPS production; however, xCOD removal did not change significantly at DO concentrations above 0.7 mg/L. In this study, the lowest COD removal efficiency was observed at Stage 3 (44.3±3.7%), where the DO concentration was the lowest (0.2±0.02 mg/L) and the d_{50} value was the highest (157±15 μm). Decreasing the DO concentration by reducing aeration may have resulted in a gentler shear force on the flocs, leading to the formation of larger flocs with a reduced specific surface area. Additionally, the lowest EPS production at Stage 3 could have caused the formation of larger but weaker flocs, potentially resulting in higher particle concentrations in the effluent. Furthermore, the low DO concentration at Stage 3 hindered sCOD assimilation for biomass growth. Increasing the DO concentration from 0.2±0.02 mg/L to 0.8±0.05 mg/L at Stage 4 reduced the d_{50} values in the A reactor sludge from 157±15 μm to 126±13 μm. Additionally, it increased EPS production and biomass growth, resulting in a higher COD removal efficiency at Stage 4 (53.4±2.6%) compared to Stage 3 (44.3±3.7%). Although xCOD removal efficiencies were very similar at Stage 1 and Stage 4, COD capture by biomass was higher at Stage 1, possibly due to lower EPS production at Stage 4 compared to Stage 1.

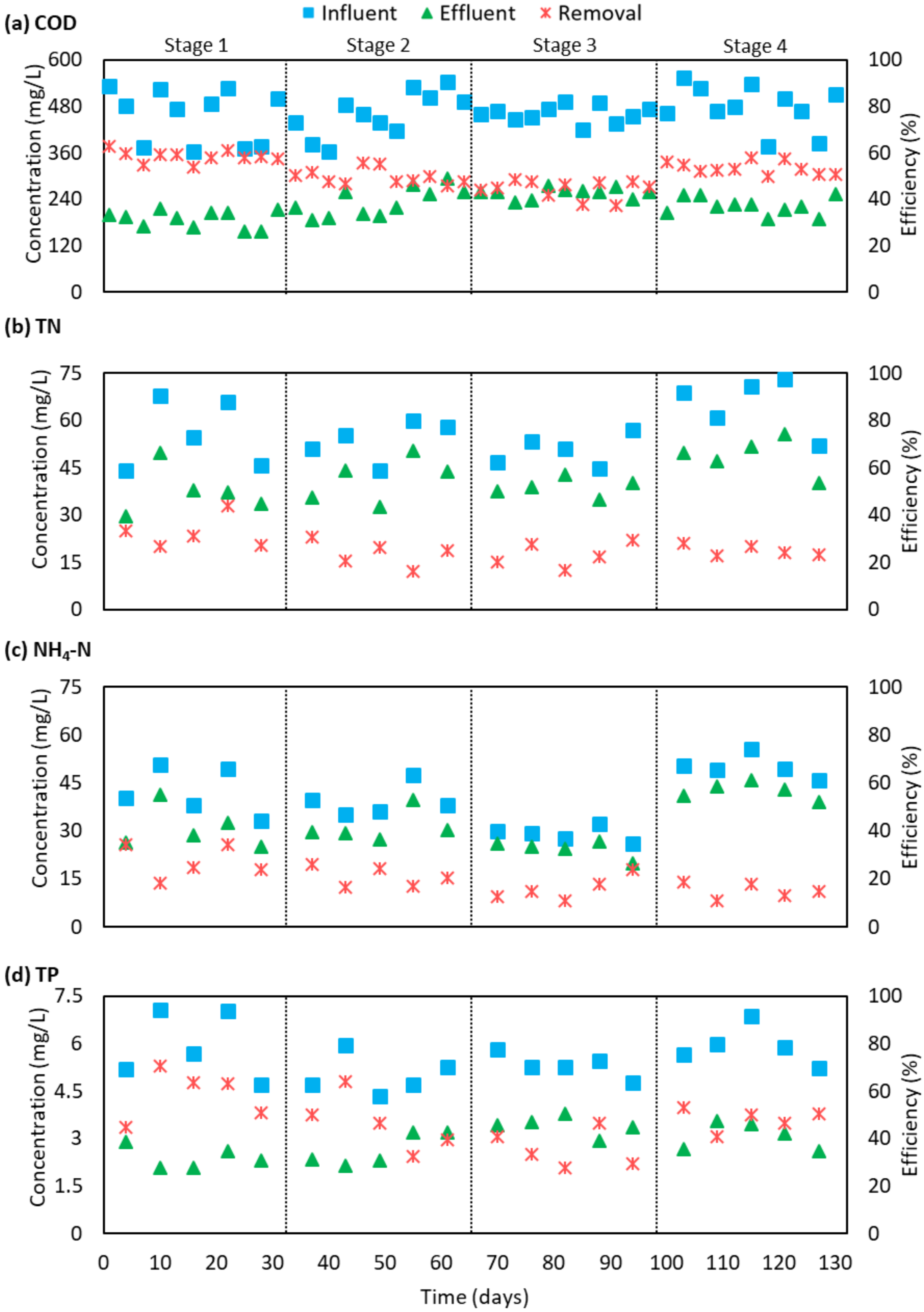

Figure 4.3 : Influent and effluent concentrations and removal efficiencies of different parameters at each stage: (a) COD, (b) TN, (c) NH_4-N, (d) TP.

Figure 4.4 provides information on the COD fractions in the influent and effluent of the HRAS system for each stage. The xCOD fraction accounted for more than half of the influent COD (54-61%) throughout the entire experimental study. The HRAS process demonstrated effective removal of this xCOD fraction. PSD measurements conducted on the effluent revealed that 48% of the particles were classified as large particles, with sizes ranging from 100 to 1000 µm, at Stage 1, while this percentage increased to 59% at the other stages.

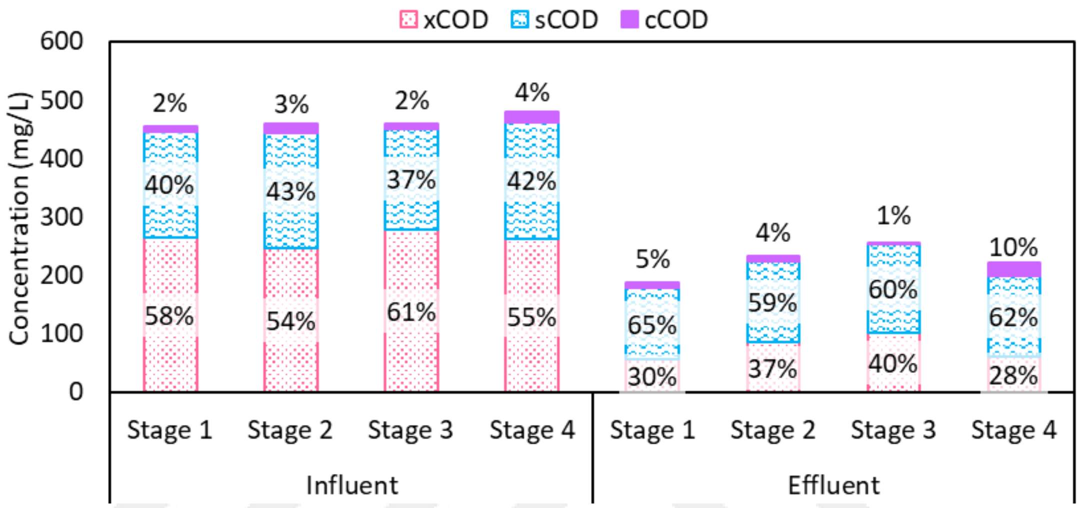

Figure 4.4 : COD fractions of influent and effluent.

4.1.3 Mass balance

The primary goal of the HRAS process is to maximize the capture of carbon in the waste sludge while maintaining high effluent quality, thereby reducing the pollution load on downstream treatment processes. This is achieved by minimizing the loss of COD through oxidation and maximizing COD capture to the sludge line. The concentration of tCOD in the waste sludge reflects the amount of harvested COD, with the highest concentration observed at Stage 1 (13.7±3.0 g COD/L) and the lowest at Stage 3 (8.2±1.2 g COD/L). The COD/VSS ratio indicates the amount of COD captured by biomass, which ranged from 1.49 to 1.58 across the operational stages. Figure 4.5 illustrates the pathways of COD redirection at each stage.

Stage 1 exhibited the lowest percentage of non-biomass COD in the effluent at 28.4%. Reducing the HRT to 54±6 min in Stage 2 led to decreased oxidation and biomass growth compared to Stage 1, which had an HRT of 77±1 min. However, due to the lower production of EPS relative to Stage 1, a greater proportion of xCOD escaped the system through the effluent in Stage 2. The COD losses associated with mineralization ranged from 9.0% to 20.1% at each stage, consistent with previous HRAS studies reported in the literature (Miller, 2015; Rahman et al., 2019; Cao et al., 2020). Stage 4 exhibited the lowest COD redirection, likely attributed to a higher COD loss through oxidation. This stage had the highest levels of COD oxidation (20.1%) and biomass growth (12.0%), primarily due to the highest DO concentration (0.8±0.05 mg/L) in the aeration tank. Stage 3 showed the highest percentages of COD redirection (62.4%) and biosorption (54.0%). Conversely, the percentage of COD harvested in the waste sludge (41.5%) was nearly identical to that of Stage 1 (41.7%), as biomass escape through the effluent (20.8%) was highest in Stage 3. This may be attributed to the formation of weak flocs at Stage 3 due to low EPS production. Although lower DO levels limited oxidation and favored carbon redirection, the weak flocs resulted in effluent quality deterioration and hindered COD harvesting.

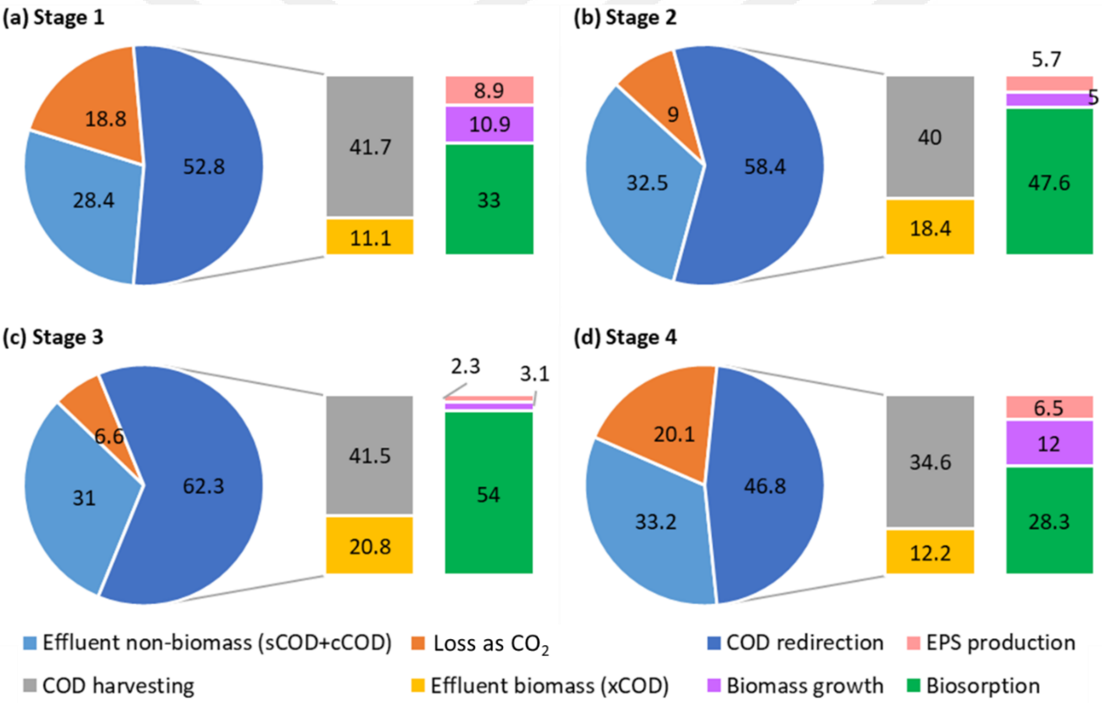

Figure 4.5 : COD pathways of each stage: (a) Stage 1, (b) Stage 2, (c) Stage 3, (d) Stage 4.

The COD that is harvested in the waste sludge during the HRAS process can be effectively converted into CH_4 through anaerobic digestion, thereby generating energy. One advantage of HRAS systems is that the waste sludge contains higher levels of N and P compared to primary sludge. As a result, the recovery of N and P from the supernatant of anaerobic digesters through magnesium ammonium phosphate (MAP) precipitation is enhanced (Stumpf et al., 2008).

An alternative strategy for managing the sludge is to co-digest dewatered waste sludge (with a dry matter content of 20-40%) along with organic solid waste in dry thermophilic anaerobic digesters. This approach integrates the treatment of sludge with solid waste management (Mata-Alvarez et al., 2000). Additionally, the digested sludge can be utilized as a beneficial soil amendment.

Figure 4.6 provides an overview of the mass balance of COD, N, and N throughout the pilot-scale HRAS system at each stage. In HRAS systems, the removal of N and P is primarily attributed to biosorption and capture mechanisms. The highest N and P capture rates were achieved at Stage 1, which also exhibited the highest COD capture. Although the N and P removal efficiencies in HRAS systems are superior to those in primary sedimentation, they are lower compared to conventional biological nutrient removal processes.

Considering both effluent quality and harvested COD, it can be concluded that the operational conditions applied at Stage 1, characterized by an HRT of 77±1 min and a DO concentration of 0.5±0.03 mg/L, represent the optimal configuration.

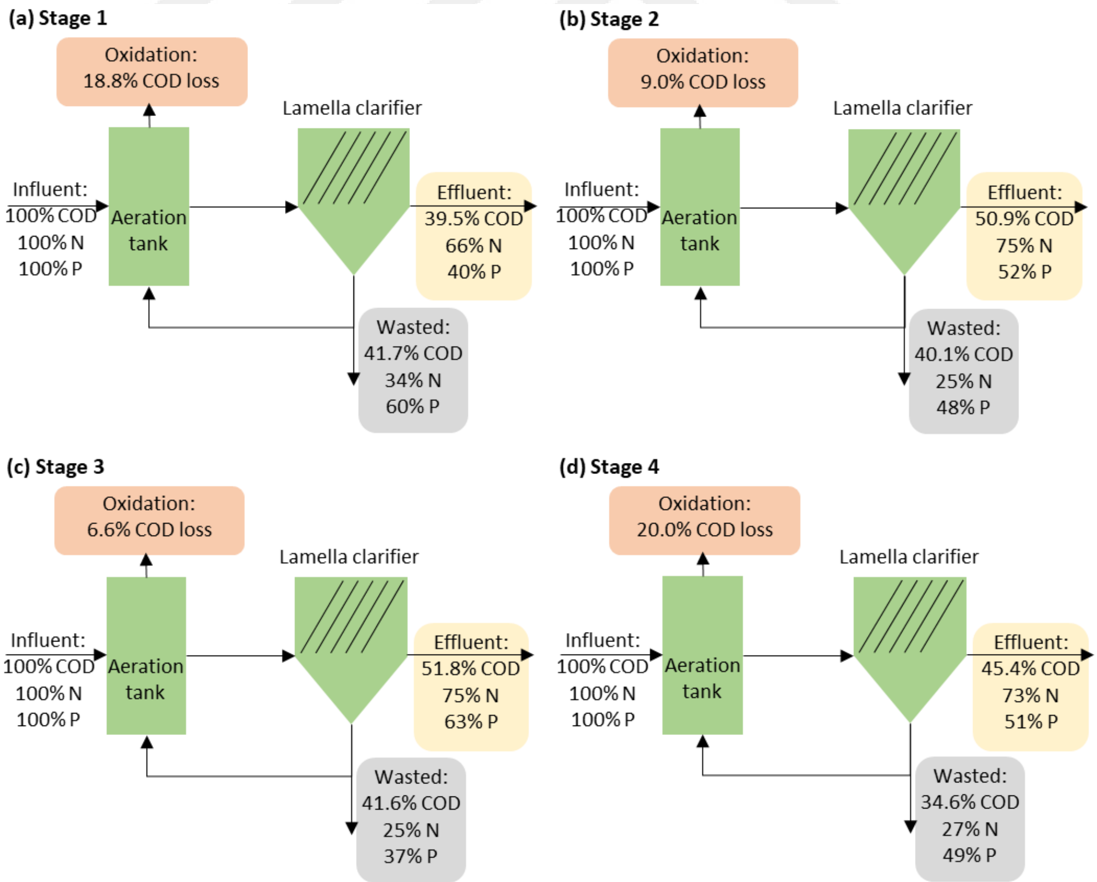

Figure 4.6 : COD, N, and P mass balances: (a) Stage 1, (b) Stage 2, (c) Stage 3, and (d) Stage 4.

4.2 Study 2 (Modelling of High-Rate Activated Sludge Process)

4.2.1 Performance of the pilot-scale HRAS system

Figure 4.7 illustrates the influent and effluent concentrations of tCOD, TN, and TP, as well as their respective removal efficiencies. The strength of the influent wastewater remained consistent during both the calibration and validation periods. Over the entire operational period, the removal efficiencies for tCOD, sCOD, and xCOD were measured as 64±3%, 42±6%, and 81±5%, respectively. The tCOD removal efficiency reported in the literature ranges from 52% to 87% (Ge et al., 2017; Cao et al., 2020; Taboada-Santos et al., 2020; Wett et al., 2020; Rey-Martinez et al., 2021). The sCOD removal efficiency of 48.2% reported by Cao et al. (2020) aligns with the results obtained in this study. For TN and NH_4-N, the removal efficiencies of the system were measured as 22±2% and 15.6±3%, respectively. Wett et al. (2020) achieved a 22% removal of NH_4-N, which is consistent with the findings of this study. However, Miller et al. (2016) reported a lower NH_4-N removal efficiency of 15%, while Cao et al. (2020) reported 9% NH_4-N removal, both lower than the results obtained in the pilot system. The TP removal efficiency of the pilot-scale HRAS system was 56±5%, which is notably higher than the values reported in the literature (2-34%) (Miller et al., 2016; Ge et al., 2017; Taboada-Santos et al., 2020). The significant TP removal efficiency achieved in the pilot plant could be attributed to the precipitation of phosphate salts, such as calcium phosphate, facilitated by the presence of calcium in the wastewater.

The DO concentration in the aeration tank remained constant at 0.48±0.03 mg/L, and the SRT variated within the range of 0.54±0.08 d during the monitoring period (as shown in Figure 4.7). Additionally, the temperature in the aeration tank increased from an average of 13.1±0.7 °C in the calibration period to 16.8±1.4 °C during the validation period.

4.2.2 Model calibration

4.2.2.1 Sensitivity analysis

To represent the SS model output group, the MLSS concentration was selected, while for the COD model output group, the effluent sCOD, xCOD, and cCOD were chosen. As for the N model output group, the effluent NH_4-N and TN concentrations were selected, and for the P model output group, the effluent sTP and xTP concentrations were chosen.

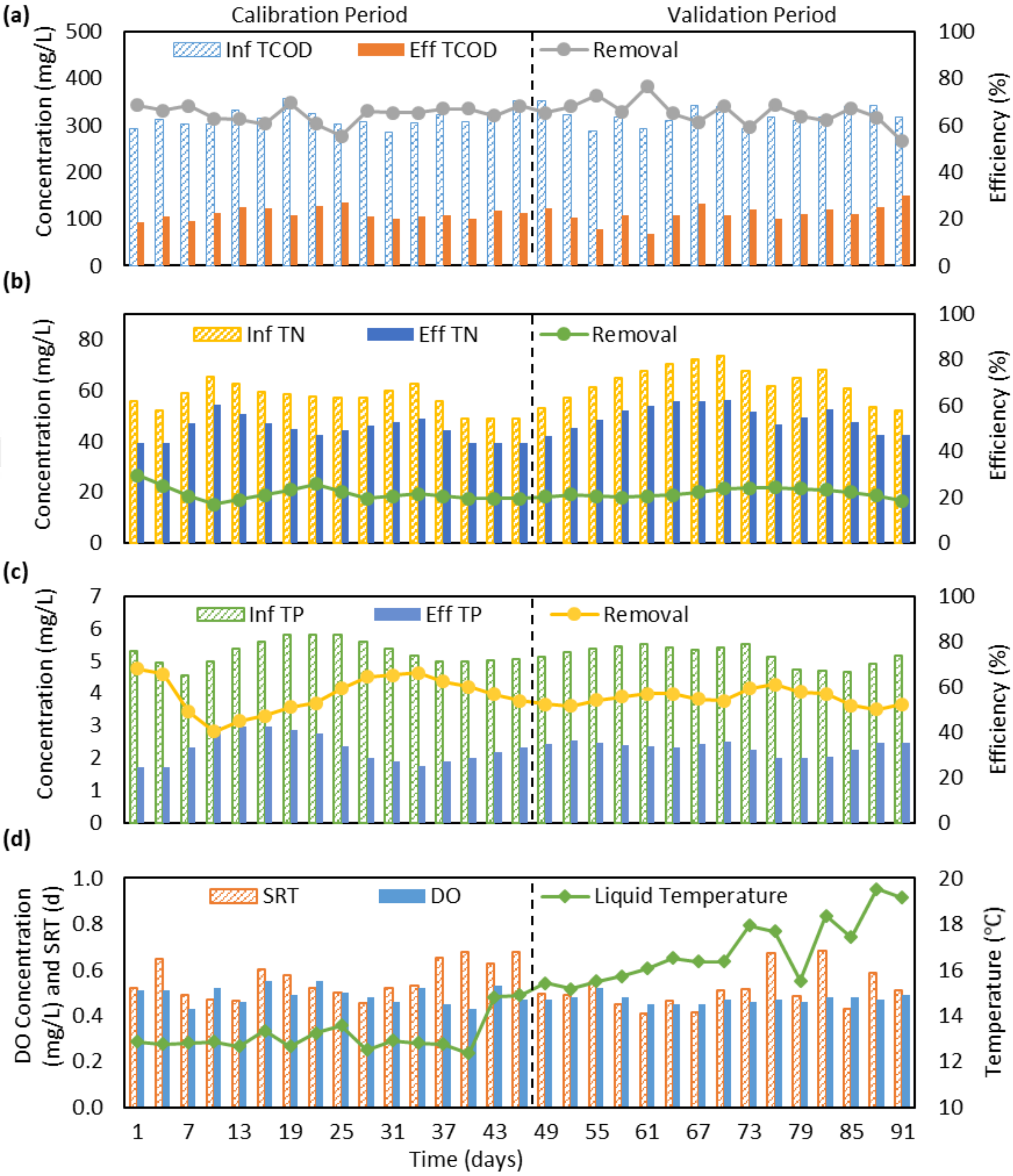

Figure 4.7 : Influent and effluent concentrations and removal efficiencies of (a) tCOD, (b) TN, (c) TP; (d) DO concentration, SRT value and temperature variations.

In Figure 4.8, the sensitivity indexes of each model parameter for the selected model outputs are presented. For the MLSS model output, Y_H was identified as the most influential parameter, followed by Y_{STO} and K_{S1}. The sorted sensitivity indexes varied for the COD model output group depending on the specific COD fraction. µ and YH were found to be the most influential parameters for effluent sCOD and xCOD, with index values exceeding 0.95. However, for cCOD, k_{ADS} (was determined to be more influential than μ. Under the N model outputs, the effluent TN concentration was found to be sensitive to more parameters compared to NH_4-N. On the other hand, the effluent sTP and xTP concentrations under the P model output group exhibited similar sensitivity to similar model parameters.

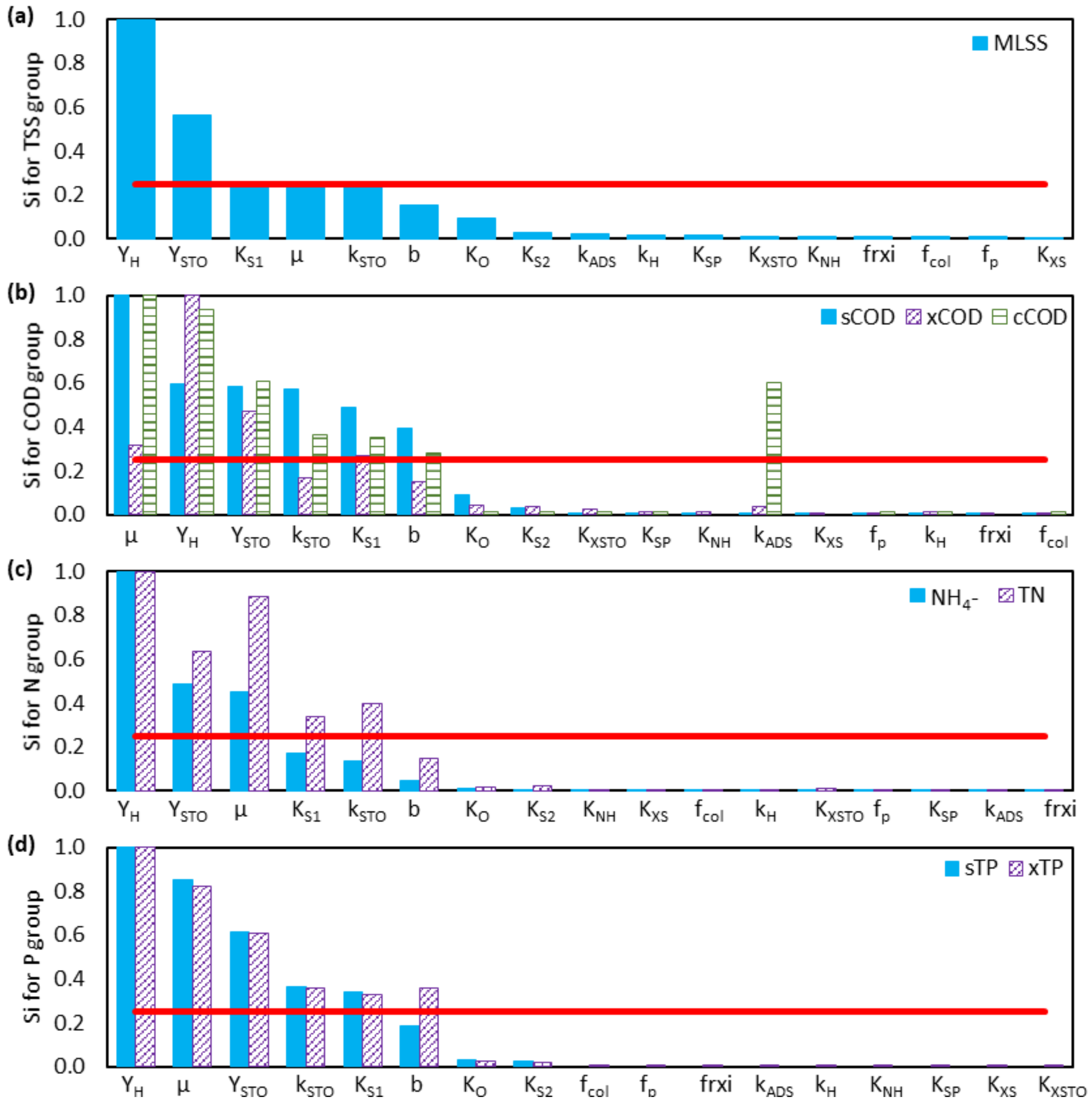

Figure 4.8 : Scaled sensitivity indexes for model outputs.

Table 4.2 provides a summary of the sorted sensitivity indexes for the most sensitive model parameters concerning the selected model outputs and overall model efficiency. Overall, μ was identified as the most influential parameter for the model's overall efficiency. However, Y_H had a greater impact on multiple model outputs compared to μ. This finding is consistent with the study by Fortela et al. (2019), which also reported Y_{STO}, Y_H, k_{STO}, b, and μ as the most sensitive parameters for the ASM3 model. Parameters with a sorted sensitivity index below 0.25 were deemed not influential for the HRAS model and were excluded from the final calibration step. The sensitivity analysis helped reduce the number of parameters requiring calibration and prevented overparameterization.

Table 4.2 : Sorted sensitivity indexes of the most sensitive model parameters.

Model parameters	MLSS	sCOD	xCOD	cCOD	NH_4-N	TN	sTP	xTP	Overall
μ	0.25	1.00	0.31	1.00	0.45	0.88	0.85	0.82	1.00
Y_H	1.00	0.60	1.00	0.93	1.00	1.00	1.00	1.00	0.60
Y_{STO}	0.56	0.58	0.47	0.61	0.49	0.64	0.61	0.61	0.59
k_{STO}	0.25	0.58	0.17	0.36	0.14	0.40	0.37	0.36	0.59
K_{S1}	0.26	0.49	0.27	0.36	0.17	0.34	0.34	0.33	0.49
b	0.16	0.40	0.15	0.28	0.05	0.15	0.18	0.36	0.40
k_{ADS}	0.03	0.00	0.04	0.61	0.00	0.00	0.00	0.00	0.00

4.2.2.2 Parameter estimation and calibration evaluation

Table 4.3 presents the model parameter values estimated using the "Optimizer Tool" in GPS-X. The estimated value for μ in this study is closer to the values reported in the ASM1 model and the model developed by Hauduc et al. (2019). However, to match the observed NH_4-N and sTP concentrations in the effluent, a higher Y_H value compared to other models listed in Table 4.3 was assigned. The estimated values for Y_{STO}, k_{STO}, and K_{XSTO} were similar to the values reported in the study by Makinia et al. (2006) and the ASM3 model. Conversely, a higher parameter value for K_{S1} was required to elevate the effluent sCOD concentrations to the observed values.

Figure 4.9 illustrates the comparison between the model outputs and the observed data for both the calibration and validation periods. Lower MAE and RMSE values indicate a better fit, but what is considered acceptable varies depending on the data scale and context. To standardize the evaluation, the MAE and RMSE values were normalized by dividing them by the average observed values for the corresponding model output. If the normalized MAE and RMSE values exceeded 90%, they were considered to have good accuracy, while values above 70% were considered to have medium accuracy. Based on the normalized MAE as a measure of goodness-of-fit, the model demonstrated good accuracy in estimating MLSS and TCOD. The normalized MAE values for all model outputs during the calibration and validation periods ranged from 66 to 94 and 63 to 91, respectively, except for CCOD. The lowest efficiency was observed for CCOD due to the model consistently underestimating this parameter. When considering the normalized RMSE, the model only showed good accuracy for

MLSS during the calibration period. The normalized RMSE values for other model outputs might have been adversely affected by outliers. RMSE is more sensitive to extreme errors compared to MAE because it squares the errors initially, penalizing large errors more heavily. This sensitivity to extreme errors could explain the discrepancy in performance between the two metrics. In conclusion, the calibrated HRAS model successfully captures the dynamic behaviors of the pilot-scale HRAS system.

Table 4.3 : Estimated model parameters for model calibration and comparison of them with the literature.

Symbol	Unit	ASM1	ASM3	Karahan et al. (2006)*	Makinia et al. (2006)	Smitshuijzen et al. (2016)	Hauduc et al. (2019)**	This study
μ	1/d	6	2	3	1.4-4.0	12	2-6	5.6
Y_H	g COD/ g COD	0.67	0.63	0.73	0.63	0.5	0.67-0.6	0.75
Y_{STO}	g COD/ g COD	-	0.85	0.91	0.85-0.95	-	-	0.95
k_{STO}	1/d	-	5	25	4.0-5.2	-	-	5.1
K_{S1}	g COD/m^3	20	2	20	2	4	5-0.5	29.6
b	1/d	0.62	0.2	0.1	0.62	0.6	0.2-0.6	0.62
k_{ADS}	1/d	-	-	0.62	0.14-2.8***	-	-	0.17
K_{XSTO}	g COD/m^3	-	1	0.4	0.1-3.0****	-		1

** Experiments with starch.*
*** Given for ordinary and adsorptive heterotrophs, respectively.*
**** m^3/g COD d.*
***** g COD/g COD.*

Table 4.4 : The average magnitude of the errors for the model calibration and validation.

Model output	MAE (mg/L)		RMSE (mg/L)		Average Observed Value (mg/L)		Normalized MAE (%)		Normalized RMSE (%)	
	Cal.	Val.	Cal.	Val.	Cal.	Val.	Cal.	Val.	Cal.	Val.
MLSS	204	244	250	292	644	740	94	91	92	89
tCOD	14	16	17	21	56	38	90	90	88	86
sCOD	16	20	20	24	40	53	82	78	79	73
cCOD	7	8	11	11	28	24	10	26	-46	-4
xCOD	10	10	12	12	48	39	78	79	73	76
TN	5.7	5.9	7.6	7.2	15.2	14.1	88	90	86	87
SNH	4.7	5.5	5.1	6.8	14.3	18.5	87	87	84	83
TP	0.4	0.5	0.6	0.6	1.3	1.0	84	87	81	83
sTP	0.4	0.4	0.4	0.4	1.1	1.0	72	63	68	55
xTP	0.5	0.6	0.6	0.6	1.6	0.7	66	78	57	71

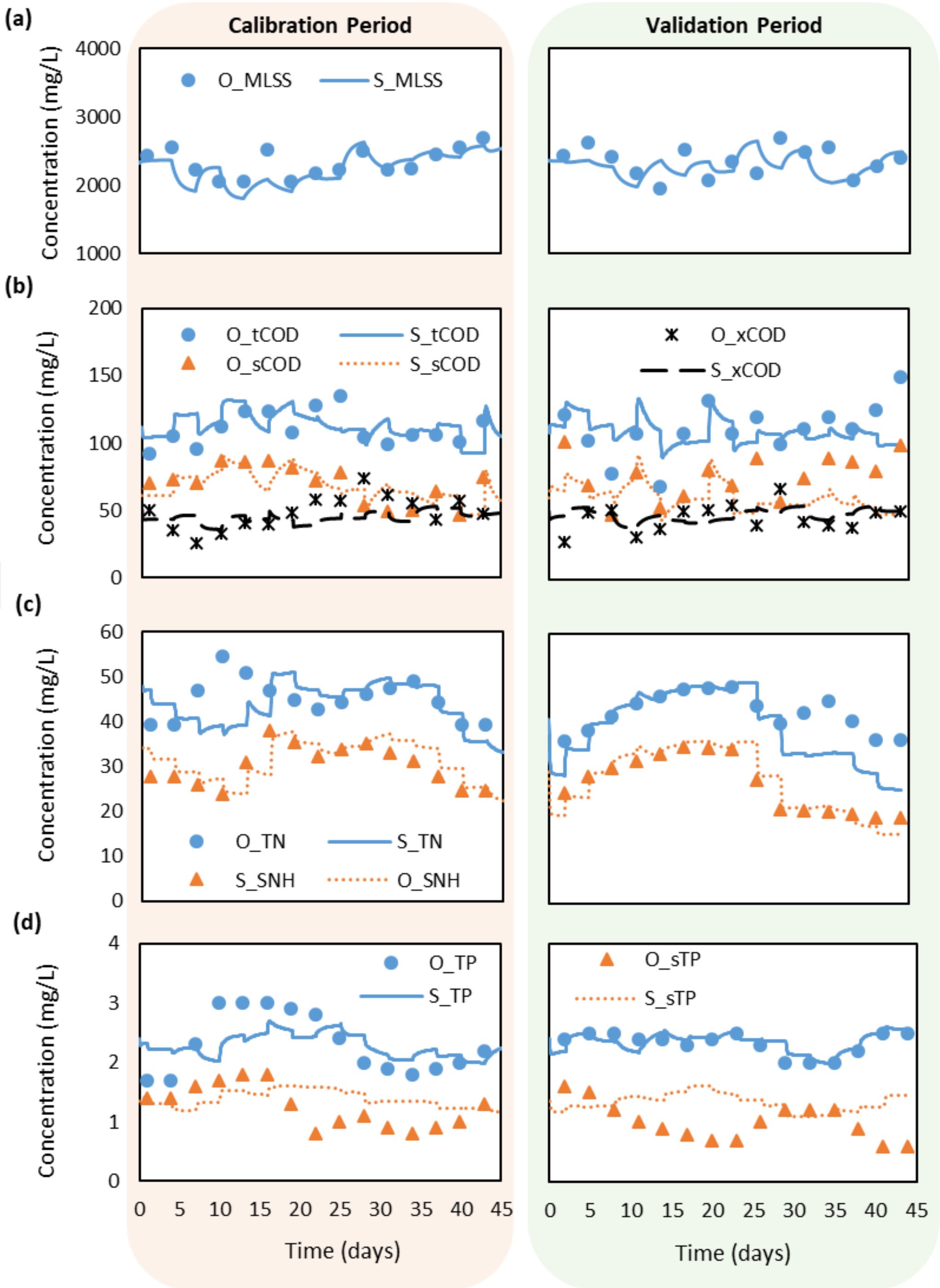

Figure 4.9 : Comparison of observed data and simulation results of (a) MLSS, (b) COD fractions, (c) N fractions, and (d) P fractions for calibration and validation periods.

4.2.2.3 Uncertainty analysis

The combination of uncertainty analysis and sensitivity analysis is a valuable approach to enhance the robustness of a model while reducing the complexity of calibration (Mannina et al., 2018). In Figure 4.10, uncertainty bands, calibrated model output, and observed data profiles are presented for MLSS, sCOD, SNH, and sTP. These model outputs were chosen to represent each model output group. The width of the uncertainty band varies based on the number of sensitive parameters and their corresponding sensitivity index magnitudes for the specific model output (Mannina et al., 2012). Specifically, the widest uncertainty band was observed for sCOD concentration, which was influenced by six model parameters (μ, Y_H, Y_{STO}, k_{STO}, K_S, and b) with sorted sensitivity indexes ranging from 0.4 to 1. On the other hand, even though the same model parameters were influential for sTP, their sorted sensitivity indexes ranged from 0.18 to 1, resulting in the thinnest uncertainty band for this model output.

A high percentage of observed data (90% for MLSS, 97% for sCOD, and 84% for SNH falls within the uncertainty band, indicating the robustness of the model for these model outputs. However, the calibrated model profile for sCOD tends to be lower than the observed data, suggesting an overestimation of this parameter. Similarly, the model underestimates the effluent SNH concentration. This implies a trade-off between the model efficiencies of these two outputs, as the same model parameters influence both. The percentage of observed data within the uncertainty band for sTP is lower (27%), indicating the need for improvement in simulating the dynamic behavior of sTP in the effluent. The influential model parameters for sTP are also influential for other model outputs, leading to a trade-off between their efficiencies. Although the HRAS model was calibrated with high efficiency overall, improving the efficiency for sTP would require calibrating other parameters that are not correlated with other outputs. However, these parameters (K_O and K_{S2}) have very low sorted sensitivity indexes (0.03 and 0.02), making it unlikely that calibrating them would significantly increase the efficiency for sTP. The higher variation in the observed data profile for sTP may be attributed to changes in wastewater characteristics throughout the monitoring period, which are not reflected in the model input data, particularly the P fractions of SS and SI. Despite assuming these fractions as 0, this assumption may be the reason for the low percentage of observed data falling within the uncertainty band. Another reason for the low prediction efficiency of sTP in the effluent could be the precipitation of phosphate salts, which was not included in the model.

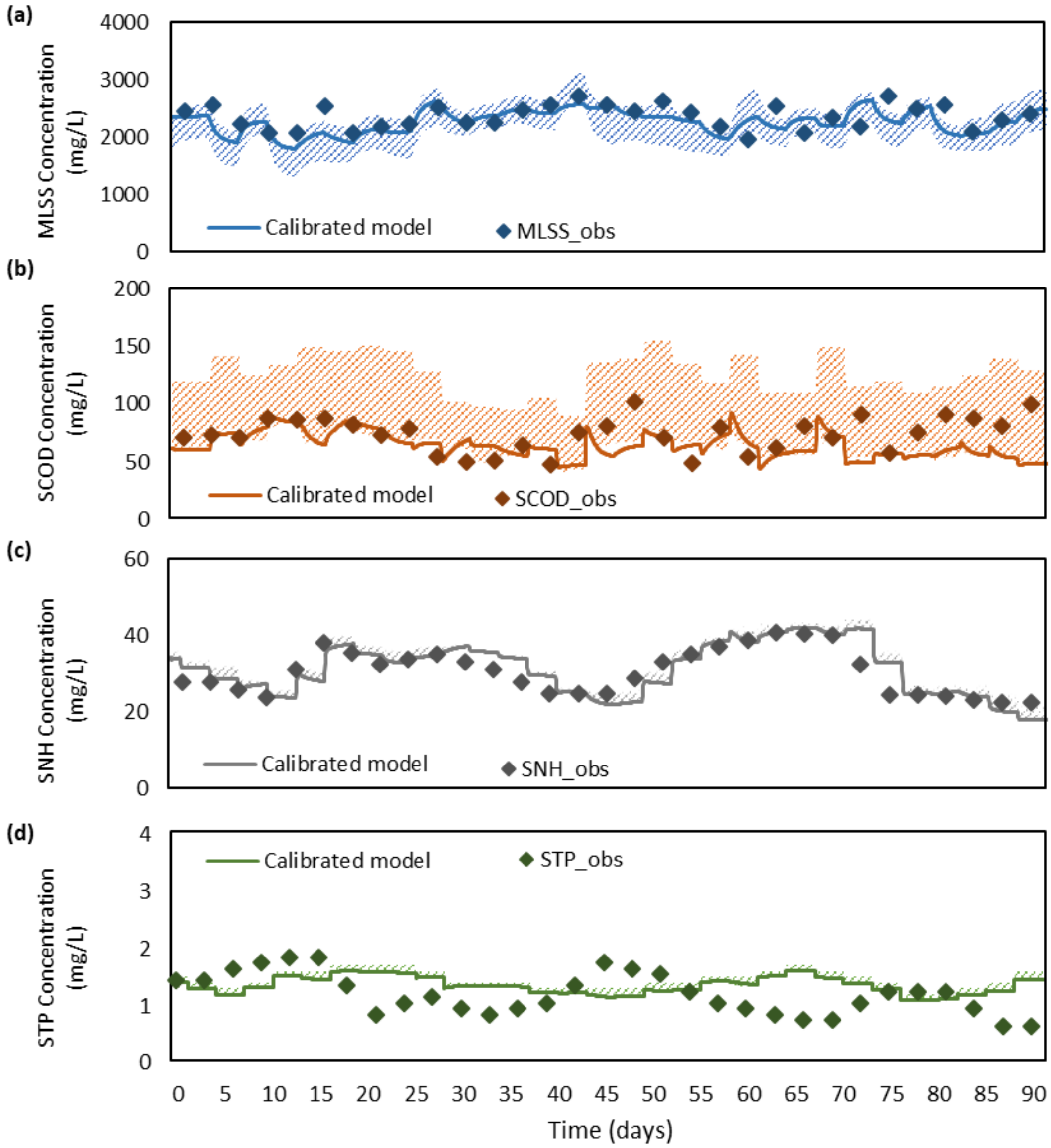

Figure 4.10 : Uncertainty bands and calibrated model output profiles.

4.3 Study 3 (Integration of Membrane Filtration and The HRAS Process to Produce Industrial Water)

4.3.1 Experimental studies

4.3.1.1 Pre-treatment experiment

The effluent of the aerated grit chamber of a full-scale WWTP underwent pre-treatment, namely DMF via MF and UF membranes and the HRAS process. Figure 4.11 shows the flux variations of the MF and UF membranes during the operation. Due to a 90% recovery rate for each membrane, the UF membrane required a longer operation time to collect the same volume of permeate than the MF membrane. The average flux for the MF membrane was 78±13 L/m^2/h, while for the UF membrane, it was 47±9 L/m^2/h.

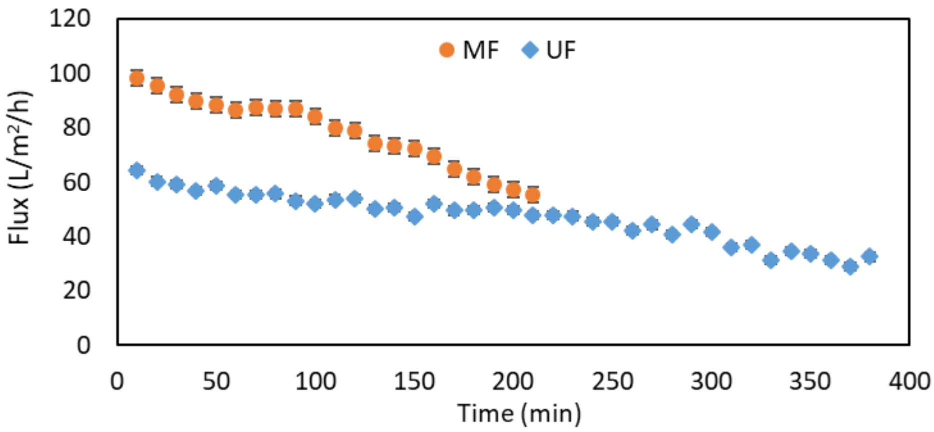

Figure 4.11 : Flux variations of MF and UF membranes.

Figure 4.12 illustrates the removal efficiencies achieved by different pre-treatment methods for conventional parameters, ions, and heavy metals. Among the alternatives, DMF via UF membrane demonstrated the highest treatment performance for each parameter, followed by DMF via MF membrane and the HRAS process (Figure 4.12). The effluent BOD_5 concentrations were 7.9±1.0 mg/L, 19.8±7.2 mg/L, and 108±12.1 mg/L for DMF via UF membrane, DMF via MF membrane, and the HRAS process, respectively. Both DMF via MF and UF membranes effectively removed TSS, with removal efficiencies exceeding 99% (permeate TSS concentrations were below 3 mg/L). Similarly, in a study by Lateef et al. (2013), DMF (via MF membrane) achieved TSS removal efficiencies of over 99% for the treatment of domestic wastewater with initial TSS concentrations of 129 and 411 mg/L. In contrast, the effluent from the HRAS system had a TSS concentration of 46±3 mg/L. The fecal coliform levels in the permeate of DMF via UF membrane were measured at 85 cfu/100 mL. For the permeate of DMF via MF membrane and the effluent from the HRAS process, the fecal coliform levels were 3.1×10^3 cfu/100 mL and 1.3×10^7 cfu/100 mL, respectively. The log removals of fecal coliform achieved by DMF via UF and MF membranes, and the HRAS process, were 5.5±0.2, 0.9±0.1, and 0.2±0.1, respectively. Consistent with this study, Capodaglio (2021) reported that filtration through UF and MF membranes resulted in log removals of bacteria ranging from 5-6 and 4-5, respectively. The pH values of the effluents from each pre-treatment method ranged between 7.4 and 7.9. DMF of raw municipal wastewater via UF membrane successfully produced reclaimed water suitable for use as cooling water, meeting the quality criteria outlined in the US

EPA water reuse guidelines (US EPA, 2012). However, the fecal coliform levels in the permeate of DMF via MF membrane exceeded the suggested guideline value of 200 cfu/100 mL. The HRAS process, with effluent fecal coliform, TSS, and BOD_5 values exceeding the guideline values (30 mg/L for TSS and BOD_5), did not meet the criteria for producing cooling water.

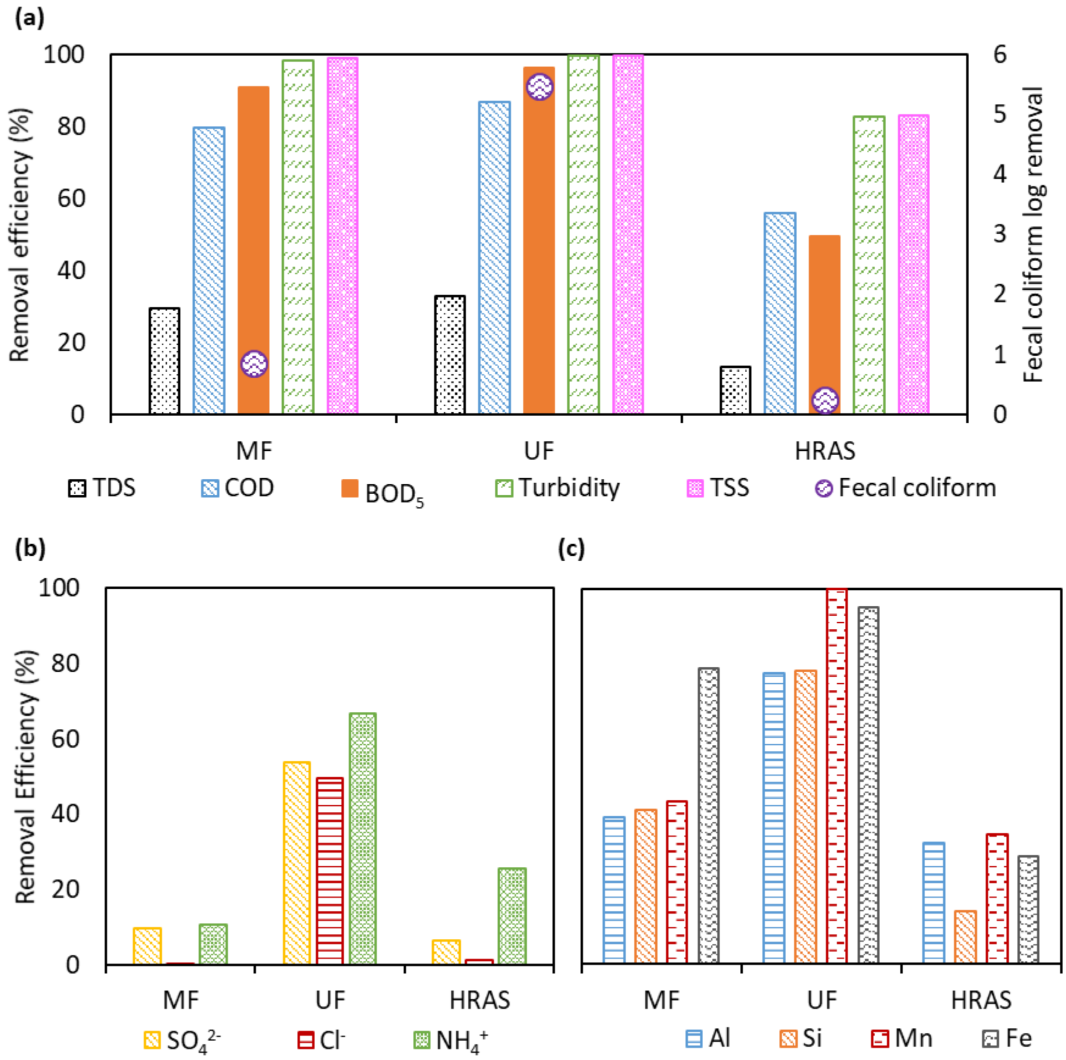

Figure 4.12 : Treatment efficiencies for different pre-treatment alternatives: (a) Conventional parameters; (b) Ions and (c) Heavy metals.

The TDS concentration in the raw wastewater (4,039±55 mg/L) was reduced to 2,706±58 mg/L, 2,850±411 mg/L, and 3,497±112 mg/L after undergoing DMF via UF and MF membranes, and the HRAS process, respectively. The TS concentrations measured after pre-treatment were below the recommended limit value of 70,000 mg/L for cooling tower systems with recirculating water (Cherchi et al., 2019). Turbidity levels in the effluents of DMF via UF and MF membranes, and the HRAS process were 1.1±0.2 NTU, 4.1±1.6 NTU, and 42.1±2.6 NTU, respectively. The literature on DMF of municipal wastewater has reported turbidity levels below 2 NTU for MF permeate (Kim et al., 2007) and below 0.2 NTU for UF permeate (Ravazzini et al., 2005). The slightly higher turbidity values observed in this study may be attributed to the characteristics of the raw wastewater. For instance, Ahn and Song (1999) and Perez et al. (2022) reported turbidity levels of 4.2 NTU in the permeate of MF and 2.98 NTU in the permeate of UF, respectively, after filtration of secondary treatment effluent.

The COD concentrations in the permeate of the DMF process using UF and MF membranes were measured at 55 mg/L and 84 mg/L, respectively. These values align with the recommended COD concentration of <100 mg/L for cooling tower recirculating waters (Cherchi et al., 2019). Jin et al. (2016) reported a COD removal efficiency of 60% using direct MF filtration for domestic wastewater, while Ravazzini et al. (2005) achieved a COD removal efficiency of 40% using direct UF filtration for municipal wastewater. It is noteworthy that the COD removal efficiencies obtained in this study for DMF via UF and MF membranes were higher than those reported in other studies. However, as pointed out by Ravazzini et al. (2005), the efficiency of membrane filtration in removing turbidity, COD, BOD_5, and TDS is heavily influenced by the particulate content of the influent, resulting in varying treatment efficiencies for different wastewater characteristics. For the HRAS system, the COD concentration in the effluent was measured at 184 mg/L.

The HRAS process has lower NH_4^+ removal efficiency compared to CAS systems, as the primary nitrogen removal mechanism in HRAS is assimilation rather than nitrification (Ge et al., 2017). While ammonia can be corrosive, particularly for copper alloy-based cooling systems, it does not pose a corrosive effect on cooling systems made of stainless steel (San Diego County Water Authority, 2009). Therefore, if copper-based alloys are used in cooling systems, the target ammonia concentration for reclaimed water is set to <2 mg/L (Cherchi et al., 2019). Mn was not detected in the permeate of DMF via UF, while its concentration in the permeate of DMF via MF was measured at 0.039±0.007 mg/L, and in the HRAS effluent, it was 0.045±0.016 mg/L. Mn can cause corrosion in stainless steel components of cooling systems. However, the measured Mn concentrations in the effluents of the pre-treatment alternatives were below the suggested concentration (0.5 mg/L) for reclaimed water (Cherchi et al., 2019). The HRAS system showed the lowest Si removal among the pre-treatment alternatives (Figure 4.12); nevertheless, the Si concentration in the effluent of each pre-treatment alternative was below the suggested limit (50 mg/L) for once-through cooling towers (Tchobanoglous et al., 2003). Moreover, the Al and Fe concentrations in the raw wastewater (Table 3.4) were also below the recommended concentrations (1 mg/L for Al and 0.5 mg/L for Fe) for make-up water in cooling tower recirculation systems (Cherchi et al., 2019).

4.3.1.2 Final-treatment experiments

The NF and RO membranes were fed with the effluent from the DMF via MF and UF, and HRAS processes. In the NF system, the average flux values for C1, C2, and C3 were 41±2.5 $L/m^2/h$, 42±2.9 $L/m^2/h$, and 37±1.9 $L/m^2/h$, respectively. In C3, where the TSS concentration in the HRAS effluent was higher (46±3 mg/L) compared to the DMF systems (<3 mg/L for each), a 10% reduction in the NF membrane flux was observed compared to the permeate from C1. For the RO filtration, the average flux values for C4, C5, and C6 were 6.8±0.4 $L/m^2/h$, 7.7±0.6 $L/m^2/h$, and 6.1±0.2 $L/m^2/h$, respectively. Due to the smaller pore size of the RO membrane compared to the NF membrane, the flux in the RO system was significantly lower than that in the NF system. The flux in the RO system fed with DMF via MF permeate was 13% lower, and for the RO system fed with HRAS effluent, it was 22% lower compared to the RO system fed with DMF via UF permeate.

Each treatment configuration successfully met the criteria for producing cooling tower makeup water according to the US EPA (2012) water reuse guideline (Table 4.5). Figure 4.13 illustrates the removal efficiencies of ions and heavy metals for each treatment configuration. Among the configurations, C3 (HRAS+NF) achieved the lowest removal efficiency for ions and heavy metals. The concentrations of NH_4^+, Cl^-, and $SO4^{2-}$ in the permeate of C3 were measured as 17.7±0.4 mg/L, 592±83 mg/L, and 41.5±0.3 mg/L, respectively. However, even these ion concentrations in the permeate of C3 were below the suggested limits (Cl^-: 600 mg/L; SO_4^{2-}: 680 mg/L; NH_4^+ concentration is not critical if other parameters meet the recommendations for cooling waters (Tchobanoglous et al., 2003). The Cl^- removal efficiencies of the NF membranes were found to be 91.9%, 91.1%, and 91.5% in C1, C2, and C3, respectively. Similarly, Lin Lin et al. (2009) reported a Cl- removal efficiency of 94% using the NF90 membrane filtration. Regarding heavy metals, all treatment configurations produced effluents free of heavy metals, except for the NF permeate in C3. The highest Si and Al concentrations were detected in the permeate of C3, with values of 1.99±0.09 mg/L and 0.044±0.001 mg/L, respectively. The total hardness concentrations after NF membrane filtration in C1, C2, and C3 were measured as 42±3 mg $CaCO_3$/L, 39±2 mg $CaCO_3$/L, and 45±4 mg $CaCO_3$/L, respectively, resulting in NF removal efficiencies above 92% for all cases.

Table 4.5 : Permeate qualities for different treatment alternatives.

Parameters	Units	C1	C2	C3	C4	C5	C6	Recommendations for water reuse in cooling towers *
TSS	mg/L	<2	<2	8.2±0.8	<2	<2	<2	30
BOD_5	mg/L	2.3±0.3	<2	4.5±0.4	<2	<2	<2	30
Fecal coliform	cfu/100 mL	ND**	ND**	ND**	ND**	ND**	ND**	200
pH	-	8.0±0.1	7.3±0.1	8.0±0.2	7.9±0.2	7.3±0.1	7.9±0.1	6-9

** US EPA (2012)*
*** ND: Not detected*

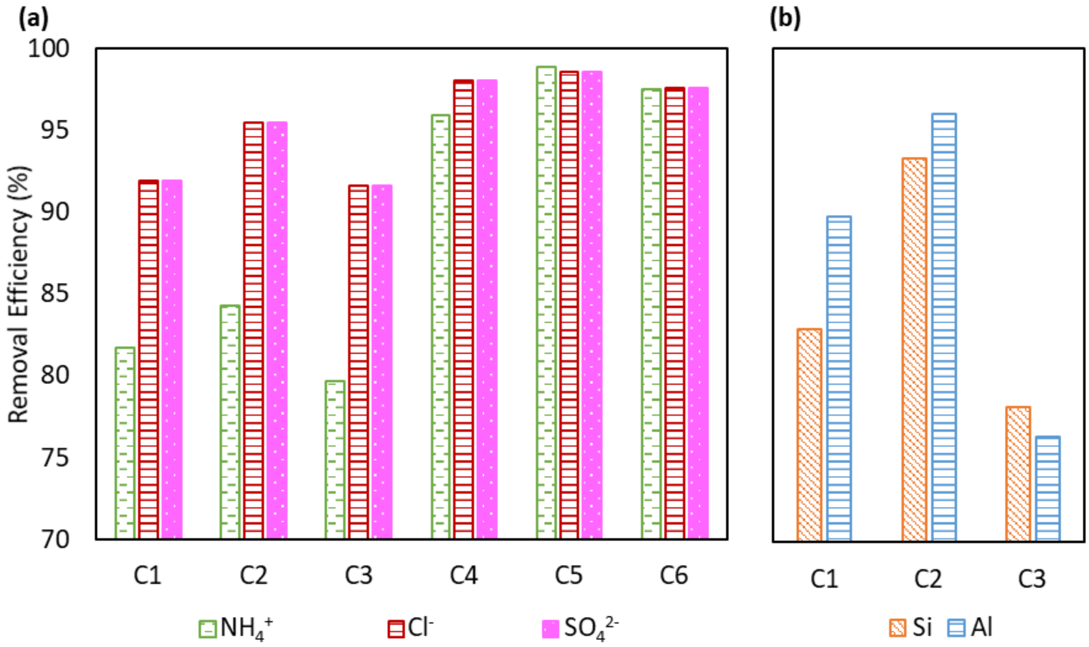

Figure 4.13 : Treatment efficiencies for different treatment alternatives: (a) Ions; (b) Heavy metals (Si and Al were not detected in the permeate of C4, C5, and C6).

4.3.2 Economic evaluation

The costs associated with six treatment configuration scenarios (Figure 3.7) were compared for treating raw wastewater to produce cooling tower makeup water. It was assumed that the waste sludges produced from DMF trials and HRAS were sent to anaerobic digestion for biogas production and the costs related to sludge treatment units were not considered. Capital and O&M costs were estimated for both pre-treatment options (DMF via MF and UF membranes, and HRAS process) and final treatment alternatives (NF and RO). A recovery rate of 90% was selected for DMF via MF and UF membranes, while the HRAS system had a recovery rate of 98%. For the final-treatment using NF and RO membranes, a water recovery rate of 75% was chosen. The permeate flow rate for each configuration was set at 432 m^3/day (5 L/s).

The present capital costs for a plant operation period of 30 years were calculated as 222,222 € for DMF via MF, 246,914 € for DMF via UF, and 104,069 € for the HRAS process. Diamantis et al. (2014) estimated the capital cost of an HRAS system with a capacity of 96 m^3/d (6.7 times less than the conceptual HRAS system used in this study) at 25,000 €. The O&M costs for DMF via MF and UF membranes were estimated at 56,837 €/year and 63,152 €/year, respectively. In contrast, the O&M cost for the HRAS process was 5,873 €/year. Due to lower energy and maintenance requirements compared to membrane filtration, the O&M cost of the HRAS system was estimated to be almost 10 times lower than that of direct filtration. The total unit cost (annual capital + O&M) for the pre-treatment options of DMF via MF and UF membranes, and HRAS process, were estimated to be 0.51 €/m^3 of treated wastewater, 0.56 €/m^3 of treated wastewater, and 0.11 €/m^3 of treated wastewater, respectively.

The present capital costs for the NF membrane systems in C1, C2, and C3 were calculated to be the same, 154,400 €. For the systems utilizing RO as the final treatment, the present capital costs for C5, C4, and C6 were determined to be 160,834 €. The O&M costs for the NF membrane systems (C1, C2, and C3) were estimated at 49,196 €/year. Similarly, the O&M costs for the RO membrane systems (C5, C4, and C6) were calculated to be 51,246 €/year.

Figure 4.14 provides a summary of the annual costs in euros (€/year), while Figure 4.15 (a) illustrates the unit annual capital costs (€/m^3 wastewater/year), and Figure 4.15 (b) shows the unit O&M costs (€/m^3 wastewater/year) for each treatment scenario.

Among the scenarios, C3 had the lowest total annual cost at 81,932 €/year, while the highest total annual cost was estimated for C5 at 156,775 €/year (Figure 4.15 (a)).

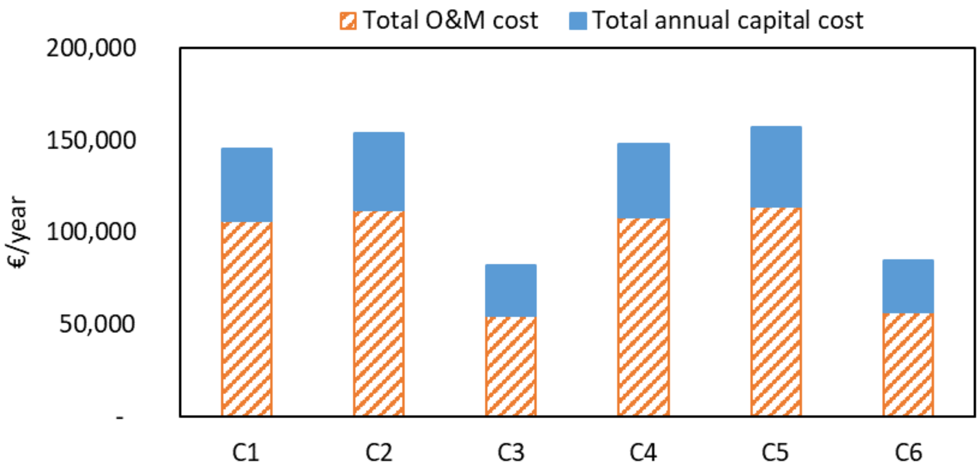

Figure 4.14 : Total Q&M and annual capital costs of treatment configurations.

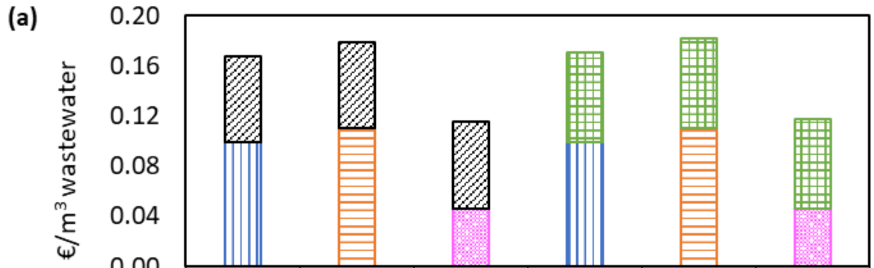

	C1	C2	C3	C4	C5	C6
RO unit annual capital cost	-	-	-	0.072	0.072	0.072
NF unit annual capital cost	0.069	0.069	0.069	-	-	-
HRAS unit annual capital cost	-	-	0.046	-	-	0.046
UF unit annual capital cost	-	0.110	-	-	0.110	-
MF unit annual capital cost	0.099	-	-	0.099	-	-

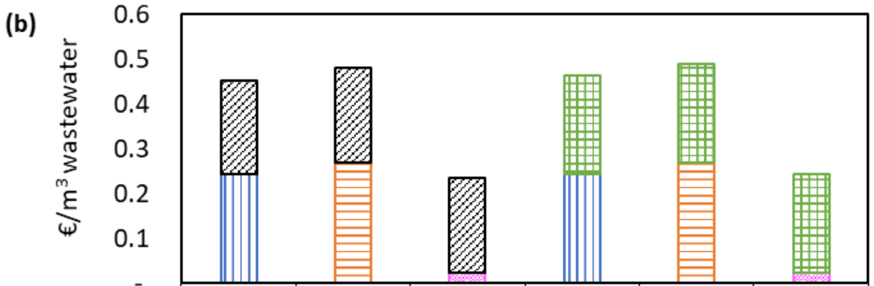

	C1	C2	C3	C4	C5	C6
RO unit O&M cost	-	-	-	0.22	0.22	0.22
NF unit O&M cost	0.21	0.21	0.21	-	-	-
HRAS unit O&M cost	-	-	0.025	-	-	0.03
UF unit O&M cost	-	0.27	-	-	0.27	-
MF unit O&M cost	0.24	-	-	0.24	-	-

Figure 4.15 : Unit annual capital and O&M costs fraction of each treatment configuration.

The production cost of cooling tower makeup water in C3 was determined to be 0.38 €/m^3 wastewater (0.52 €/m^3 reclaimed water). The HRAS process exhibited lower pre-treatment performance, leading to increased costs for the subsequent final treatment. However, the overall cost of treatment configurations incorporating HRAS appeared to be lower compared to other alternatives, as the HRAS process costs were lower than DMF via MF and UF membranes. Kehrein et al. (2021) and Perez et al. (2022) estimated the treatment costs of secondary treatment effluent using UF+RO configurations as 0.67 €/m^3 reclaimed water (Capacity: 2,400 m^3/day; 20 years of operation) and 0.57 €/m^3 feed water (Capacity: 480 m^3/day; 12 years of operation), respectively. The treatment cost of C5 in this study was estimated to be 0.67 €/m^3 wastewater (0.99 €/m^3 reclaimed water). The cost of secondary treatment (CAS process) typically ranges from 0.1 to 3.0 €/m^3 wastewater (Ozgun et al., 2021). Since HRAS systems have a footprint about 6 times smaller (HRT of the HRAS process: 75 min; HRT of the CAS: 8 hours) and a DO concentration in the aeration tank about 4 times lower (DO of the HRAS process: 0.5 mg/L; DO of the CAS: 2 mg/L) compared to CAS systems (secondary treatment), employing the HRAS process before the final treatment would offer financial advantages. This study demonstrates that the HRAS+NF treatment configuration shows promise in terms of water quality and economic evaluation for producing suitable cooling tower makeup water.

4.4 Study 4 (Alternative Post-Treatment Options to The HRAS Process for Producing Irrigation Water)

4.4.1 Membrane filtration experiments

The UF membrane filtration of the HRAS process effluent exhibited the highest removal efficiency for TSS, turbidity, BOD_5, NH_4-N, and PO_4-P among all post-treatment alternatives (Figure 4.16). The TSS concentration in the permeate of UF membrane filtration was 3.0±0.6 mg/L (93% removal efficiency), while it was 8.1±1.1 mg/L (82% removal efficiency) in the permeate of MF membrane filtration. Previous studies by Michael-Kordatou et al. (2015) and Perez et al. (2022) reported TSS concentrations of 3-9 mg/L and 0-6 mg/L, respectively, in the permeate of UF membranes used for filtering secondary effluents. Turbidity levels measured in the permeates of UF and MF membranes were 2.6±0.1 NTU and 7.1±1.2 NTU, respectively. Ahn and Song (1999) observed turbidity levels of 0-4.2 NTU in the permeate of MF membranes used for treating secondary effluents. For UF membrane permeate turbidity, Cosenza et al. (2022) and Perez et al. (2022) reported values of <1 NTU and 0-2.98 NTU, respectively. BOD_5 concentrations in the permeate of UF and MF membranes were 3.4±0.2 mg/L (97% removal efficiency) and 11±2.6 mg/L (91% removal efficiency), respectively. Cosenza et al. (2022) reported BOD_5 concentrations in the range of 4.1-8.9 mg/L in the permeate of UF membranes. NH_4-N and PO_4-P concentrations in the permeate of the UF membrane were 20.9±2.4 mg/L (33% removal) and 0.85±0.2 mg/L (29% removal), respectively. Perez et al. (2022) observed 28% NH_4-N removal through UF membrane filtration of secondary effluent. Filtration via the MF membrane resulted in NH_4-N concentrations of 27.5±2.7 mg/L (12% removal) and PO_4-P concentrations of 0.97±0.10 mg/L (19% removal) in the permeate. The results of UF and MF membrane filtrations of the HRAS process effluent demonstrated similar removal efficiencies for TSS, turbidity, BOD_5, NH_4-N, and PO_4-P compared to the filtration of secondary treatment effluents reported in the literature.

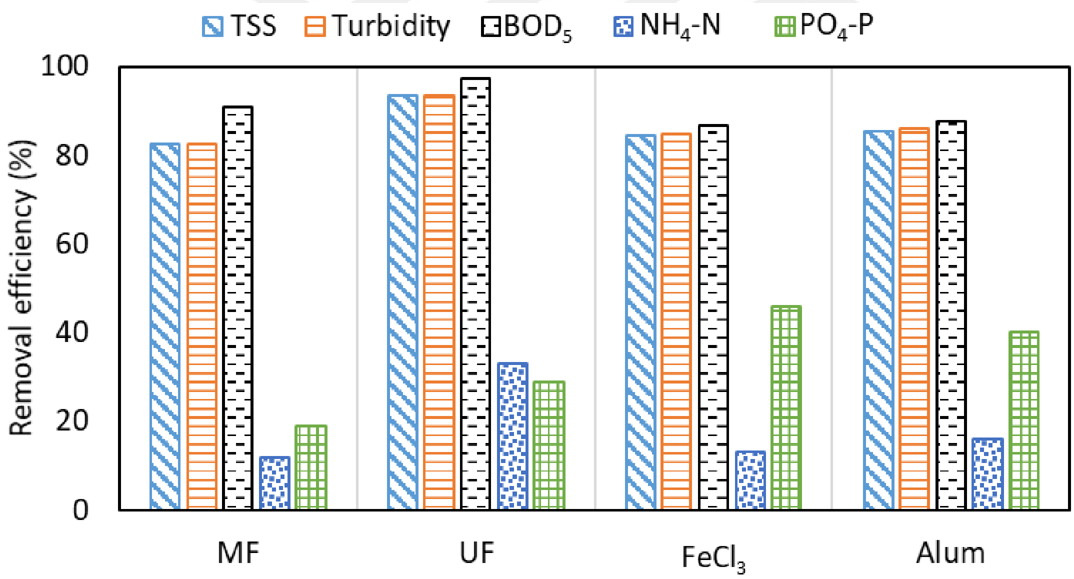

Figure 4.16 : The performance of membrane filtration via MF and UF membranes and coagulation with $FeCl_3$ and alum.

The UF and MF membranes exhibited *E. coli* capture efficiencies of log 4.3 (168±18 cfu/100 mL of *E. coli* count in the permeate) and log 3.1 (2195±50 cfu/100 mL of *E. coli* count in the permeate), respectively. Previous studies by Gomez et al. (2006), Falsanisi et al. (2010), and Perez et al. (2022) reported *E. coli* counts of <100 cfu/100 mL in the permeate of UF membranes used for treating secondary effluents. However, similar to the findings of this study, Atanasova et al. (2017) reported an *E. coli* count of 1.1×10^2 cfu/100 mL in the permeate of a UF membrane used for treating hotel greywater containing >106 cfu/100 mL of *E. coli*. The flux values for filtration via the MF and UF membranes were 143±3 L/m^2/h and 64±4 L/m^2/h, respectively.

4.4.2 Coagulation tests

Figure 4.17 shows the turbidity values and TSS concentrations measured in the supernatant during jar tests. When $FeCl_3$ was dosed at 30 mg/L, turbidity of 7 NTU was achieved; however, the TSS concentration exceeded 10 mg/L. Consequently, the $FeCl_3$ dose was increased to 50 mg/L. To achieve turbidity and TSS values lower than 10 NTU and 10 mg/L, respectively, an alum dose of 100 mg/L was selected.

Coagulation with a dose of 50 mg/L of $FeCl_3$ resulted in a TSS concentration of 7.1±2.0 mg/L, turbidity of 5.8±1.2 NTU, BOD_5 concentration of 16±4.0 mg/L, NH_4-N concentration of 27.1±3.2 mg/L, and PO_4-P concentration of 0.65±0.10 mg/L in the supernatant. Coagulation with a dose of 100 mg/L of alum yielded similar results except for PO_4-P (Figure 4.16): TSS concentration of 6.7±1.4 mg/L, turbidity of 6.5±0.9 NTU, BOD_5 concentration of 15±4.4 mg/L, and NH_4-N concentration of 26.2±4.7 mg/L. The PO_4-P concentration in the supernatant of coagulation with alum was 0.72±0.12 mg/L. Coagulation with $FeCl_3$ resulted in slightly higher removal of PO_4-P (46%) compared to coagulation with alum (40%).

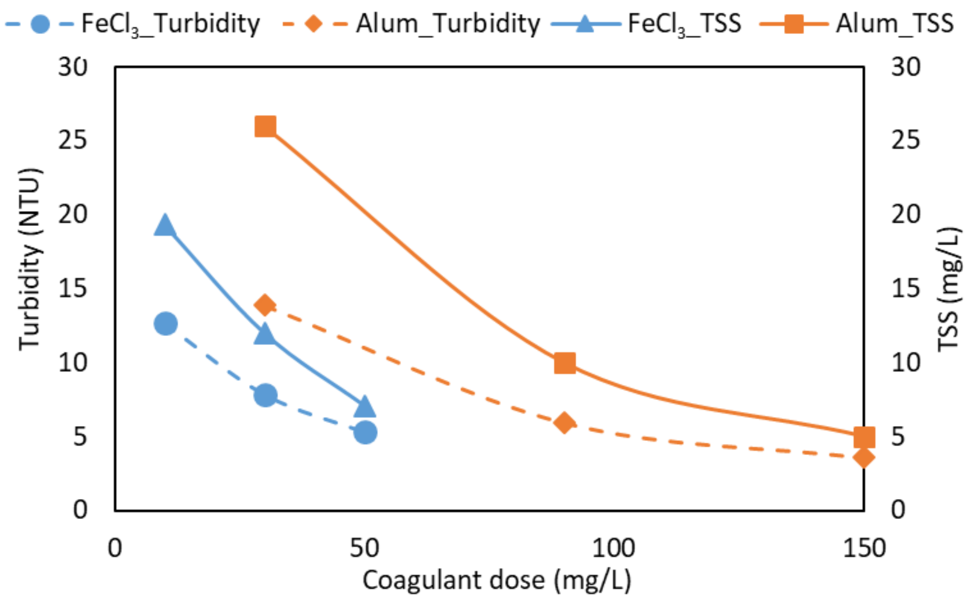

Figure 4.17 : Turbidity values and TSS concentrations observed in the supernatant of jar tests with different doses of (a) $FeCl_3$ and (b) alum.

The sludge resulting from post-treatment involving iron (A3) and alum (A4) precipitation should be managed carefully. After dewatering the iron sludge and alum sludge, dewatering liquor and solids should be handled separately. Nitrogen and phosphorus in the dewatering liquor can be captured by crystallization via the formation of struvite (Ping et al., 2016). The remaining liquor can be sent back to the beginning of the HRAS process. The iron-containing dewatering liquor in A3 can be sent to the anaerobic digester since iron in the dewatering liquor may be beneficial to biogas production (Salehin et al., 2020). Dewatered iron-containing sludge can be used to produce construction material (Koppel et al., 2017) or iron-rich biochar (wu et al., 2020). Liang and Zhou (2022) noted that it is essential to conduct extensive life cycle assessments (LCA) and evaluate life cycle costs (LCC) on a large scale to expedite the advancement of iron sludge reutilization. Dewatered alum-containing solids can be utilized for soil improvement (Mahdy et al., 2009; Dassanayake et al., 2015). Concerns regarding aluminum toxicity or groundwater leaching were found to be negligible within the typical agricultural pH range of 6-9, as aluminum solubility increases at lower pH levels (Goldbold et al., 2003). Nevertheless, a comprehensive analysis of heavy metals should be conducted as stated by Dassanayake et al. (2015).

4.4.3 UV disinfection

The permeates of UF membrane filtration (A2) required a UV dose of 10 mW s/cm^2 to achieve an *E. coli* count lower than 10 cfu/100 mL, which meets the criteria for Class A reclaimed water. When the supernatants of $FeCl_3$ and alum coagulation were disinfected by UV, *E. coli* reductions of >3.5 log were observed. A similar study by Nasser et al. (2006) also achieved >3 log reduction of *E. coli* in secondary effluent using a UV dose of 10 mW s/cm^2. However, the *E. coli* counts after UV disinfection of the supernatants of $FeCl_3$ and alum coagulation were higher than the Class A criteria (80 cfu/100 mL and 89 cfu/100 mL, respectively), but they were suitable for Class B irrigation water (Table 4.6). Class A reclaimed water can be used for all types of crops, while Class B reclaimed water is not suitable for root crops that are consumed raw.

Table 4.6 provides the reclaimed water characteristics for the post-treatment alternatives. A2, which combines UF and UV, demonstrated superior treatment performance for all parameters and produced reclaimed water of Class A quality. However, A1, A2, and A4 resulted in reclaimed water of Class B quality due to BOD_5 concentrations exceeding 10 mg/L. The RWQIs for the post-treatment alternatives are calculated based on the concentrations provided in Table 4.6.

Table 4.6 : The reclaimed water quality obtained in each scenario.

Parameter	Unit	A1	A2	A3	A4	Criteria*	
		MF+UV	UF+UV	$FeCl_3$+UV	Alum+UV	(Class A)	(Class B)
TSS	mg/L	8±2	4±0.1	7±2	7±1	≤10	≤35
Turbidity	NTU	7.0±0.1	2.6±0.4	5.8±0.2	6.5±0.4	≤5	-
BOD_5	mg/L	11±2.6	3.4±0.2	16±4.0	15±4.4	≤10	≤25
E. coli	cfu/100 mL	≤10	≤10	≤100	≤100	≤10	≤100
NH_4-N	mg/L	27.5±2.4	20.9±3.2	27.1±4.7	26.2±4.0	-	-
PO_4-P	mg/L	0.97±0.21	0.85±0.15	0.65±0.17	0.72±0.11	-	-

** The EU minimum reclaimed water quality criteria (2020/741)*

Figure 4.18 provides a summarized comparison of the RWQI for each post-treatment alternative. It is evident that the effluent of A2, which exhibits the lowest concentrations of undesired parameters (TSS, turbidity, BOD_5, and *E. coli*), attains the lowest value of the undesired quality index at -0.30. Conversely, A3 represents the worst alternative in terms of concentrations of undesired parameters, resulting in a quality index of -1.0. Since A1 demonstrates the highest concentrations of desired parameters (NH_4-N and PO_4-P), it acquires the highest desired quality index of 1.0. Overall, A2 generates a Class A quality reclaimed water with the highest RWQI value of 0.52. The RWQIs for A1, A3, and A4 are 0.12, -0.17, and -0.12, respectively. An RWQI below zero signifies that these alternatives are relatively worse compared to others. In conclusion, A2 (UF+ UV) yields the most valuable reclaimed water, while A3 ($FeCl_3$ + UV) produces the least valuable reclaimed water for irrigation purposes.

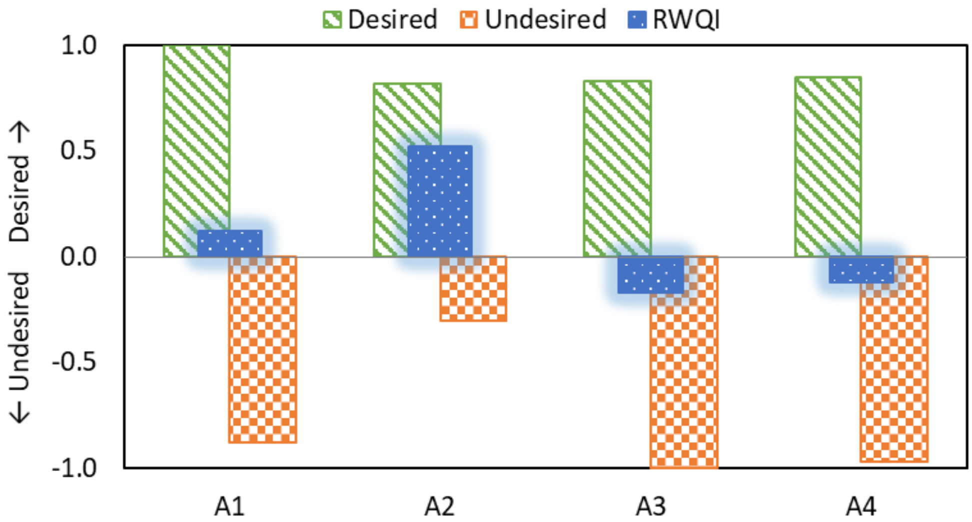

Figure 4.18 : RWQIs of post-treatment alternatives.

4.4.4 Cost estimations

The energy costs for A1, A2, A3, and A4 were estimated to be 0.23 kWh/m^3, 0.27 kWh/m^3, 0.13 kWh/m^3, and 0.13 kWh/m^3, respectively. Similarly, in a study by

Kehrein et al. (2021), the energy consumption for UF+UV post-treatment of a secondary treatment effluent was estimated to be 0.2 kWh/m^3. Among the alternatives, the highest treatment cost was calculated for A2 (UF+UV) post-treatment configuration, amounting to 5.5 €cents/m^3. The treatment costs for A1, A3, and A4 were 4.9 €cents/m^3, 4.1 €cents/m^3, and 4.8 €cents/m^3, respectively (Figure 4.19).

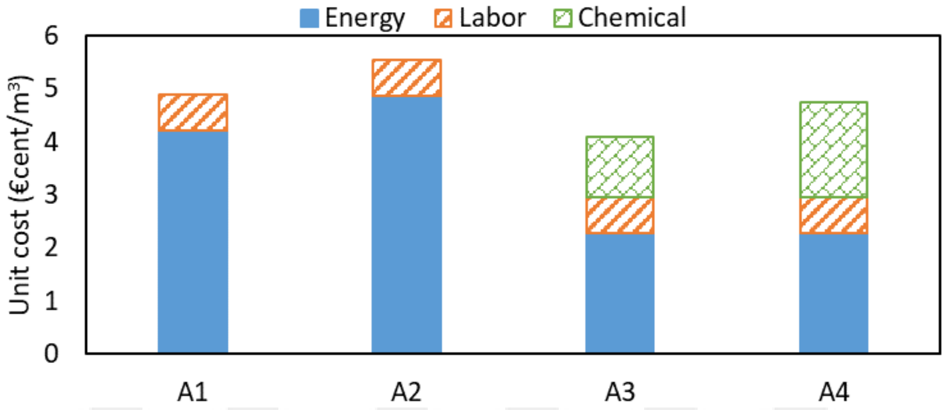

Figure 4.19 : Treatment costs of post-treatment alternatives.

4.5 Study 5 (Examination of The Impact of Adding WTP Sludge to The HRAS Process)

4.5.1 Jar tests

The sludge from the aeration tank of the HRAS plant was treated with alum sludge and iron sludge at a dose of 0.3 mL/L HRAS process sludge, containing 3% solids. The addition of iron sludge resulted in improved removal efficiencies of TSS, COD, and TP by 1.3%, 2.6%, and 3.0%, respectively, compared to the control jar (Figure 4.20). Alum sludge addition also led to increased removal efficiencies of TSS, COD, and TP by 1.0%, 0.4%, and 0.6%, respectively. Based on these results, iron sludge performed better, likely due to its higher coagulant content (11-14% iron content) compared to alum sludge (4-6% alum content). Consequently, iron sludge was chosen for implementation in the pilot-scale HRAS process. The increase in removal efficiencies in this study was lower than the values reported in the literature. Guan et al. (2005) achieved a COD removal efficiency increase from 30-40% to 40-50% by dosing 20 mg of Al/L. The lower increase in removal efficiency in this study may be attributed to the lower dosage of WTP sludge (1.1 mg Al/L for alum sludge and 8 mg Fe/L for iron sludge on average) to avoid raising the inert matter content of the waste sludge from the HRAS plant, thereby maintaining the anaerobic digestibility of the HRAS process sludge.

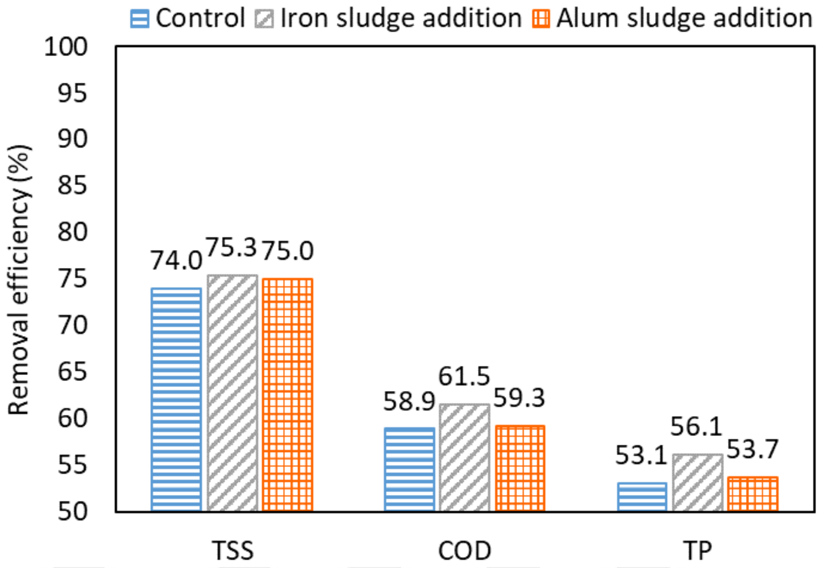

Figure 4.20 : Jar tests results.

4.5.2 Pilot-scale experiments

4.5.2.1 Treatment performance

The HRAS system was monitored for the concentrations of different COD fractions (xCOD, cCOD, and sCOD) and TSS in the influent and effluent at each stage (Figure 4.21). The tCOD removal efficiency remained stable at around 60% throughout the operation. After the addition of iron sludge in Stage 2, the average removal efficiency of xCOD increased from 75% to 81%. The effluent concentrations of sCOD were similar in Stages 1 and 2, resulting in removal efficiencies of 41% and 40% respectively. The average TSS concentration in the effluent was slightly lower in Stage 2 (47 mg/L) compared to Stage 1 (54 mg/L). The average TSS removal efficiencies in Stages 1 and 2 were around 78% and 80% respectively. The xCOD concentration in the effluent decreased from 34% to 22% in Stage 2 due to higher xCOD removal efficiency. Overall, the addition of iron sludge to the HRAS system improved the removal of particulate matter as expected.

The addition of WTP sludge to the HRAS system did not have an impact on the removal of TN (Stage 1: 22.1±5.3%; Stage 2: 23.1±1.4%) and ammonium-nitrogen (NH_4-N) (Stage 1: 15.1±5.3%; Stage 2: 16.1±1.7%), as the removal efficiencies were similar at each stage (Table 4.7). It was not expected to observe higher TN and NH_4-

N removal efficiencies in the HRAS system regardless of WTP sludge addition because the primary removal mechanism in the HRAS process is biomass assimilation without nitrification (Rahman et al., 2016). Similarly, the addition of WTP sludge did not affect the removal efficiency of TP in the system (p-value: 0.45).

Table 4.7 : TN, NH_4-N, and TP concentrations in the influent and effluent, and their removal efficiencies in the HRAS system.

Parameter	Stage 1			Stage 2		
	Concentration (mg/L)		Removal efficiency (%)	Concentration (mg/L)		Removal efficiency (%)
	Influent	Effluent		Influent	Effluent	
TN	57.1±3.7	44.4±2.6	22.1±5.3	56.3±4.4	43.3±3.0	23.1±1.4
NH_4-N	36.5±3.9	30.9±3.0	15.1±5.3	37.2±2.2	31.2±2.2	16.1±1.7
TP	4.95±0.32	1.97±0.20	60.1±4.1	4.80±0.32	1.73±0.15	63.8±2.3

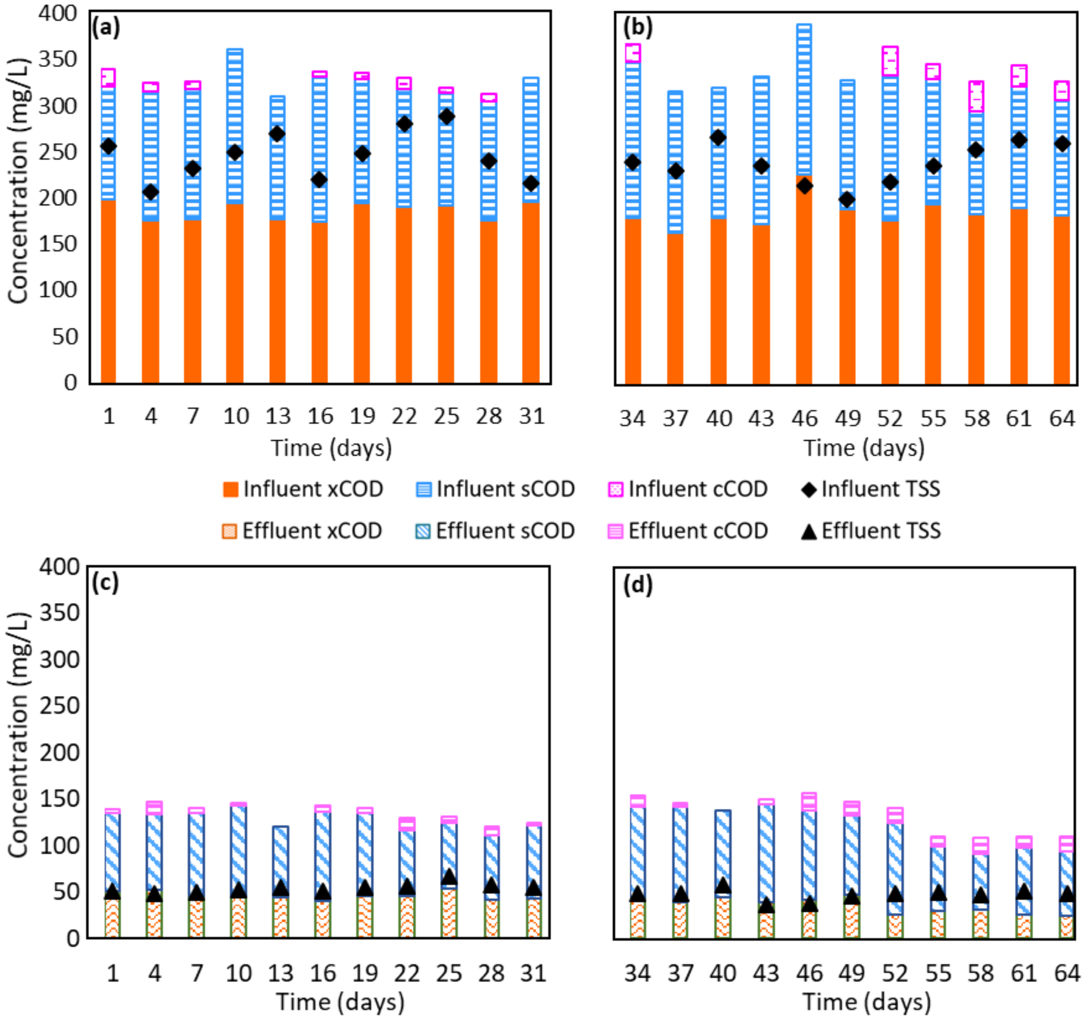

Figure 4.21 : Concentrations of COD fractions and TSS: (a) influent of Stage 1; (b) influent of Stage 2; (c) effluent of Stage 1; (d) effluent of Stage 2.

4.5.2.2 Sludge characteristics

The HRAS system maintained a MLSS concentration range of 2000-3000 mg/L at each stage of operation (Figure 4.22) similar to the MLSS concentration range observed in full-scale HRAS plants (de Graff et al., 2016). The ratio of MLVSS/MLSS remained stable throughout the operation, with values of 0.70±0.03 and 0.69±0.03 at Stage 1 and Stage 2, respectively. The d_{50} value of the sludge in the aeration tank significantly increased after the addition of WTP sludge. The average d_{50} values were 96±3 μm at Stage 1 and 163±14 μm at Stage 2. This increase in d_{50} value can be attributed to the coagulant properties of iron in the WTP sludge, leading to the aggregation of flocs. Consequently, the settleability of the sludge improved when iron sludge was introduced into the HRAS system. The SVI after 5 min of settling (SVI_5) decreased from 72±10 mL/g to 59±6 mL/g, and the SVI after 10 min of settling (SVI_{10}) decreased from 54±9 mL/g to 45±4 mL/g at Stage 2 (Figure 4.22). Additionally, the SVI after 30 min of settling SVI_{30} was slightly lower (Stage 1: 38±6 mL/g; Stage 2: 32±4 mL/g) compared to values reported in the literature (37-60 mL/g) (Guven et al., 2019).

The TS concentration of the excess sludge remained relatively stable, with values around 13.8 g/L at Stage 1 and 12.3 g/L at Stage 2. However, there was a notable difference in the VS concentration between the two stages. The addition of WTP sludge led to a decrease in the VS concentration in the excess sludge, as expected due to the predominantly inorganic composition of iron sludge (Marguti et al., 2018). The average VS concentration was approximately 7.6 g/L at Stage 1 and 5.8 g/L at Stage 2, resulting in VS/TS ratios of 0.55±0.07 and 0.47±0.04, respectively. Furthermore, the filterability of the excess sludge improved following the addition of WTP sludge, as indicated by a decrease in the normalized CST from 1.44±0.2 to 0.95±0.1 sec/g TSS/L.

The microstructure of the excess sludge was investigated at each stage using ESEM (Figure 4.23). The results showed that the addition of iron sludge caused a noticeable alteration in the morphology of the sludge. In Stage 1, the sludge consisted of small floc-like particles with irregular shapes. However, in Stage 2, these particles exhibited a bonding phenomenon, leading to the formation of larger particles. This observation was further supported by the higher d_{50} values measured in Stage 2, indicating an increase in particle size compared to Stage 1.

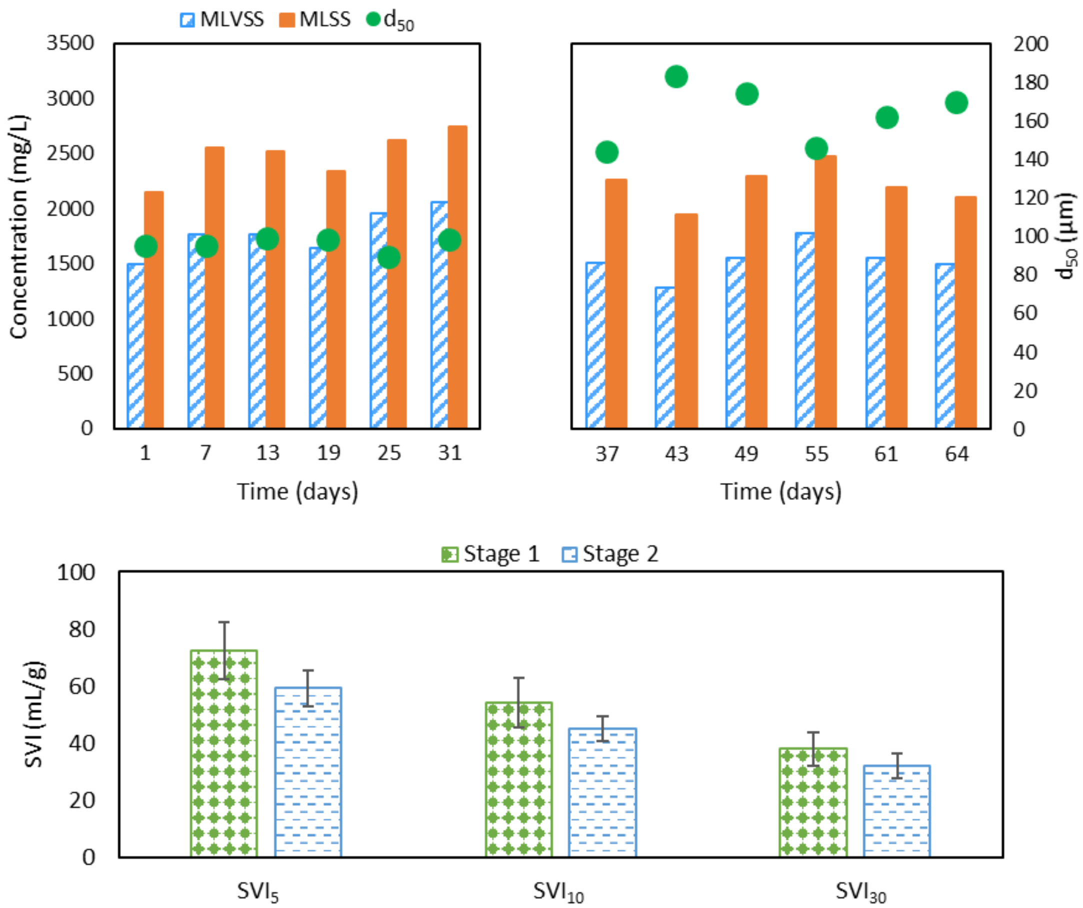

Figure 4.22 : MLSS and MLVSS concentrations and d_{50} values of (a) Stage 1 and (b) Stage 2; (c) SVI values of each stage.

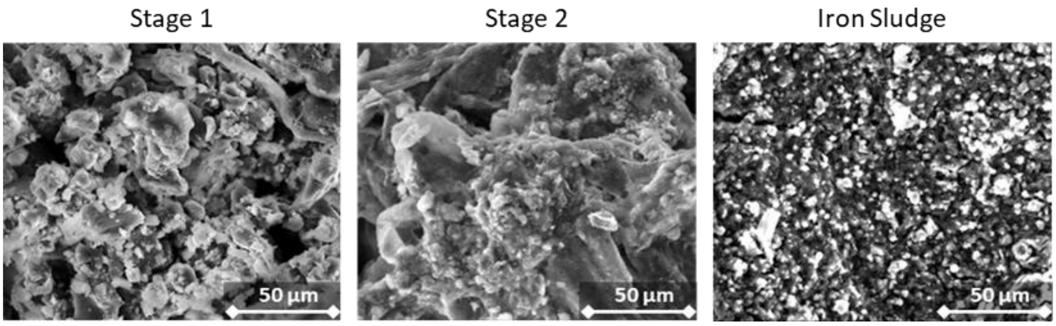

Figure 4.23 : ESEM images: (a) excess sludge at Stage 1; (b) excess sludge at Stage 2; (c) iron sludge.

The impact of WTP sludge addition on the digestibility of excess sludge from the HRAS process is a significant factor to consider, given the changes in the sludge characteristics. To assess the digestibility, a BMP test was conducted for the HRAS process sludge at each stage (Figure 4.24). The results revealed that the addition of iron sludge negatively affected the digestibility of the HRAS process sludge, leading to a reduction in BMP by approximately 8.8% at Stage 2. The average BMP values were measured as 330 mL CH_4/g VS at Stage 1 and 301 mL CH_4/g VS at Stage 2. The decrease in digestibility observed in Stage 2 could be attributed to the inorganic content present in the WTP sludge. Additionally, the formation of larger flocs may have created a "cage" effect, limiting the accessibility of anaerobic bacteria and enzymes to the organic matter within the flocs. Previous studies by Lin et al. (2017) and Shewa et al. (2020) have reported similar effects caused by the presence of large flocs on sludge digestibility.

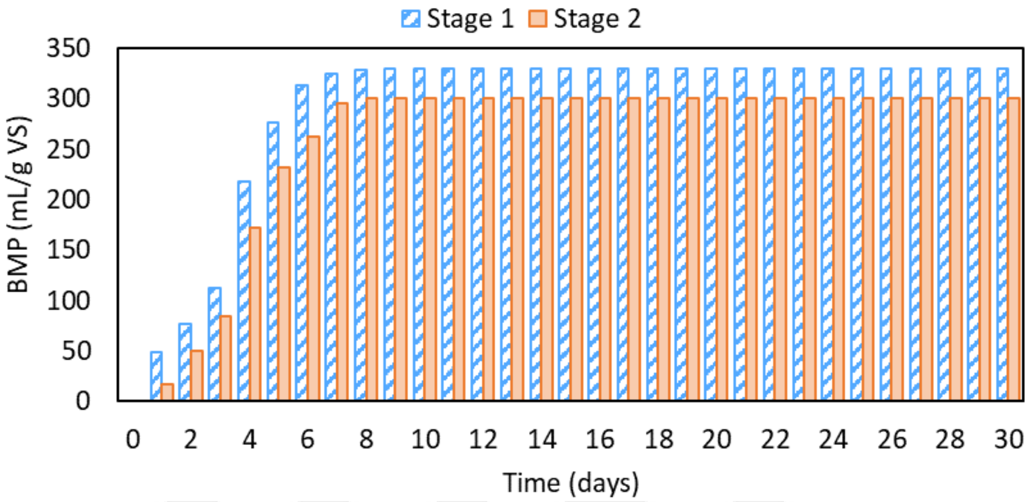

Figure 4.24 : BMP test results.

4.5.3 Scenario analysis

In the scenario analysis, the integration of iron sludge management with the HRAS system was evaluated in terms of both treatment performance and economic aspects. The study examined various factors such as sludge transfer, sludge disposal, energy recovery from excess sludge from the HRAS process, and effluent quality. Based on the experimental results, it was observed that the addition of a low dose of iron sludge to the HRAS system had a limited improvement in treatment performance. In Scenario 1, the EQI for a HRAS process with a capacity of 1,000,000 PE was calculated as 234 kg pollution/day. When iron sludge was added in Scenario 2, the EQI decreased by 2% to 229 kg pollution/day.

Table 4.8 provides a cost estimation for different sludge management scenarios. In Scenario 2, the amount of iron sludge to be sent to the HRAS plant was determined as 16.5 tons/day. In Scenario 1, this amount of iron sludge was sent to a landfill. Since the distances between the WTP and the landfill area, as well as the WTP and the HRAS plant, were the same, the cost of transporting the iron sludge remained the same in each scenario. In Scenario 2, as there was no sludge disposal cost from the WTP, the total cost of landfill disposal and sludge transfer was reduced by 98% (Figure 4.25).

The total energy consumption by the HRAS plant in Scenario 1 was calculated as 13,761 MWh/year, corresponding to an energy cost of 1,662,336 €/year. In Scenario 2, the energy consumption for sludge treatment (including waste sludge pumping, sludge thickening, anaerobic digestion, and sludge dewatering) increased by 10% due to the introduction of iron sludge to the HRAS plant. The total energy consumption of the HRAS system, including wastewater and sludge treatment, increased by 5.6% to 14,534 MWh/year, resulting in an energy cost of 1,755,671 €/year in Scenario 2. The estimated specific energy consumptions in this study (Scenario 1: 0.189 kWh/m^3; Scenario 2: 0.199 kWh/m^3) were consistent with the literature. Tertiary wastewater treatment plants have reported energy consumptions ranging from 0.2 kWh/m^3 to 0.29 ± 0.08 kWh/m^3. The addition of iron sludge in Scenario 2 led to a 9% decrease in BMP of the excess sludge from the HRAS process compared to Scenario 1, as observed in the experimental study. Consequently, the total energy (electricity and heat) production potential from the biogas generated in the anaerobic digester decreased by 7% from 0.34 kWh/m^3 wastewater to 0.32 kWh/m^3 wastewater in Scenario 2. The energy surplus decreased by 23% from 1,358,421 €/year to 1,042,371 €/year in Scenario 2.

Table 4.8 : Cost estimation of the different sludge management scenarios.

Cost (€/year)	Scenario 1	Scenario 2
WTP sludge transport	46,042	46,042
WTP sludge landfill disposal	1,505,625	-
WTP sludge transfer cost	**1,551,667**	**46,042**
HRAS plant energy consumption	1,662,336	1,755,671
HRAS plant energy production	3,020,757	2,798,041
HRAS plant energy surplus	**1,358,421**	**1,042,371**
HRAS process sludge transportation	168,969	185,606
HRAS process sludge landfill disposal	5,525,488	6,069,509
HRAS process sludge transfer cost	**5,694,458**	**6,255,115**
HRAS plant chemical consumption	35,969	28,809
Grand total cost	***5,923,672***	***5,287,595***

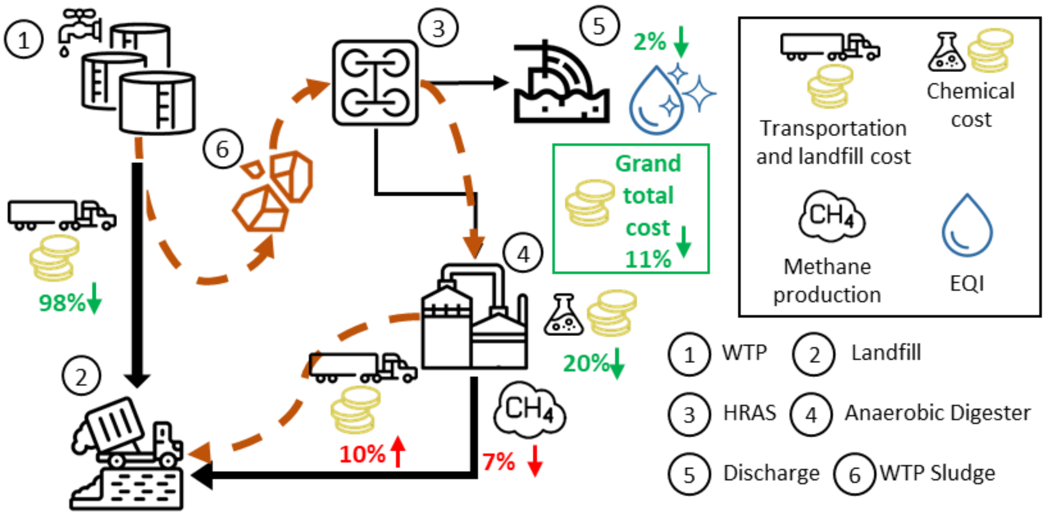

Figure 4.25 : Overall evaluation.

5. CONCLUSIONS AND FUTURE PERSPECTIVES

5.1 Conclusions

This thesis focuses on optimizing and investigating the inclusion of the HRAS process in the circular economy concept not only from an energy but also water and material recovery point of view. In order to enhance the effluent quality of the HRAS process, a lamella clarifier was chosen over a conventional clarifier and the system was optimized at a pilot scale. The results from Study 1 demonstrate that the HRAS process, especially when coupled with a lamella clarifier, exhibits improved efficiency in removing particulate matter. Study 2 focused on modelling and elucidating the biological parameters of the HRAS system, providing valuable insights for subsequent investigations. Typically, reclaimed water is produced by subjecting the effluent of the CAS process to post-treatment steps. However, due to its low energy consumption and smaller footprint requirements, the post-treated effluent from the HRAS process emerges as a viable option for water reuse. Studies 3 and 4 further explored the integration of the HRAS process in reclaimed water production systems. Additionally, Study 5 investigated the use of WTP sludge as an alternative to coagulants, aiming to enhance particulate matter and P removal in HRAS plants and increase material circularity.

In **Study 1**, the focus was on determining the optimal operational conditions for a pilot-scale HRAS system coupled with a lamella clarifier for municipal wastewater treatment. The investigation involved testing different HRTs of 75 and 50 min, as well as different DO concentrations of 0.2, 0.5, and 0.8 mg/L. After conducting the study, several conclusions were drawn:

Firstly, the use of a lamella clarifier resulted in lower concentrations of TSS in the effluent, while requiring a smaller footprint for settling compared to a study that employed a conventional clarifier with similar reactor volumes, HRT values, and influent characteristics.

Among the tested conditions, Stage 1, characterized by an HRT of 75 minutes and a DO concentration of 0.5 mg/L, was identified as the optimum operational condition. Because Stage 1 demonstrated the best effluent quality, highest carbon capture, and the highest production of EPS, which play a role in flocculation. The average removal efficiencies for various parameters were as follows: TSS (80±5%), tCOD (58±3%), TN (32±6%), NH_4-N (27±7%), and TP (58±10%). Additionally, 41.7% of the influent COD was harvested through excess sludge during this stage.

As for the HRT effect on the HRAS process, it was found that reducing the HRT from 75 to 50 min increased biosorption by reducing COD loss through oxidation, but it also resulted in increased COD loss through the effluent.

Regarding the DO concentration effect on the HRAS process, it was determined that lower DO concentrations promoted carbon redirection, but it led to weak floc formation due to low EPS production, resulting in increased loss of xCOD through the effluent and negatively impacting carbon capture. Despite increased biosorption and carbon redirection, carbon capture did not increase in the HRAS system. Higher DO concentrations enhanced COD oxidation and hydrolysis of particulate matter, leading to more particles escaping the system through the effluent.

According to the results obtained from Study 1, it has been shown that the particulate matter removal efficiency of the HRAS process increases with the lamella clarifier and the TSS concentration in the effluent can decrease to an average of 60 mg/L when optimum conditions are provided for this system configuration.

The HRAS model utilized in **Study 2** incorporates ASM1 and ASM3, integrating colloidal substrate adsorption and soluble substrate storage. To ensure accuracy, the model was calibrated using a stepwise approach with dynamic data obtained from the pilot-scale HRAS plant. The study identified several influential model parameters for HRAS systems, including μ, Y_H, Y_{STO}, k_{STO}, b, and K_{S1}. The calibrated model demonstrated efficiencies above 70% of normalized MAE for MLSS, tCOD, sCOD, xCOD, TN, SNH, TP, sTP, and xTP. However, the uncertainty analysis revealed certain discrepancies, indicating that the calibrated model underestimated sCOD. Further analysis of the dynamic profiles of uncertainty bands and observed data revealed a potential for improvement in estimating the dynamic behavior of sTP. The discrepancies observed may be attributed to the variations in wastewater characteristics throughout the monitoring period, particularly concerning the P fractions of S_S and S_I, which were not dynamically considered in the model. Another factor contributing to the reduced predictive accuracy of sTP in the effluent could be the formation of phosphate salt precipitates, which were not accounted for in the model.

In **Study 3**, both experimental and cost analysis components were conducted. In the experimental phase, six treatment configurations (C1-C6) were examined, incorporating different small-footprint pre-treatment options such as DMF with MF and UF membranes, and HRAS, along with final treatment alternatives including NF and RO. The exceptional performance of NF and RO membranes ensured that the reclaimed water in each scenario met the required quality standards for cooling tower makeup water.

Among the pre-treatment options, the HRAS process produced effluent with the lowest quality in terms of turbidity, measuring 42.1±2.6 NTU, in contrast to the DMF permeates obtained through MF and UF membranes, which exhibited turbidity levels below 5 NTU. However, the following cost analysis demonstrated that the C3 configuration (HRAS + NF) achieved the most cost-effective treatment, with a cost of 0.38 €/m^3 of wastewater. This cost advantage stemmed from the lower expenses associated with the HRAS process compared to DMF via MF and UF membranes.

Study 3 established that the C3 configuration (HRAS + NF) has the potential to generate water suitable for use as makeup water in cooling towers. Consequently, the proposed alternative reclaimed water production system presents an opportunity to reduce the water footprint of industries while simultaneously promoting the circularity of water resources.

In **Study 4**, various post-treatment alternatives were compared to generate irrigation water from the effluent of the HRAS process. Among the alternatives considered, UF membrane filtration exhibited superior treatment performance in comparison to MF membrane filtration, $FeCl_3$ coagulation, and alum coagulation.

UV disinfection was implemented at the final stage of all treatment options to eliminate pathogens. The concentration of TSS in the reclaimed water played a crucial role in the success of UV disinfection. The membrane filtration techniques effectively removed particulate matter, while the coagulant doses were adjusted to achieve TSS concentrations below 10 mg/L in the supernatant. Coagulation tests demonstrated that $FeCl_3$ and alum coagulants required doses of 50 mg/L and 100 mg/L, respectively, to achieve TSS concentrations below the desired threshold.

The produced irrigation water quality of each alternative was compared to the minimum reclaimed water quality criteria by EUCO Regulation no. 2020/741. Among the alternatives, only UF membrane filtration followed by UV disinfection (referred to as A2) produced reclaimed water of Class A quality, meeting the highest standards. In fact, A2 attained the highest RWQI value of 0.52. However, it is important to note that A2 also had the highest operating cost of 5.5 €cents/m^3. On the other hand, alternatives A1 (MF+UV), A3 ($FeCl_3$ coagulation + UV), and A4 (alum coagulation + UV) produced reclaimed water of Class B quality. As expected, the operating costs decreased with a decrease in the reclaimed water quality. Among these alternatives, A3 yielded the lowest operating cost of 4.1 €cents/m^3, along with an RWQI of -0.17. The energy consumption per unit of volume for A1, A2, A3, and A4 was calculated to be 0.23 kWh/m^3, 0.27 kWh/m^3, 0.13 kWh/m^3, and 0.13 kWh/m^3, respectively. These values align with previous studies reported in the literature, indicating consistency in the estimated energy requirements for the different treatment alternatives. The findings of this study demonstrate that the effluent of the HRAS process can be effectively utilized for the production of irrigation water at comparable costs to traditional CAS systems. Moreover, the HRAS process exhibits advantages such as low energy consumption and a smaller footprint requirement compared to CAS systems. These results indicate that the HRAS process effluent holds significant potential in promoting water and nutrient circularity, contributing to sustainable development efforts.

Study 5 focused on investigating the impact of using WTP sludge in a HRAS system. Jar tests were conducted to compare the performance of iron sludge and alum sludge in terms of removal efficiency. The results indicated that iron sludge outperformed alum sludge in removing particulates. By incorporating iron sludge into the HRAS system, there was a slight increase in the removal efficiencies of TSS and xCOD from 78% and 75% to 80% and 81%, respectively. Consequently, the environmental impact of the HRAS plant, as measured by the EQI, improved by 2% through the use of iron sludge.

Furthermore, iron sludge addition to the HRAS process increased the d_{50} value of the sludge in the aeration tank from 96±3 to 163±14 μm. This increase in particle size enhanced sludge settleability and dewaterability which would decrease the cost of sludge treatment. However, BMP tests revealed that the addition of iron sludge decreased the BMP of HRAS process sludge by 8.9%.

In addition to the experimental studies, cost estimations were carried out for two different sludge management scenarios, considering sludge transfer and disposal, and wastewater treatment costs. The scenario analysis also took into account the energy savings resulting from the production of biogas. The results indicated that the use of WTP sludge in the HRAS plant led to an estimated 11% reduction in the grand total cost. This finding highlights the potential for achieving mutual benefits for both WTPs and WWTPs in terms of financial and environmental aspects through the integration of resources. Therefore, the integration of water and wastewater treatment plants should be considered to promote resource circularity and maximize the efficiency of resource utilization.

5.2 Future Perspectives

This thesis has demonstrated the potential of the HRAS process to contribute to water and material recovery within the circular economy framework, in addition to energy recovery. In the future, the HRAS process can be advanced within the context of the circular economy by exploring or suggesting the following issues:

- To enhance the accuracy of the HRAS model in estimating sTP, it may be necessary to simulate the precipitation of phosphate salts. Additionally, conducting respirometric analysis can lead to a more precise model. However, these improvements would necessitate obtaining additional data on wastewater characteristics and increasing the complexity of the model.
- To further explore water reuse and nutrient recovery aspects, a more comprehensive economic analysis could be conducted by investigating various treatment combinations of membrane filtration and coagulations at the pilot scale. Additionally, the impact of coagulation before membrane filtration on membrane fouling can be explored.
- In this thesis, the integration of WTP sludge into the HRAS process was examined without treating the WTP sludge first, resulting in limited enhancement of the HRAS process's treatment performance. Future research

may involve conducting pilot-scale tests to refine this approach, with the goal of increasing treatment efficiency and biogas production. One potential route for enhancement is the implementation of coagulant recovery processes, such as acidification. Such research could provide valuable insights into the circular relationship between water and wastewater treatment plants.

REFERENCES

Abdelrahman, A. M., Aras, M. F., Cicekalan, B., Fakioglu, M., Cingoz, S., Basa, S., Guven, H., Ozgun, H., Ozturk, İ., Koyuncu, I., van Lier, J.B., Volcke, E.I.P., & Ersahin, M. E. (2022). Primary and A-sludge treatment by anaerobic membrane bioreactors in view of energy-positive wastewater treatment plants. *Bioresource Technology,* ***351***, 126965.

Abo-El-Enein, S. A., Shebl, A., & El-Dahab, S. A. (2017). Drinking water treatment sludge as an efficient adsorbent for heavy metals removal. *Applied Clay Science,* ***146***, 343-349.

Ahmad, T., Ahmad, K., & Alam, M. (2016). Sustainable management of water treatment sludge through 3 'R' concept. *Journal of Cleaner Production,* ***124***, 1-13.

Ahn, K. H., & Song, K. G. (1999). Treatment of domestic wastewater using microfiltration for reuse of wastewater. *Desalination*, ***126***(1-3), 7-14.

Appels, L., Baeyens, J., Degrève, J., & Dewil, R. (2008). Principles and potential of the anaerobic digestion of waste-activated sludge. *Progress in Energy and Combustion Science,* ***34***(6), 755-781.

AQUASTAT (2020). Retrieved May 26, 2023, from http://www.fao.org/nr/water/aquastat/data/query/index.html

Atanasova, N., Dalmau, M., Comas, J., Poch, M., Rodriguez-Roda, I., & Buttiglieri, G. (2017). Optimized MBR for greywater reuse systems in hotel facilities. *Journal of Environmental Management,* ***193***, 503-511.

Barker, P. S., & Dold, P. L. (1997). General model for biological nutrient removal activated-sludge systems: model presentation. *Water Environment Research,* ***69***(5), 969-984.

Boehnke, B., Schulze-Rettmer, R., & Zuckut, S. W. (1998). Cost-effective reduction of high-strength wastewater by adsorption-based activated sludge technology. *Water Engineering & Management,* ***145***(12), 31-34.

Bolan, N. S., Thangarajan, R., Seshadri, B., Jena, U., Das, K. C., Wang, H., & Naidu, R. (2013). Landfills as a biorefinery to produce biomass and capture biogas. *Bioresource Technology,* ***135***, 578-587.

Campo, G., Cerutti, A., Lastella, C., Leo, A., Panepinto, D., Zanetti, M., & Ruffino, B. (2021). Production and destination of sewage sludge in the Piemonte Region (Italy): the results of a survey for a future sustainable management. International *Journal of Environmental Research and Public Health,* ***18***(7), 3556.

Cao, S., Lu, D., Phua, K., Yan, W., Le, C., Tao, G., & Zhou, Y. (2020). Organics transformation and energy production potential in a high rate A-stage system: A demo-scale study. *Bioresource Technology, **295***, 122300.

Capodaglio, A. G. (2021). Fit-for-purpose urban wastewater reuse: Analysis of issues and available technologies for sustainable multiple barrier approaches. *Critical Reviews in Environmental Science and Technology, **51***(15), 1619-1666.

Chen, C. Y., Wang, S. W., Kim, H., Pan, S. Y., Fan, C., & Lin, Y. J. (2021). Non-conventional water reuse in agriculture: A circular water economy. *Water Research, **199***, 117193.

Chen, L., Tian, Y., Cao, C., Zhang, S., & Zhang, S. (2012). Sensitivity and uncertainty analyses of an extended ASM3-SMP model describing membrane bioreactor operation. *Journal of Membrane Science, **389***, 99-109.

Cherchi, C., Kesaano, M., Badruzzaman, M., Schwab, K., & Jacangelo, J. G. (2019). Municipal reclaimed water for multi-purpose applications in the power sector: A review. *Journal of Environmental Management, **236***, 561-570.

Copp J.B. (2002). *The COST Simulation Benchmark: Description and Simulator Manual*. Luxembourg: Office for Official Publications of the European Communities.

Cosenza, A., Gulhan, H., Maida, C. M., & Mannina, G. (2022). Nutrient recovery from wastewater treatment by ultrafiltration membrane for water reuse in view of a circular economy perspective. *Bioresource Technology, **363***, 127929.

Dai, H., Chen, W., Dai, Z., Li, X., & Lu, X. (2017). Efficient model calibration method based on phase experiments for anaerobic–anoxic/nitrifying (A2N) two-sludge process. *Environmental Science and Pollution Research, **24***, 19211-19222.

Dassanayake, K., Jayasinghe, G., Surapaneni, A., & Hetherington, C. (2015). A review on alum sludge reuse with special reference to agricultural applications and future challenges. *Waste Management*, ***38***, 321-335.

De Graaff, M. S., van Den Brand, T. P., Roest, K., Zandvoort, M. H., Duin, O., & Van Loosdrecht, M. C. (2016). Full-scale highly-loaded wastewater treatment processes (A-stage) to increase energy production from wastewater: performance and design guidelines. *Environmental Engineering Science, **33***(8), 571-577.

Diamantis, V., Eftaxias, A., Bundervoet, B., & Verstraete, W. (2014). Performance of the biosorptive activated sludge (BAS) as pre-treatment to UF for decentralized wastewater reuse. *Bioresource Technology, **156***, 314-321.

Dignac, M. F., Urbain, V., Rybacki, D., Bruchet, A., Snidaro, D., & Scribe, P. (1998). Chemical description of extracellular polymers: implication on activated sludge floc structure. *Water Science and Technology, **38***(8-9), 45-53.

DuBois, M., Gilles, K. A., Hamilton, J. K., Rebers, P. T., & Smith, F. (1956). Colorimetric method for determination of sugars and related substances. *Analytical Chemistry*, ***28***(3), 350-356.

EEA (2013). *Typical charge (gate fee and landfill tax) for legal landfilling of non-hazardous municipal waste in EU Member States and regions*. Retrieve April 20, 2022 from https://www.eea.europa.eu/data-and-maps/figures/typical-charge-gate-fee-and

European Council (EC) (2020). *Water reuse for agricultural irrigation: Council adopts new rules*. Retrieved July 30, 2020, from https://www.consilium.europa.eu/en/press/press-releases/2020/04/07/water-reuse-for-agricultural-irrigation-council-ado pts-new-rules/

European Parliament, Council of the European Union (2002). Regulation (EC) No 2150/2002 of the European Parliament and of the Council of 25 November 2002 on waste statistics, 25 November 2002. Retrieved from https://eur-lex.europa.eu/legal-content/en/ALL/?uri=CELEX:32002R2150

Eurostat (2022). *Electricity price statistics*. Retrieved April 11, 2022, from https://ec.europa.eu/eurostat/statistics-explained/index.php?title=Electricity_price_statistics#Electricity_prices_for_non-household_consumers

Falsanisi, D., Liberti, L., & Notarnicola, M. (2010). Ultrafiltration (UF) pilot plant for municipal wastewater reuse in agriculture: impact of the operation mode on process performance. *Water*, ***2***(4), 872-885.

Fortela, D. L. B., Farmer, K., Zappi, A., Sharp, W. W., Revellame, E., Gang, D., & Zappi, M. (2019). A Methodology for Global Sensitivity Analysis of Activated Sludge Models: Case Study with Activated Sludge Model No. 3 (ASM 3). *Water Environment Research*, ***91***(9), 865-876.

Frolund, B., Griebe, T., & Nielsen, P. H. (1995). Enzymatic activity in the activated-sludge floc matrix. *Applied Microbiology and Biotechnology*, ***43***, 755-761.

Fujisaki, K. (2010). Enhancement of settling tank capacity using a new type of tube settler. *Water Science and Technology*, ***62***(6), 1213-1220.

Garrido, J. M., Fdz-Polanco, M., & Fdz-Polanco, F. (2013). Working with energy and mass balances: a conceptual framework to understand the limits of municipal wastewater treatment. *Water Science and Technology*, ***67***(10), 2294-2301.

Ge, H., Batstone, D. J., Mouiche, M., Hu, S., & Keller, J. (2017). Nutrient removal and energy recovery from high-rate activated sludge processes–Impact of sludge age. *Bioresource Technology*, ***245***, 1155-1161.

Gernaey, K. V., Van Loosdrecht, M. C., Henze, M., Lind, M., & Jørgensen, S. B. (2004). Activated sludge wastewater treatment plant modelling and simulation: state of the art. *Environmental Modelling & Software*, ***19***(9), 763-783.

Gernaey, K.V. & Jorgensen, S.B. (2004). Benchmarking combined biological phosphorus and nitrogen removal wastewater treatment processes. *Control Engineering Practice,* ***12***, 357-373.

Gitis, V., & Hankins, N. (2018). Water treatment chemicals: Trends and challenges. *Journal of Water Process Engineering*, ***25***, 34-38.

Goldbold, P., Lewin, K., Graham, A., & Barker, P. (2003). The potential reuse of water utility products as secondary commercial materials. WRC Report No. UC, 6081.

Gómez, M. D., De la Rua, A., Garralón, G., Plaza, F., Hontoria, E., & Gómez, M. A. (2006). Urban wastewater disinfection by filtration technologies. *Desalination,* ***190***(1-3), 16-28.

Guan, X. H., Chen, G. H., & Shang, C. (2005). Re-use of water treatment works sludge to enhance particulate pollutant removal from sewage. *Water Research*, ***39***(15), 3433-3440.

Guven, H., Dereli, R. K., Ozgun, H., Ersahin, M. E., & Ozturk, I. (2019). Towards sustainable and energy efficient municipal wastewater treatment by up-concentration of organics. *Progress in Energy and Combustion Science,* ***70***, 145-168.

Guven, H., Ersahin, M. E., Dereli, R. K., Ozgun, H., Sancar, D., & Ozturk, I. (2017). Effect of hydraulic retention time on the performance of high-rate activated sludge system: a pilot-scale study. *Water, Air, & Soil Pollution,* ***228***, 1-10.

Hauduc, H., Al-Omari, A., Wett, B., Jimenez, J., De Clippeleir, H., Rahman, A., Wadhawan, T., & Takacs, I. (2019). Colloids, flocculation and carbon capture–a comprehensive plant-wide model. *Water Science and Technology,* ***79***(1), 15-25.

Hauduc, H., Rieger, L., Takács, I., Héduit, A., Vanrolleghem, P. A., & Gillot, S. (2010). A systematic approach for model verification: application on seven published activated sludge models. *Water Science and Technology,* ***61***(4), 825-839.

He, C., Wang, K., Fang, K., Gong, H., Jin, Z., He, Q., & Wang, Q. (2021). Up-concentration processes of organics for municipal wastewater treatment: New trends in separation. *Science of The Total Environment*, ***787***, 147690.

Henze, M., Gujer, W., Mino, T., & CM, M. (2000). M. van Loosdrecht in: Activated sludge models ASM1, ASM2, ASM2d and ASM3.

Hidalgo, A. M., Murcia, M. D., Gomez, M., Gomez, E., García-Izquierdo, C., & Solano, C. (2017). Possible uses for sludge from drinking water treatment plants. *Journal of Environmental Engineering,* ***143***(3), 04016088.

Hube, S., Eskafi, M., Hrafnkelsdóttir, K. F., Bjarnadóttir, B., Bjarnadóttir, M. Á., Axelsdóttir, S., & Wu, B. (2020). Direct membrane filtration for wastewater treatment and resource recovery: A review. *Science of The Total Environment*, ***710***, 136375.

Jenkins, D., & Wanner, J. (Eds.). (2014). *Activated Sludge-100 Years and Counting*. London: IWA publishing.

Jimenez, J. A., La Motta, E. J., & Parker, D. S. (2007). Effect of operational parameters on the removal of particulate chemical oxygen demand in the activated sludge process. *Water Environment Research*, ***79***(9), 984-990.

Jimenez, J., Miller, M., Bott, C., Murthy, S., De Clippeleir, H., & Wett, B. (2015). High-rate activated sludge system for carbon management–Evaluation of crucial process mechanisms and design parameters. *Water Research*, ***87***, 476-482.

Judd, S., & Jefferson, B. (Eds.). (2003). *Membranes for Industrial Wastewater Recovery and Re-Use*. Oxford: Elsevier.

Kacprzak, M., Neczaj, E., Fijałkowski, K., Grobelak, A., Grosser, A., Worwag, M., Rorat, A., Brattebo, H., Almas, A., & Singh, B. R. (2017). Sewage sludge disposal strategies for sustainable development. *Environmental Research*, ***156***, 39-46.

Kappel, A., Ottosen, L. M., & Kirkelund, G. M. (2017). Colour, compressive strength and workability of mortars with an iron rich sewage sludge ash. *Construction and Building Materials*, ***157***, 1199-1205.

Karahan, Ö., van Loosdrecht, M. C., & Orhon, D. (2006). Modeling the utilization of starch by activated sludge for simultaneous substrate storage and microbial growth. *Biotechnology and Bioengineering*, ***94***(1), 43-53.

Kehrein, P., Jafari, M., Slagt, M., Cornelissen, E., Osseweijer, P., Posada, J., & van Loosdrecht, M. (2021). A techno-economic analysis of membrane-based advanced treatment processes for the reuse of municipal wastewater. *Journal of Water Reuse and Desalination*, ***11***(4), 705-725.

Kim, J. O., Jung, J. T., & Chung, J. (2007). Treatment performance of metal membrane microfiltration and electrodialysis integrated system for wastewater reclamation. *Desalination*, ***202***(1-3), 343-350.

Kinyua, M. N., Elliott, M., Wett, B., Murthy, S., Chandran, K., & Bott, C. B. (2017). The role of extracellular polymeric substances on carbon capture in a high rate activated sludge A-stage system. *Chemical Engineering Journal*, ***322***, 428-434.

Kolisch, G., & Schirmer, G. (2004). Lamella separators in the upgrading of a large urban sewage treatment plant. *Water Science and Technology*, ***50***(7), 205-212.

Krishna, C., & Van Loosdrecht, M. C. (1999). Substrate flux into storage and growth in relation to activated sludge modeling. *Water Research*, ***33***(14), 3149-3161.

Lateef, S. K., Soh, B. Z., & Kimura, K. (2013). Direct membrane filtration of municipal wastewater with chemically enhanced backwash for recovery of organic matter. *Bioresource Technology*, ***150***, 149-155.

Lazarova, V., Asano, T., Bahri, A., & Anderson, J. (Eds.). (2013). *Milestones in Water Reuse: The Best Success Stories*. London: IWA Publishing.

Li, X. Y., & Yang, S. F. (2007). Influence of loosely bound extracellular polymeric substances (EPS) on the flocculation, sedimentation and dewaterability of activated sludge. *Water Research, **41***(5), 1022-1030.

Liang, J., & Zhou, Y. (2022). Iron-based advanced oxidation processes for enhancing sludge dewaterability: State of the art, challenges, and sludge reuse. *Water Research, **218***, 118499.

Lin Lin, W., Xuan, Z., Meng, Z., & Xu Zhou, C. (2009). Desalination of reclaimed water by nanofiltration in an artificial groundwater recharge system. *Journal of Water Supply: Research and Technology—AQUA, **58***(7), 463-469.

Lin, L., Li, R. H., Yang, Z. Y., & Li, X. Y. (2017). Effect of coagulant on acidogenic fermentation of sludge from enhanced primary sedimentation for resource recovery: Comparison between $FeCl_3$ and PACl. *Chemical Engineering Journal, **325***, 681-689.

Liu, Y., Gu, J., & Zhang, M. (2019). *AB Processes: Towards Energy Self-Sufficient Municipal Wastewater Treatment*. London: IWA Publishing.

Longo, S., d'Antoni, B. M., Bongards, M., Chaparro, A., Cronrath, A., Fatone, F., Lema, J.M., Mauricio-Iglesias, M., Soares, A., & Hospido, A. (2016). Monitoring and diagnosis of energy consumption in wastewater treatment plants. A state of the art and proposals for improvement. *Applied Energy, **179***, 1251-1268.

Mahdy, A. M., Elkhatib, E. A., Fathi, N. O., & Lin, Z. Q. (2009). Effects of co-application of biosolids and water treatment residuals on corn growth and bioavailable phosphorus and aluminum in alkaline soils in Egypt. *Journal of Environmental Quality, **38***(4), 1501-1510.

Makinia, J., Rosenwinkel, K. H., & Phan, L. C. (2006). Modification of ASM3 for the determination of biomass adsorption/storage capacity in bulking sludge control. *Water Science and Technology, **53***(3), 91-99.

Mancell-Egala, W. A., De Clippeleir, H., Su, C., Takacs, I., Novak, J. T., & Murthy, S. N. (2017). Novel stokesian metrics that quantify collision efficiency, floc strength, and discrete settling behavior. *Water Environment Research, **89***(7), 586-597.

Mannina, G., Cosenza, A., & Viviani, G. (2012). Uncertainty assessment of a model for biological nitrogen and phosphorus removal: Application to a large wastewater treatment plant. *Physics and Chemistry of the Earth, Parts A/B/C, **42***, 61-69.

Mannina, G., Cosenza, A., Vanrolleghem, P. A., & Viviani, G. (2011). A practical protocol for calibration of nutrient removal wastewater treatment models. *Journal of Hydroinformatics, **13***(4), 575-595.

Mannina, G., Cosenza, A., Viviani, G., & Ekama, G. A. (2018). Sensitivity and uncertainty analysis of an integrated ASM2d MBR model for wastewater treatment. *Chemical Engineering Journal, **351***, 579-588.

Mannina, G., Gulhan, H., & Ni, B. J. (2022). Water Reuse from wastewater treatment: The transition towards Circular Economy in the water sector. *Bioresource Technology,* 127951.

Marguti, A. L., Ferreira Filho, S. S., & Piveli, R. P. (2018). Full-scale effects of addition of sludge from water treatment stations into processes of sewage treatment by conventional activated sludge. *Journal of Environmental Management, **215***, 283-293.

Marufuzzaman, M., Ekşioğlu, S. D., & Hernandez, R. (2015). Truck versus pipeline transportation cost analysis of wastewater sludge. *Transportation Research Part A: Policy and Practice, **74***, 14-30.

Mata-Alvarez, J., Macé, S., & Llabres, P. (2000). Anaerobic digestion of organic solid wastes. An overview of research achievements and perspectives. *Bioresource Technology, **74***(1), 3-16.

McCarty, P. L., Bae, J., & Kim, J. (2011). Domestic wastewater treatment as a net energy producer–can this be achieved?. *Environmental Science and Technology, **45***(17), 7100–7106

Meerburg, F. A., Vlaeminck, S. E., Roume, H., Seuntjens, D., Pieper, D. H., Jauregui, R., Vilchez-Vargas, R. & Boon, N. (2016). High-rate activated sludge communities have a distinctly different structure compared to low-rate sludge communities, and are less sensitive towards environmental and operational variables. *Water Research, **100***, 137-145.

Michael-Kordatou, I., Michael, C., Duan, X., He, X., Dionysiou, D. D., Mills, M. A., & Fatta-Kassinos, D. (2015). Dissolved effluent organic matter: characteristics and potential implications in wastewater treatment and reuse applications. *Water Research, **77***, 213-248.

Miller, M. W. (2015). *Optimizing high-rate activated sludge: organic substrate for biological nitrogen removal and energy recovery* (Doctoral dissertation). VIRGINIA Polytechnic Institute and State University, Blacksburg, Virginia, USA.

Miller, M.W., De Armond, J., Elliott, M., Kinyua, M., Kinnear, D., Wett, B., Murthy, S., & Bott, C.B. (2016). Settling and Dewatering Characteristics of an A-stage Activated Sludge Process Proceeded by Shortcut Biological Nitrogen Removal. International Journal of Water and *Wastewater Treatment, **2***(5).

Modin, O., Saheb Alam, S., Persson, F., & Wilén, B. M. (2015). Sorption and release of organics by primary, anaerobic, and aerobic activated sludge mixed with raw municipal wastewater. *PloS One, **10***(3), e0119371.

Morgenroth, E., Kommedal, R., & Harremoës, P. (2002). Processes and modeling of hydrolysis of particulate organic matter in aerobic wastewater treatment–a review. *Water Science and Technology, **45***(6), 25-40.

Nair, A. T., & Ahammed, M. M. (2014). Coagulant recovery from water treatment plant sludge and reuse in post-treatment of UASB reactor effluent treating municipal wastewater. *Environmental Science and Pollution Research, **21***, 10407-10418.

Nascimento, T. A., Fdz-Polanco, F., & Peña, M. (2020). Membrane-based technologies for the up-concentration of municipal wastewater: A review of pretreatment intensification. *Separation & Purification Reviews, **49***(1), 1-19.

Nogaj, T. M., Randall, A. A., Jimenez, J. A., Takacs, I., Bott, C. B., Miller, M. W., Murthy, S., & Wett, B. (2013). Mathematical modeling of carbon removal in the high-rate activated sludge system: model presentation and application. *Proceedings of the 86th Annual Water Environment Federation Technical Exposition and Conference*, Chicago, Illinois, USA, October 5-9.

Nogaj, T., Randall, A., Jimenez, J., Takacs, I., Bott, C., Miller, M., Murthy, S., & Wett, B. (2015). Modeling of organic substrate transformation in the high-rate activated sludge process. *Water Science and Technology, **71***(7), 971-979.

Orhon, D., & Artan, N. (1994). *Modeling of Activated Sludge Systems*. Basel: Technomic Publishing.

Ozgun, H., Cicekalan, B., Akdag, Y., Koyuncu, I., & Ozturk, I. (2021). Comparative evaluation of cost for preliminary and tertiary municipal wastewater treatment plants in Istanbul. *Science of the Total Environment, **778***, 146258.

Perez, G., Gomez, P., Ortiz, I., & Urtiaga, A. (2022). Techno-economic assessment of a membrane-based wastewater reclamation process. *Desalination, **522***, 115409.

Perry, R.H., Green, D.W., Southard, M.Z. (2018). *Perry's Chemical Engineers' Handbook.* 9th Edition, New York: McGraw-Hill Education.

Ping, Q., Li, Y., Wu, X., Yang, L., & Wang, L. (2016). Characterization of morphology and component of struvite pellets crystallized from sludge dewatering liquor: Effects of total suspended solid and phosphate concentrations. *Journal of Hazardous Materials, **310***, 261-269.

Rahman, A., De Clippeleir, H., Thomas, W., Jimenez, J. A., Wett, B., Al-Omari, A., Murthy, S., Riffat, R., & Bott, C. (2019). A-stage and high-rate contact-stabilization performance comparison for carbon and nutrient redirection from high-strength municipal wastewater. *Chemical Engineering Journal, **357***, 737-749.

Rahman, A., Hasan, M., Meerburg, F., Jimenez, J. A., Miller, M. W., Bott, C. B., Al-Omari, A., Murthy, S., Shaw, A., de Clippeleir, H., & Riffat, R. (2020). Moving forward with A-stage and high-rate contact-stabilization for energy efficient water resource recovery facility: Mechanisms, factors, practical approach, and guidelines. *Journal of Water Process Engineering, **36***, 101329.

Rahman, A., Meerburg, F. A., Ravadagundhi, S., Wett, B., Jimenez, J., Bott, C., Al-Omari, A., Riffat, R., Murthy, S., & De Clippeleir, H. (2016). Bioflocculation management through high-rate contact-stabilization: a promising technology to recover organic carbon from low-strength wastewater. *Water Research, **104***, 485-496.

Rahman, A., Yapuwa, H., Baserba, M. G., Rosso, D., Jimenez, J. A., Bott, C., Al-Omari, A., Murthy, S., Riffat, R., & De Clippeleir, H. (2017). Methods for quantification of biosorption in high-rate activated sludge systems. *Biochemical Engineering Journal*, ***128***, 33-44.

Ravazzini, A. M., Van Nieuwenhuijzen, A. F., & Van Der Graaf, J. H. M. J. (2005). Direct ultrafiltration of municipal wastewater: comparison between filtration of raw sewage and primary clarifier effluent. *Desalination*, ***178***(1-3), 51-62.

Rebosura Jr, M., Salehin, S., Pikaar, I., Kulandaivelu, J., Jiang, G., Keller, J., Sharma, K., & Yuan, Z. (2020). Effects of in-sewer dosing of iron-rich drinking water sludge on wastewater collection and treatment systems. *Water Research*, ***171***, 115396.

Rey-Martínez, N., Barreiro-López, A., Guisasola, A., & Baeza, J. A. (2021). Comparing continuous and batch operation for high-rate treatment of urban wastewater. *Biomass and Bioenergy*, ***149***, 106077.

Ricart, S., & Rico, A. M. (2019). Assessing technical and social driving factors of water reuse in agriculture: A review on risks, regulation and the yuck factor. *Agricultural Water Management*, ***217***, 426-439.

Salehin, S., Rebosura, M., Keller, J., Gernjak, W., Donose, B. C., Yuan, Z., & Pikaar, I. (2020). Recovery of in-sewer dosed iron from digested sludge at downstream treatment plants and its reuse potential. *Water Research*, ***174***, 115627.

San Diego County Water Authority (SDCWA). (2009). *Technical Information for Cooling Towers Using Recycled Water*. Retrieved from https://www.sdcwa.org/sites/default/files/files/water-management/recycled/techinfo-cooling-towers.pdf

Sancho, I., Lopez-Palau, S., Arespacochaga, N., & Cortina, J. L. (2019). New concepts on carbon redirection in wastewater treatment plants: A review. *Science of the Total Environment*, ***647***, 1373-1384.

Shewa, W. A., Dong, T., Mu, W., Murray, K., & Dagnew, M. (2020). The impact of chemically enhanced primary treatment on the downstream liquid and solid train processes. *Water Environment Research*, ***92***(3), 359-368.

Shin, H. S., Kang, S. T., & Nam, S. Y. (2000). Effect of carbohydrates to protein in EPS on sludge settling characteristics. *Biotechnology and Bioprocess Engineering*, ***5***, 460-464.

Smitshuijzen, J., Pérez, J., Duin, O., & van Loosdrecht, M. C. (2016). A simple model to describe the performance of highly-loaded aerobic COD removal reactors. *Biochemical Engineering Journal*, ***112***, 94-102.

Smol, M., Adam, C., & Preisner, M. (2020). Circular economy model framework in the European water and wastewater sector. *Journal of Material Cycles and Waste Management*, ***22***, 682-697.

Stumpf, D., Zhu, H., Heinzmann, B., & Kraume, M. (2008). Phosphorus recovery in aerated systems by MAP precipitation: optimizing operational conditions. *Water Science and Technology*, ***58***(10), 1977-1983.

Sweetapple, C., Fu, G., & Butler, D. (2013). Identifying key sources of uncertainty in the modelling of greenhouse gas emissions from wastewater treatment. *Water Research, **47***(13), 4652-4665.

Taboada-Santos, A., Rivadulla, E., Paredes, L., Carballa, M., Romalde, J., & Lema, J. M. (2020). Comprehensive comparison of chemically enhanced primary treatment and high-rate activated sludge in novel wastewater treatment plant configurations. *Water Research, **169***, 115258.

Tchobanoglous, G., Burton, F. L., & Stensel, H. D. (2003). *Wastewater Engineering: Treatment and Reuse*, Metcalf & Eddy Inc. Singapore: McGraw-Hill, Inc.

Trzcinski, A. P., Wang, C., Zhang, D., Ang, W. S., Lin, L. L., Niwa, T., Fukuzaki, Y., & Ng, W. J. (2017). Performance of A-stage process treating combined municipal-industrial wastewater. *Water Science and Technology, **75***(1), 228-238.

Turner, T., Wheeler, R., Stone, A., & Oliver, I. (2019). Potential alternative reuse pathways for water treatment residuals: Remaining barriers and questions—A review. *Water, Air, & Soil Pollution, **230***(9), 227.

US EPA (2012). Guidelines for water reuse. Washington: US EPA.

Üstün, G. E., Solmaz, S. K. A., Çiner, F., & Başkaya, H. S. (2011). Tertiary treatment of a secondary effluent by the coupling of coagulation–flocculation–disinfection for irrigation reuse. *Desalination, **277***(1-3), 207-212.

Van Winckel, T., Liu, X., Vlaeminck, S. E., Takács, I., Al-Omari, A., Sturm, B., Kjellerup, B. V., Murthy, S. N., & De Clippeleir, H. (2019). Overcoming floc formation limitations in high-rate activated sludge systems. *Chemosphere, **215***, 342-352.

Versprille, A. I., Zuurveen, B., & Stein, T. (1985). The A–B process: a novel two stage wastewater treatment system. *Water Science and Technology, **17***(2-3), 235-246.

Wan, J., Gu, J., Zhao, Q., & Liu, Y. (2016). COD capture: a feasible option towards energy self-sufficient domestic wastewater treatment. *Scientific Reports, **6***(1), 1-9.

Wett, B., Aichinger, P., Hell, M., Andersen, M., Wellym, L., Fukuzaki, Y., Cao, Y.S., Tao, G., Jimenez, J., Takacs, I., Bott, C., & Murthy, S. (2020). Operational and structural A-stage improvements for high-rate carbon removal. *Water Environment Research, **92***, 1983-1989.

Wilén, B. M., Jin, B., & Lant, P. (2003). The influence of key chemical constituents in activated sludge on surface and flocculating properties. *Water Research, **37***(9), 2127-2139.

Wilfert, P., Mandalidis, A., Dugulan, A. I., Goubitz, K., Korving, L., Temmink, H., Witkamp G., & Van Loosdrecht, M. C. M. (2016). Vivianite as an important iron phosphate precipitate in sewage treatment plants. *Water Research, **104***, 449-460.

Winkler, S., Müller-Rechberger, H., Nowak, O., Svardal, K., & Wandl, G. (2001). A new approach towards modelling of the carbon degradation cycle at two-stage activated sludge plants. *Water Science and Technology*, ***43***(7), 19-27.

Wu, B., Dai, X., & Chai, X. (2020). Critical review on dewatering of sewage sludge: Influential mechanism, conditioning technologies and implications to sludge re-utilizations. *Water Research*, ***180***, 115912.

Zhao, Y. X., Li, P., Li, R. H., & Li, X. Y. (2020). Characterization and mitigation of the fouling of flat-sheet ceramic membranes for direct filtration of the coagulated domestic wastewater. *Journal of Hazardous Materials*, ***385***, 121557.

CURRICULUM VITAE

Name Surname : Hazal GÜLHAN

EDUCATION :

- **B.Sc.** : 2014, Istanbul Technical University, Civil Engineering Faculty, Environmental Engieering
- **M.Sc.** : 2017, Istanbul Technical University, Graduate School, Environmental Sciences Engineering and Management Program

PROFESSIONAL EXPERIENCE AND REWARDS:

- 2018-… Research Assisstant at Istanbul Technical University
- 2022-2023 Research Fellow at University of Palermo (Italy)

PUBLICATIONS, PRESENTATIONS AND PATENTS ON THE THESIS:

- **Gulhan, H.,** Hamidi, M. N., Abdelrahman, A. M., Fakioglu, M., Mese, B., Yoruk, M., Kurt, E. S., Koyuncu, I., Guven, H., Ozgun, H., Ersahin, M. E., & Ozturk, I. (2022). Long term experiences in a pilot-scale high-rate activated sludge system with lamella clarifier: Effluent quality and carbon capture. *Journal of Water Process Engineering*, *49*, 103138. https://doi.org/10.1016/j.jwpe.2022.103138

OTHER PUBLICATIONS, PRESENTATIONS AND PATENTS:

National Journal Papers

- **Gülhan, H.**, Erşahin, M. E., Dereli, R. K., Özgün, H., Erkan, F. D., Özdemir, Ö., & Öztürk, İ. (2018). Tam ölçekli bir ileri biyolojik evsel atıksu arıtma tesisinin matematiksel modellemesi. *Çukurova Üniversitesi Mühendislik-Mimarlık Fakültesi Dergisi, 33*(4), 213-224.

- **Gülhan, H.,** Dereli, R. K., Özgün, H., Erşahin, M. E., & Öztürk, İ. (2018). İleri biyolojik atıksu arıtma tesislerinde işletme parametrelerinin doğrudan sera gazı emisyon miktarı üzerindeki etkilerinin belirlenmesi. *Pamukkale Üniversitesi Mühendislik Bilimleri Dergisi, 24*(6), 1117-1124.

- **Gülhan, H.,** Özgün, H., Erşahin, M. E., Dereli, R. K., & Öztürk, İ. (2018). İstanbul'daki biyolojik atıksu arıtma tesislerinin sera gazı emisyonunun modelleme metodu ile tahmini. *Fırat Üniversitesi Mühendislik Bilimleri Dergisi, 30*(1), 59-67.

International Journal Papers

- Fakioglu, M., **Gulhan, H.**, Ozgun, H., Ersahin, M. E., & Ozturk, I. (2020). Determination of optimum operational conditions for the removal of 2-MIB from drinking water by peroxone process: a pilot-scale study. *Water Supply, 20*(6), 2339-2347.

- Fakioglu, M., **Gulhan, H.**, Ozgun, H., Ersahin, M. E., & Ozturk, I. (2021). Removal of taste and odor causing compounds from drinking water sources by peroxone process: laboratory and pilot scale studies. *Ozone: Science & Engineering, 43*(6), 527-537.

- **Gulhan, H.**, Dereli, R. K., Ersahin, M. E., & Koyuncu, İ. (2022). Dynamic modeling of a full-scale membrane bioreactor performance for landfill leachate treatment. *Bioprocess and Biosystems Engineering, 45*(2), 345-352.

- Daskiran, F., **Gulhan, H.**, Guven, H., Ozgun, H., & Ersahin, M. E. (2022). Comparative evaluation of different operation scenarios for a full-scale wastewater treatment plant: Modeling coupled with life cycle assessment. *Journal of Cleaner Production, 341*, 130864.

- Kosar, S., Isik, O., Cicekalan, B., **Gulhan, H.**, Kurt, E. S., Atli, E., Basa, S., Ozgun, H., Koyuncu, I., van Loosdrecht, M. C. M., & Ersahin, M. E. (2022). Impact of primary sedimentation on granulation and treatment performance of municipal wastewater by aerobic granular sludge process. *Journal of Environmental Management, 315*, 115191.

- Kosar, S., Isik, O., Akdag, Y., **Gulhan, H.**, Koyuncu, I., Ozgun, H., & Ersahin, M. E. (2022). Impact of seed sludge characteristics on granulation and performance of aerobic granular sludge process. *Journal of Cleaner Production, 363*, 132424.

- Mannina, G., **Gulhan, H.**, & Ni, B. J. (2022). Water reuse from wastewater treatment: The transition towards circular economy in the water sector. *Bioresource Technology*, 127951.

- Cosenza, A., **Gulhan, H.**, Maida, C. M., & Mannina, G. (2022). Nutrient recovery from wastewater treatment by ultrafiltration membrane for water reuse in view of a circular economy perspective. *Bioresource Technology, 363*, 127929.

- Kosar, S., Isik, O., Cicekalan, B., **Gulhan, H.**, Cingoz, S., Yoruk, M., Ozgun, H., Koyuncu, I., van Loosdrecht, M. C. M., & Ersahin, M. E. (2023). Coupling high-rate activated sludge process with aerobic granular sludge process for sustainable municipal wastewater treatment. *Journal of Environmental Management, 325*, 116549.

- Abdelrahman, A. M., Kosar, S., **Gulhan, H.,** Cicekalan, B., Ucas, G., Atli, E., Guven, H., Ozgun, H., Oztuk, I., Koyuncu, I., van Lier, J. B., Volcke, E. I. P., & Ersahin, M. E. (2023). Impact of primary treatment methods on sludge characteristics and digestibility, and wastewater treatment plant-wide economics. *Water Research*, *235*, 119920.

- Mannina, G., Ni, B. J., Makinia, J., Harmand, J., Alliet, M., Brepols, C., Ruano, M. V., Robles, A., Heran, M., **Gulhan, H.**, Rodriguez-Roda, I., & Comas, J. (2023). Biological processes modelling for MBR systems: A review of the state-of-the-art focusing on SMP and EPS. *Water Research*, 120275.

International Symposiums

- **Gulhan, H.**, Fakioglu, M., Ersahin, M.E., Ozgun, H., & Ozturk, I. (2018). Determination of Optimum Operational Conditions for the Removal of 2-Methylisoborneol and Geosmin from Drinking Water by Peroxone Process. In ICOEST 2018. *Proceedings of the 4th International Conference on Environmental Science and Technology,* Ukraine, 19-23 Seprember.

- Fakioglu, M., **Gulhan, H.**, Ozgun, H., Ersahin, M. E., & Ozturk, I. (2019). Determination of Optimum Operational Conditions for the Removal of 2-MIB from Drinking Water by Peroxone Process: A Pilot Scale Study. In IWA YWP 2019. *Proceedings of 11th Eastern European Young Water Professionals Conference,* Czech Republic, 1-5 October.

- Abdelrahman, A. M., Kosar, S., Cicekalan, C., **Gulhan, H.**, Cingoz, S., Buyukbuberoglu, F. B., Guven, H., Ozgun, H., Ozturk, I., Koyuncu, I., Van Lier, J. B., Volcke, E., Ersahin, M. E. (2022). Effect of wastewater treatment configuration on sludge digestion: an economic analysis. *Presented in 17th IWA World Conference on Anaerobic Digestion*, USA, 17 June.

- **Gulhan, H.**, Cosenza, A., Mannina, G. (2022). Resources recovery from wastewater treatment plants: full-scale optimization by using a mathematical model including greenhouse gas emissions. *Presented in iEMSs 2022 Conference,* Belgium, 4-8 July.

- Cosenza, A., **Gulhan, H.**, Mannina, G. (2022). Enhancing membrane bioreactor optimization for water reuse: A pilot-scale experimental study. In AGRO 2022. *The Book of Abstracts of 11th IWA International Symposium on Waste Management Problems in Agro Industry,* Poland, 26-28 October.

- Mannina, G., Ni, B. J., Makinia, J., Harmand, J., Alliet, M., Brepols, C., Ruano, V., Robles, V., Heran, M., Smets, I., **Gulhan, H.**, Rodriguez-Roda, I., Comas, J. (2023). Biological Processes Modelling for Integrated MBR Systems: A Review of the State-of-the-Art. Presented in ECO STP 2023. *6th IWA International Conference on eco-Technologies for Wastewater Treatment,* Spain, 26-29 June.

Book

- Öztürk, İ., Koyuncu, İ., Gömeç, Ç., Karpuzcu, M. E., Erşahin, M. E., Timur, H., Ozgün, H., Dereli, R. K., Koşkan, U., **Gülhan, H.**, Fakıoğlu, M. (2017). *Atıksu Mühendisliği*. İstanbul: İSKİ.